THE CONSEQUENCES OF A NEAR DEGENERACY OF THE $^4T_1(^4F)$ AND $^2E(^2G)$ TERMS IN A d^7 CONFIGURATION

By

DAVID LLOYD WILLIAMS

A DISSERTATION PRESENTED TO THE GRADUATE COUNCIL OF
THE UNIVERSITY OF FLORIDA
IN PARTIAL FULFILLMENT OF THE REQUIREMENTS FOR THE
DEGREE OF DOCTOR OF PHILOSOPHY

UNIVERSITY OF FLORIDA

December, 1966

ACKNOWLEDGMENTS

The author is deeply indebted to the many individuals who have provided assistance on this dissertation. First and foremost is Dr. R. Carl Stoufer, research supervisor, whose assistance and advice throughout the entire project proved invaluable.

Sincere appreciation is extended to Dr. Darwin W. Smith for his many contributions of time and effort in several phases of the project.

Acknowledgment is also given to H. M. Fisher and W. J. McCarthy for their special assistance, and to Mrs. Edwin N. Johnston for her excellent job of typing.

PREFACE

This dissertation is specifically concerned with the magnetic properties exhibited by a small class of six-coordinate octahedral cobalt(II) complexes which are anomalous in their magnetic behavior. This work is presented in two sections, the first and major portion is devoted to a theoretical calculation of magnetic susceptibility as a function of temperature for a d^7 ion, (cobalt(II)). The second section involves electron paramagnetic resonance measurements of some of these compounds, and correlation of the data with the results of the theoretical calculations.

In order to establish a basis from which to work, a general discussion of basic definitions and relationships for paramagnetic ions and their interactions with an external magnetic field is presented in the Introduction of Part I. This is immediately followed by the specific historical and experimental background which formed the motivation and direction for this study. There is a separate introduction in Part II for the electron paramagnetic resonance work.

TABLE OF CONTENTS

Page

ACKNOWLEDGMENTS ii

PREFACE iii

LIST OF TABLES. v

LIST OF FIGURES vi

PART I. MAGNETIC SUSCEPTIBILITY STUDIES

Introduction. 1

Calculations. 17

Results and Discussion. 47

PART II. ELECTRON PARAMAGNETIC RESONANCE STUDIES

Introduction. 75

Experimental. 81

Calculations. 83

Results 93

Discussion. 106

CONCLUSIONS 115

SUMMARY 118

APPENDICES. 120

BIBLIOGRAPHY. 158

BIOGRAPHICAL SKETCH 163

LIST OF TABLES

Table Page

1. Intermediate Magnetic Moments Exhibited by Anomalous Cobalt(II) Complexes 14

2. Spin-Orbit Coupling Matrix for d^7 in Units of ξ 39

3a. First-Order Zeeman Energies for ϕ States. . . . 43

3b. First-Order Zeeman Energies for Linear Combination of ϕ_3 and ϕ_5 44

4. Individual Percentage Contributions of the Five Levels to χ 53

5. Parameters of Equation (44) Used to Calculate the Curves of Figure 9 58

6. Eigenvalues for $\langle \phi_i | \underset{\sim}{L}_x + 2\underset{\sim}{S}_x | \phi_j \rangle$ 86

7. EPR g Values and Transition Probability Numbers for Transitions of the Lowest U' 91

8. The Temperature Dependence of the EPR Spectrum of $[Co(terpy)_2]SO_4 \cdot 2H_2O$. 94

9. The Temperature Dependence of the EPR Spectrum of $[Co(terpy)_2]Cl_2 \cdot 5H_2O$. 95

10. The Temperature Dependence of the EPR Spectrum of $[Co(terpy)_2](ClO_4)_2 \cdot H_2O$ 96

11. The Temperature Dependence of the EPR Spectrum of $[Co(terpy)_2]I_2 \cdot H_2O$. 97

12. The Temperature Dependence of the EPR Spectrum of $[Co(terpy)_2](NO_3)_2$. 98

13. Average g Values of $\Lambda_b \leftrightarrows \Lambda_e$ and $\Lambda_c \leftrightarrows \Lambda_d$ Transitions. 111

LIST OF FIGURES

Figure Page

1. Experimental curves of χ^{-1} vs T 15
2. Experimental curves of χ^{-1} vs T 16
3. Splitting of the d orbitals in an octahedral field. 22
4. Energy level diagram of a d^7 ion in an octahedral field 25
5. Splitting of the $^4T_1$ and ^2E terms under spin-orbit coupling. 37
6. Zero-field energy levels for a d^7 system at the cross-over point in an octahedral field. . 40
7. χ^{-1} vs T for various values of constant δ . . 48
8. Room-temperature magnetic moment vs δ 52
9. χ^{-1} vs T with $\delta = f(T)$. Parameters for curves given in Table 5. 57
10. Energy level diagram for a d^5 ion in an octahedral field 60
11. χ^{-1} vs T calculated by the Ewald model for values of δ with c = 1. 66
12. χ^{-1} vs T calculated by the Ewald model for values of δ with c = 10 and c = 20. 67
13. Splittings of magnetic states of lowest U' as a function of δ, with cross-over of E' states 92
14. EPR spectrum of $[Co(terpy)_2]SO_4 \cdot 2H_2O$ at 193°K. Signal amplitude = 250. 99
15. EPR spectrum of $[Co(terpy)_2]SO_4 \cdot 2H_2O$ at 193°K. Signal amplitude = 400,000. 100

Figure Page

16. EPR spectrum of $[Co(o\text{-}phen)_3](ClO_4)_2$ at 133°K. Signal amplitude = 160,000. 102

17. EPR spectrum of $[Co(o\text{-}phen)_3](ClO_4)_2$ at 93°K. Signal amplitude = 25,600. 103

18. EPR spectrum of $[Co(terpy)_2](NO_3)_2$ at 0°K. Signal amplitude = 63,000. 104

PART I

MAGNETIC SUSCEPTIBILITY STUDIES

Introduction[†]

Each atom or molecule that contains one or more unpaired electrons has a permanent magnetic moment, $\hat{\mu}$, arising from the spin and orbital angular momenta of the unpaired electrons. Substances having permanent magnetic moments are said to be paramagnetic. If the incomplete shells of electrons of such substances are, to a first approximation, isolated from each other, they are also said to be magnetically dilute. The particular systems considered herein have been demonstrated to be magnetically dilute [4,5] and so this will be assumed in all subsequent derivations.

In the presence of an external magnetic field, $\hat{H}$, the magnetic moments of a paramagnetic substance are quantized such that they assume one of a finite number of directions relative to the field. There is an overall tendency for the magnetic moments to align themselves in the direction of the applied field since this is the orientation of lowest energy. Hence, since a magnetic moment by convention has a north-to-south direction (see Appendix B), the substance will experience a force in the direction of the field proportional to the degree of alignment. The net positive macroscopic moment is called the magnetization, $\hat{M}$, and is simply the vector sum of the individual magnetic moments for a substance containing n magnetic ions per gram ion,

---

[†] Most of the equations and relationships established in this introduction can be found in several different textbooks. The author primarily made use of those by Griffith [1], Van Vleck [2], and Figgis [3].

$$\hat{M} = \sum_{i=1}^{n} \hat{\mu}_i \ . \qquad (1)$$

Taking the field direction to be along the z axis of a Cartesian coordinate system, the magnetic moment in the field direction, μ_z, is

$$\mu_z = \frac{\hat{\mu}\cdot\hat{H}}{|H|} \qquad (2)$$

The macroscopic moment in the field direction M_z, is obtained from the scaler product of both sides of equation (1) with the unit vector of the field. Thus,

$$M_z = \sum_{i=1}^{n} \mu_{z_i} \ . \qquad (3)$$

Because of quantization, the μ_{z_i}'s have only a limited number of possible values, each associated with an atom having an energy E_i. The total number of magnetic ions per gram ion is N, Avagadro's number, and the fraction with a magnetic moment of μ_{z_j} and energy E_j is governed by the Boltzmann factor. From these considerations, and summing over the j possible quantum states, equation (3) becomes

$$M_z = N \frac{\Sigma \mu_z e^{-E/kT}}{\Sigma e^{-E/kt}} \qquad (4)$$

where the subscript j is to be understood.

The magnitude of M_z is proportional to the field strength tending to cause alignment and an inverse function of the temperature which is tending to cause randomness. At any one temperature,

$$M_z = \chi H \qquad (5)$$

where χ is the proportionality factor and is defined as the paramagnetic susceptibility per gram ion. For alternative but equivalent definitions for these and other terms, see Appendix A.

The magnetic moment in the field direction, μ_z, is related to the energy of the ionic system in a particular electronic state, E, by the equation

$$\mu_z = - \frac{\partial E}{\partial H} , \qquad (6)$$

derived in Appendix B.

In order to calculate susceptibilities, E is expanded as a power series in H,

$$E = W_0 + HW_1 + H^2W_2 + \ldots.. \qquad (7)$$

so that W_0 corresponds to the zero-order energy of a level, W_1 to the first-order Zeeman energy, and W_2 to the second-order Zeeman energy. From equation (6), the magnetic moment in the field direction is

$$\mu_z = -W_1 - 2HW_2 - \ldots\ldots \tag{8}$$

Utilizing equations (4) through (8) yields

$$\chi = \frac{M_z}{H} = \frac{N}{H}\,\frac{\Sigma(-W_1-2HW_2 - \ldots)e^{-(W_0+HW_1+H^2W_2 + \ldots)/kT}}{\Sigma e^{-(W_0+HW_1+H^2W_2 + \ldots)/kT}}\,, \tag{9}$$

but

$$e^{-(W_0+HW_1+H^2W_2 + \ldots)/kT} = e^{-W_0/kT}(1 - \frac{HW_1}{kT}) \tag{10}$$

provided H^2 terms are neglected. Then

$$\chi = \frac{N}{H}\,\frac{\Sigma(-W_1-2W_2H - \ldots)e^{-W_0/kT}(1 - \frac{HW_1}{kT})}{\Sigma e^{-W_0/kT}(1 - \frac{HW_1}{kT})}\,. \tag{11}$$

If the substance possess no mean residual moment in the absence of the field,

$$[u_z]_{H=0}e^{-W_0/kT} = -\Sigma W_1 e^{-W_0/kT} = 0\,. \tag{12}$$

Using this and retaining only that part of χ independent of H,

$$\chi = N\,\frac{\Sigma(\frac{W_1^2}{kT} - 2W_2)e^{-W_0/kT}}{\Sigma e^{-W_0/kT}}\,. \tag{13}$$

This equation is of primary importance and will be used for the theoretical calculations of magnetic susceptibility as a function of temperature. The only physical assumptions which have been made in deriving equation (13) are that the systems are magnetically dilute, the terms of the energy expansion dependent on H are $\ll kT$, and the susceptibility is independent of the field strength. It will be shown later that within experimental error these assumptions are valid.

If one makes the assumption that the second-order Zeeman effect is negligible, that is, the terms involving W_2 are dropped, equation (13) becomes

$$\chi = N \frac{\Sigma \frac{W_1^2}{kT} e^{-W_0/kT}}{\Sigma e^{-W_0/kT}} \quad . \tag{14}$$

In the expansion of μ_z, equation (8), the $-W_1$ term represents the contribution to the magnetic moment in the z direction in a field-free system. Thus,

$$\mu_z' = -W_1 \tag{15}$$

where a prime indicates the field-free value. Equation (14) is then

$$\chi = \frac{N}{kT} \frac{\Sigma \mu_z'^2 e^{-W_0/kT}}{\Sigma e^{-W_0/kT}} \quad . \tag{16}$$

Note that equation (16) involves a sum of squared terms which will have a finite value and not average out to zero as would a sum of μ_z. Equation (16) can now be written

$$\chi = \frac{N \overline{\mu_z'^2}}{kT} \tag{17}$$

where $\overline{\mu_z'^2}$ denotes the statistical mean square of $\mu_z'^2$ averaged over the available levels of a system weighted by the Boltzmann factor. All special orientations will be equally probable when $H = 0$, and $\overline{\mu_z'^2}$ may be replaced by one third the statistical mean square of the magnetic moment μ. Hence

$$\chi = \frac{N\overline{\mu^2}}{3kT} \quad . \tag{18}$$

This relationship was derived theoretically by Langevin [6] some years after Curie [7] experimentally established the temperature dependence of χ,

$$\chi = \frac{C}{T} \quad , \tag{19}$$

which is referred to as the Curie law, C being constant for a particular substance.

In most systems the temperature dependence of χ as expressed in equation (18) is more complex and, in general, magnetic moments will not be independent of temperature over a large temperature range. However, for qualitative comparison it is convenient to define a magnetic moment independent of temperature in terms of empirical values of χ at any one temperature. This is the "effective magnetic moment" which, when substituted for $\overline{\overline{\mu^2}}$ in equation (18), is given by

$$\mu_{eff} = \left[\frac{3kT}{N\beta^2}\chi\right]^{\frac{1}{2}} = 2.828(\chi T)^{\frac{1}{2}} \qquad (20)$$

where μ_{eff} is expressed in Bohr magnetons, symbolized as β, where

$$\beta = \frac{e\,h}{2mc} = 0.9273 \times 10^{-20} \text{ erg-gauss}^{-1} . \qquad (21)$$

This will be the unit used for all magnetic moments.

The Curie law as expressed by equation (19) is obeyed by comparatively few systems with any degree of accuracy. Often it is possible to describe the variation of χ with T over a large temperature range by the Curie-Weiss law,

$$\chi = \frac{C}{T + \Theta} \quad . \qquad (22)$$

The Weiss constant Θ has physical significance only in some magnetically concentrated systems; in magnetically dilute systems it is to be regarded as empirical only and as a measure of how far the system departs from the ideality of the Curie law.

Magnetic data for most transition-metal complexes can be interpreted in terms of the Curie-Weiss law. There are, however, certain substances which exhibit anomalous magnetic properties, that is, they are not easily characterized by their magnetic moments, and the susceptibility is a more complicated function of temperature than is indicated by equation (22). It is primarily those anomalous systems which are of concern in this work.

The ground term of octahedral d^4, d^5, d^6 and d^7 complexes depends upon the strength of the ligand-field potential. A series of ligands of increasing strength will produce high-spin compounds for weak ligand fields and low-spin compounds for strong ligand fields. For a compound to be low-spin, it is necessary for the ligand field to overcome the interelectronic repulsions and force pairing of electron spins. For a d^7 cobalt(II) system there are comparatively few ligands which manifest sufficient field strengths to accomplish this, and as a result, most six-coordinate octahedral cobalt(II) complexes are high-spin with magnetic moments in the range 4.8 to 5.6 BM [8]. The few low-spin six-coordinate compounds known have magnetic moments in the range 1.73 to 2.0 BM [8,9]. Generally, compounds that can be unequivocably assigned as being either high-spin or low-spin will exhibit normal Curie-Weiss behavior, that is, $\chi^{-1}(T)$ curves will be straight lines. However, a number of complexes of cobalt, and also of iron and nickel as well, have magnetic moments intermediate between the values expected for high-spin and low-spin. These complexes often exhibit anomalous Curie-Weiss behavior, their magnetic moments being temperature dependent.

In 1924, Jackson [10] noted curvature in $\chi^{-1}(T)$ curves below liquid nitrogen temperature for some cobalt(II) sulfates, but he could offer no satisfactory explanation. In 1933, Cambi and Szego [11] found a series of iron(III) dialkyl dithiocarbamates with $\chi^{-1}(T)$ curves containing maxima and minima, and with magnetic moments intermediate between the values expected for high-spin and low-spin iron(III). They proposed a thermal equilibrium between high- and low-spin isomers as an explanation. This work was repeated in 1964 [12] with the same results and conclusions being reached. It should be noted that Bozza [13] in 1933 also proposed a high-spin $\rightleftharpoons$ low-spin equilibrium to explain anomalous magnetic behavior. Cambi proposed a similar explanation for some anomalous cobalt(II) complexes [14] (the oxamide, isonitrosomalonamide, and pyridine isonitrosomalonamide) and estimated the transition energy between the two isomers as 1000cal. Also about this time, Janes [15] noted an anomalous temperature dependence of susceptibility for some cobalt(II) salts and attributed it to a thermal distribution of the electron population over the multiplet levels of the high-spin ground term.

Calvin and Barkelew [16] observed an anomalous temperature dependence of the susceptibility for some planar tetradentate complexes of cobalt(II) and attributed the behavior to a loss of magnetic entropy. By this, they meant that degeneracies of magnetic states were being removed by distortions in crystal symmetry, and that these distortions were a function of temperature. One of their anomalous compounds was restudied by Figgis and Nyholm [17] who discounted their explanation and ascribed the curvature in the $\chi^{-1}(T)$ curve to a large second-order Zeeman effect (the second-order Zeeman contribution to the susceptibility is sometimes called "temperature independent paramagnetism," or the "high-frequency contribution").

For a number of years there has been considerable interest in magnetically anomalous tetracoordinated nickel(II) complexes. French, Magee, and Sheffield [18] observed that solid, diamagnetic bis(formylcamphorethylenediamine)nickel(II) displayed weak paramagnetism in methanol and they postulated a planar ⇆ tetrahedral equilibrium in solution. Further studies by Willis and Mellor [19] seemed to indicate the same type of equilibrium, but in pyridine they postulated the association of two pyridine molecules to give an octahedral configuration, and hence, a planar ⇆ octahedral equilibrium. This idea was further strengthened by the isolation of these pyridine-coordinated species [20]. The hypothesis of a conformational equilibrium such as that between planar and tetrahedral forms, fell out of favor, and the idea of molecular association plus the new concept of an electronic equilibrium became the accepted explanation

[21,22]. The idea of an equilibrium between singlet and triplet states was placed on a quantitative basis by the calculations and investigations of Maki [23,24], and Ballhausen and Liehr [25]. This general idea of high-spin and low-spin forms existing simultaneously was anticipated by Griffith [26] who estimated that such an equilibrium should occur when the difference between the ligand-field strength and the mean pairing energy was less than 2000cm^{-1}. Subsequently, various authors have used the idea of a singlet ⇌ triplet equilibrium in studies of tetracoordinate nickel(II) complexes [27,28,29,30,31].

In 1963, Eaton, Phillips, and Caldwell [32] demonstrated the existence of a truly planar ⇌ tetrahedral equilibrium for some bis(N,N-disubstituted aminotroponimine)-nickel(II) complexes, and concluded that the Maki-Ballhausen-Liehr explanation and the conformational equilibrium explanation were both valid mechanisms. Further studies [33,34] support the conclusions of Eaton _et al_. Recently, the existence of a planar ⇌ tetrahedral equilibrium of cobalt(II) complexes in solution has been observed [35,36]. There has also been a tetrahedral ⇌ octahedral equilibrium observed for cobalt(II) [37,38], and another involving octahedral, pyramidal and tetrahedral species [39].

Studies of magnetically anomalous iron(II) complexes are beginning to appear in the literature [40,41,42,43].

Iron(II) is a d^6 ion, and a quintet $\rightleftharpoons$ singlet equilibrium has been postulated [43] to explain the magnetic behavior.

Figgins and Busch [44] studied a series of six-coordinate octahedral cobalt(II) complexes and observed room-temperature magnetic moments intermediate between the expected high-spin and low-spin values. They postulated an equilibrium mixture of high-spin and low-spin states as an explanation. The magnetic moment of bis(2,6-pyridindialdihydrazone)cobalt(II) iodide was measured over a 300° temperature range by Stoufer, Busch, and Hadley [45] and found to depend markedly on the temperature. Again a high-spin $\rightleftharpoons$ low-spin equilibrium was proposed and the equilibrium constant at various temperatures was calculated. Cossee [46] measured the magnetic susceptibility of Co^{2+} ions in octahedral interstices of an oxide lattice over the range 300° to 1200°K and noted curvature in $\chi^{-1}(T)$ curves. He explained the anomalous behavior by a Boltzmann distribution over the three levels which arise from the splitting of the high-spin ground term by spin-orbit coupling (vide infra). In 1963, Hogg and Wilkins [47] examined some terpyridine complexes of cobalt(II) and found intermediate magnetic moments. They suggested a high-spin $\rightleftharpoons$ low-spin equilibrium, but concluded it cannot be simple, and that the magnetic moment of either the high-spin or low-spin form or both, must be temperature dependent.

Most of the motivation for this dissertation is derived from the work of Stoufer, Smith, Clevenger, and Norris [4] who investigated six octahedral cobalt(II) complexes with intermediate magnetic moments, and presented $\chi^{-1}(T)$ curves for each. Other cobalt(II) complexes exhibiting similar behavior have also been found by Fisher [5] and Ramirez [48]. A tabulation of some of these compounds and their room-temperature magnetic moments is given in Table 1, and plots of χ^{-1} versus T are shown in Figures 1 and 2. In their paper, Stoufer et al. conclude that the only qualitative explanation for this anomalous magnetic behavior consistent with the experimental data involves a model in which there is a distribution of magnetic ions among two or more low-lying electronic levels. They also concur with the suggestion of Hogg and Wilkins that the characteristics of each level are temperature dependent. Data are presented which indicate that other possible explanations are improbable. Careful chemical analysis eliminates the possibility of paramagnetic or diamagnetic impurities such as Co(III) from causing the anomalies. All magnetic susceptibilities were measured at different field strengths and found to be independent of the applied magnetic field. This fact precludes the existence of ferromagnetic interaction and justifies the assumption used in the derivation of equation (13) that χ

TABLE 1

INTERMEDIATE MAGNETIC MOMENTS EXHIBITED BY ANOMALOUS COBALT(II) COMPLEXES

	Compound	Room Temperature Moments	Reference
I.	$[Co(terpy)_2]Cl_2\cdot 5H_2O$	2.51	5
II.	$[Co)PdAdH)_2]I_2$	2.85	5
III.	$[Co(BMI)_3]I_2\cdot H_2O$	2.91	4
IV.	$[Co(PBI)_2]I_2$	3.72	4
V.	$[Co(terpy)_2](ClO_4)_2\cdot H_2O$ (anoxic)	3.84	5
VI.	$[Co(PvdH)_3]I_2$	4.41	4
VII.	$[Co(GdH)_3]Br_2$	3.18	5
VIII.	$[Co(terpy)_2]SO_4\cdot 2H_2O$	2.98	5
IX.	$[Co(terpy)_2]I_2\cdot H_2O$	3.30	5
X.	$[Co(PvdH)_3](NO_3)_2$	4.11	5
XI.	$[Co(PvdH)_3]Br_2$	4.23	5
XII.	$[Co(terpy)_2](NO_3)_2$	2.96	5

Abbreviations: terpy, 2,2',2" - terpyridine; PdAdH, 2,6-pyridindialdihydrazone; BMI, biacetylbis(methylimine); PBI, 2,6-pyridindialbis(benzylimine); PvdH, pyruvaldihydrazone; GdH, glyoxaldihydrazone.

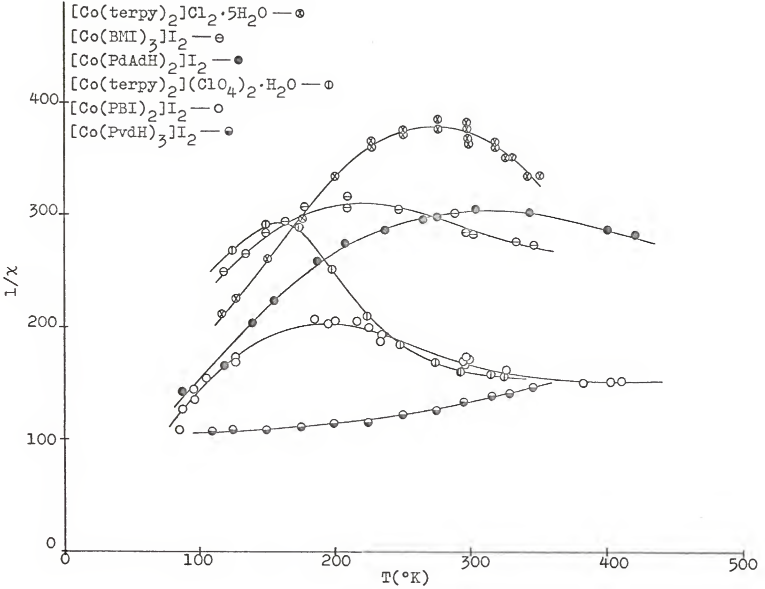

Fig. 1.-Experimental curves of χ^{-1} vs T.

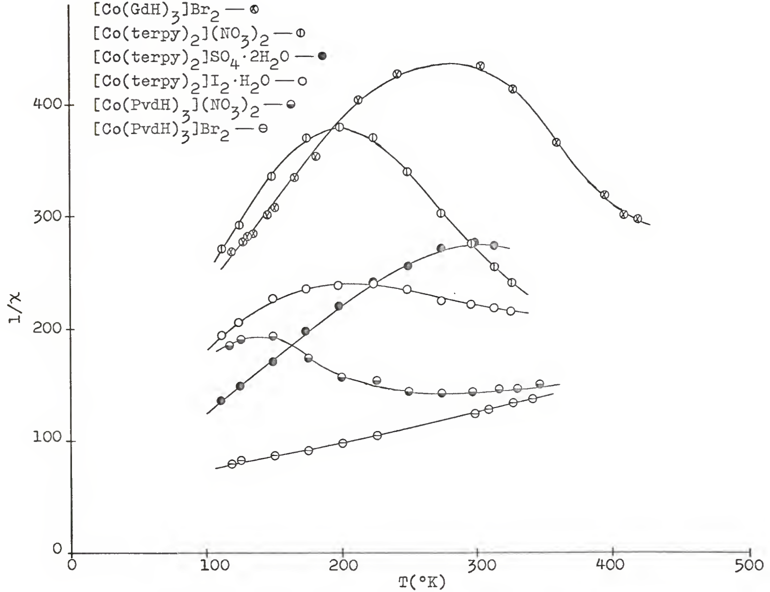

Fig. 2.-Experimental curves of χ^{-1} vs T.

is independent of H. Also, close examination of the experimental curves finds that they do not bear the characteristics associated with antiferromagnetic interaction, and thus this possibility is ruled out. With the elimination of the possibility of ferro- or antiferromagnetism, the assumption that these systems are magnetically dilute is justified.

Spin-orbit coupling allows the simple high-spin $\rightleftarrows$ low-spin two-level model to become a five-level model [4, 49]. It is the purpose of the first part of this dissertation to quantitatively investigate this five-level model and theoretically calculate magnetic susceptibilities as a function of temperature.

Recently, Ewald, Martin, Ross, and White [50] have examined the anomalous behavior of iron(III) complexes using a model similar to the one mentioned above for cobalt(II). A high-spin $\rightleftarrows$ low-spin equilibrium had been previously proposed for the iron(III) compound ferromyoglobin hydroxide [51,52] as well as for the dithiocarbamates mentioned earlier. The Ewald model will be examined in detail in Results and Discussion.

Calculations

In simplest terms, the energy expectation value, E, for any system can be obtained from the wave function Ψ describing that system and the Hamiltonian operator $\mathcal{H}$,

$$E = \langle \Psi | \mathcal{H} | \Psi \rangle \ . \tag{23}$$

Equation (23) is expressed in the bra and ket notation of Dirac [53], and for the purposes of this dissertation, can be defined by the following:

$$\left.\begin{aligned} \langle \Psi | \mathcal{H} | \Psi \rangle &= \int \Psi^* \mathcal{H} \Psi \, d\tau \\ \langle \Psi | \Psi \rangle &= \int \Psi^* \Psi \, d\tau \end{aligned}\right\} \tag{24}$$

Throughout the calculations, the single-electron approximation will be assumed. Under this approximation, the n electrons are distributed among the single-electron orbitals with due regard to the spin of the final state. The Pauli principle declares that all wave functions must be antisymmetrical in every pair of electrons. In other words, an interchange of two electrons must change the sign of the wave function. This physical principle can be built into the mathematical formalism by using determinantal wave functions. These are of the form

$$\Psi = \frac{1}{\sqrt{n!}} \begin{vmatrix} \phi_1(1) & \phi_1(2) & \cdots & \phi_1(n) \\ \phi_2(1) & \phi_2(2) & \cdots & \phi_2(n) \\ \cdots & \cdots & \cdots & \cdots \\ \phi_n(1) & \phi_n(2) & \cdots & \phi_n(n) \end{vmatrix} = \frac{1}{\sqrt{n!}} \left\{ \phi_i(j) \right\} \tag{25}$$

where ϕ is an orthonormal single-electron wave function of both space and spin.

The hydrogenic wave functions, that is, the orbitals s, p, d, etc., are eigenfunctions of the Hamiltonian operator

$$\mathcal{H}_o = -\frac{\hbar^2}{2m}\nabla^2 - \frac{Ze^2}{r} \quad (26)$$

where Z is the "effective" nuclear charge. For an atom having n electrons,

$$\mathcal{H}_o = -\sum_{i=1}^{n}\frac{\hbar^2}{2m}\nabla_i^2 + \frac{Z_i e^2}{r_i} \quad (27)$$

By means of perturbation theory, it is possible to separate the total Hamiltonian into several parts and approximate the energy by regarding the smaller interactions as perturbations on the larger ones. The exact order of the several parts depends on the particular system under investigation. An electron paramagnetic resonance investigation of several of the magnetically anomalous complexes of cobalt(II) reveals that there is a significant amount of spin pairing in the ground level [54]. This is indicative of a large crystal-field splitting (vide infra), and this splitting has been estimated to be approximately 14,000cm^{-1}. For a splitting this large, it is reasonable to calculate the energy values for the pertinent levels of a d^7 ion in an octahedral field by the strong-field method outlined by Griffith [55]. In this strong-field coupling scheme, the crystal-field splitting energy is taken as being greater than the inter-electronic interaction energy which is greater than the spin-orbit coupling energy which again is greater than the first- and second-order Zeeman energies. This approach has been used successfully by Thornley, Windsor, and Owen [56] who worked with systems which had crystal-field splittings of only 10,000cm^{-1}. The general Hamiltonian is then written

$$\mathcal{H} = \mathcal{H}_0 + \mathcal{V} + \mathcal{H}_e + \mathcal{H}_s + \mathcal{H}_1 \qquad (28)$$

where $\mathcal{V}$ is the operator of the electrostatic crystalline field, $\mathcal{H}_e$ is the operator of the interelectronic interaction energy, $\mathcal{H}_s$ is the spin-orbit coupling operator, and $\mathcal{H}_1$ is the operator of the magnetic field interaction energy. Evaluating each of these in succession will evolve the following general scheme:

$$d^k \xrightarrow[\text{component of crystalline field}]{\overset{\mathcal{V}}{\text{high-symmetry}}} t_2^m e \xrightarrow{\overset{\mathcal{H}_e}{\text{electrostatic}}} {}^{2s+1}\Gamma \xrightarrow[\text{coupling}]{\overset{\mathcal{H}_s}{\text{spin-orbit}}}$$

configuration term

$$\Gamma' \xrightarrow[\text{field}]{\overset{\mathcal{H}_1}{\text{magnetic}}} \Gamma' M'$$

level state

A crystalline field of octahedral symmetry splits the five d orbitals into two sets, a triply degenerate set designated t_2 and lying lowest, and a doubly degenerate e set at an energy Δ above the t_2 set. For the particular case of d^7 under consideration, the low-spin configuration will be $t_2^{\,6}e$, and the high-spin configuration will be $t_2^{\,5}e^2$. These two situations are illustrated in Figure 3.

The three d orbitals which span the t_2 representation are related to the three p orbitals by what is known as the p^n isomorphism. Designating the p orbitals by their m_1 values, they are allowed to correspond to the t_2 set by

$$
\begin{aligned}
|p\ 1\rangle \sim |dt_2\ 1\rangle &= |2{-}1\rangle \sim \tfrac{\sqrt{6}}{2}(zx-iyz) \\
|p\ 0\rangle \sim |dt_2\ 0\rangle &= 1/\sqrt{2}\,(|22\rangle - |2{-}2\rangle) \sim i\sqrt{3}xy \qquad (29) \\
|p{-}1\rangle \sim |dt_2{-}1\rangle &= |21\rangle \sim -\tfrac{\sqrt{6}}{2}\,(zx+iyz)
\end{aligned}
$$

The notation in the second column is Griffith's; the functions in the third column are complex and in terms of $|1,m_1\rangle$; on the right is the common Cartesian coordinate notation. This correspondence allows one to use theory developed for field-free systems in systems having ions in other than spherically symmetrical fields. One such modification is the replacement of the operator $\underset{\sim}{L}$ by $\gamma\underset{\sim}{L}$ where γ is a real number which is unity for free ions. Under octahedral symmetry in the strong-field scheme, γ has the value -1. This very conveniently allows one to directly utilize the results obtained for free ions since, from (29),

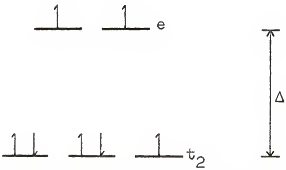

High-spin configuration, $t_2^5e^2$

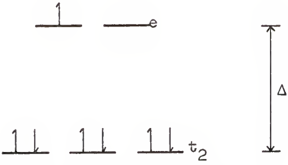

Low-spin configuration, t_2^6e

Fig. 3.-Splitting of the d orbitals in an octahedral field.

$$\langle pi|\,\underset{\sim}{l}\,|pj\rangle = -\langle dt_2i|\,\underset{\sim}{l}\,|dt_2j\rangle \qquad (30)$$

For the e set,

$$|e\theta\rangle = |20\rangle \sim 1/2(2z^2-x^2-y^2)$$

$$(31)$$

$$|e\epsilon\rangle = 1/\sqrt{2}(|22\rangle + |2-2\rangle) \sim \frac{\sqrt{3}}{2}(x^2-y^2)$$

In decreasing order of magnitude, the next energy perturbation is the electrostatic electron repulsions given by the operator

$$\mathcal{H}_e = \sum_{i<j} \frac{e^2}{r_{ij}} \qquad (32)$$

where r_{ij} is the distance separating electrons i and j. It is now necessary to ask what terms arise from each of the aforementioned configurations.

A general configuration $t_2^m e^n$ has two constituent partly-filled subshells, and the terms are obtained by coupling the allowed terms of t_2^m with those of e^n in all possible ways. The coupling of spins is by the vector coupling procedure and the coupling of the space representations is by direct products under the octahedral group O. A table of direct products is given in the table of Appendix C. The problem remaining is to find the allowed terms of t_2^m and e^n. This is accomplished by group theoretical methods by noting how the possible configurations transform under O. For example, e^2 has one triplet state and three singlet ones. These would be

$$\text{triplet:} \qquad \Psi = |\theta^+ \epsilon^+\rangle$$

$$\text{singlet:} \qquad \begin{cases} \Psi_1 = |\theta^+ \theta^-\rangle \\ \Psi_2 = |\epsilon^+ \epsilon^-\rangle \\ \Psi_3 = 1/\sqrt{2}(|\theta^+ \epsilon^-\rangle - |\theta^- \epsilon^+\rangle) \end{cases}$$

where $|a_1 \ldots\ldots a_n\rangle$ denotes a determinantal function based on the single-electron functions according to (25). The manner in which each of these transforms can be determined from their equivalent representations in terms of Cartesian coordinates as given in (29) and (31). Griffith has worked out the results for all t_2^m and e^n configurations [57]. For the particular configurations herein,

$$\begin{aligned} e &\rightarrow {}^2E \\ e^2 &\rightarrow {}^3A_2 + {}^1A_1 + {}^1E \\ t_2^5 &\rightarrow {}^2T_2 \\ t_2^6 &\rightarrow {}^1A_1 \end{aligned}$$

and, using Appendix C,

$$t_2^6 e \rightarrow {}^2E$$

$$t_2^5 e^2 \rightarrow {}^4T_1 + 2\,{}^2T_1 + 2\,{}^2T_2$$

The energy level diagram for a d^7 system as calculated by Tanabe and Sugano [58] is shown in Figure 4, and

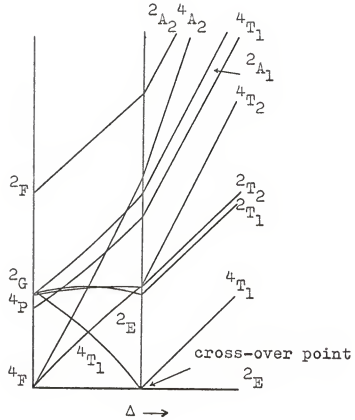

Fig. 4.-Energy level diagram of a d^7 ion in an octahedral field.

the point at which the ^2E and $^4T_1$ terms have equal energy is labelled the "cross-over point." It is presumably at this point that a transformation from high-spin to low-spin character occurs and is thus the specific region of interest. At values of Δ in the vicinity of the cross-over point, all terms other than ^2E and $^4T_1$ are of sufficiently high energy that they may be neglected.

The next problem is to find how these two terms split under spin-orbit coupling and subsequently how they mix. This is accomplished by taking the direct product of the irreducible representation for the spin part and the irreducible representation for the space part. For ^2E, the spin is 1/2, and this transforms as E' [57]. From Appendix C, it is found that under octahedral symmetry $E' \times E = U'$. This means that the ^2E term is not split by spin-orbit coupling, but does transform as a four-dimensional representation, U', under the double group O*. For $^4T_1$, the spin is 3/2 which transforms as U'. Then, $U' \times T_1 = E' + E'' + 2U'$, so that the $^4T_1$ term splits into four levels.

Spin-orbit coupling may also be viewed from a vector-coupling, or Russell-Saunders point of view, whereby a $^4T_1$ term would split into three levels corresponding to $J = 5/2$, $3/2$, and $1/2$. These arise from $\hat{J} = \hat{L} + \hat{S}$, taking all possible integer increments from $|\hat{L} + \hat{S}|$ to $|\hat{L} - \hat{S}|$. Again referring to Griffith [57], $J = 5/2$ transforms as

U' + E", J = 3/2 as U', and J = 1/2 as E'. Hence, there is a one-to-one correspondence between the three Russell-Saunders J levels and the four levels derived from group theory if the E" and one of the U' levels are degenerate. This will be shown to be the case when the actual energy of each of these levels is calculated.

To distinguish between the different U' levels, the U' symbol is followed by the term designation from which it came, for example, U'(^{2}E). However, since there are two U' levels originating from $^4T_1$ another label must be found. As shown above, the U' levels can be associated with a specific J value, and so this J value can be used to distinguish between the U' levels, that is, 5/2U'($^4T_1$) and 3/2U'($^4T_1$).

The problem now involves five levels, four arising from $^4T_1$ and one from ^{2}E. It will be seen that the degeneracy involving the 5/2U' and E" levels is lifted upon further interaction. Thus, in calculating the energy by equation (23), there should arise a five-by-five matrix.

It should be recalled that the ultimate objective is the calculation of magnetic susceptibility as a function of temperature by means of equation (13). The energies of the levels discussed above correspond to the W_0 terms of equation (13). These terms enter through the Boltzmann factor and need only be relative to a ground zero. Thus, it is the difference in energy between the $^4T_1$ and ^2E terms which is important, and their absolute energies need not be calculated. Therefore, only the spin-orbit and magnetic interaction parts of the Hamiltonian in equation (28) must be calculated explicitly.

The spin-orbit coupling Hamiltonian can be obtained from Dirac's relativistic equation [59], and for a central field of potential V, is

$$\mathcal{H}_s = - \frac{e}{2m^2c^2r} \frac{dV}{dr} \underset{\sim}{l} \cdot \underset{\sim}{s} = \xi(r) \underset{\sim}{l} \cdot \underset{\sim}{s} \ . \qquad (33)$$

V is Ze/r for a one-electron atom so $\mathcal{H}_s$ is positive. For an n-electron system,

$$\mathcal{H}_s = \sum_{i=1}^{n} \xi(r_i) \underset{\sim}{l}_i \cdot \underset{\sim}{s}_i \qquad (34)$$

Operating on wave functions which are products of radial, angular, and spin components, the radial portion can be integrated out with $\xi(r)$. The evaluation of the radial integral depends on knowing the radial part of the wave function which is assumed to depend on the quantum numbers n and l plus $\xi(r)$. As a result, the integral is customarily set equal to $h^{-2} \zeta_{nl}$, where ζ_{nl} is called the single-electron spin-orbit coupling constant for an nl orbital. Equation (34) becomes for 3d electrons (with $\zeta \equiv \zeta_{32}$)

$$\mathcal{H}_s = \zeta \sum_i \underset{\sim}{l}_i \cdot \underset{\sim}{s}_i \qquad (35)$$

A typical function can be written as $|t_2^5e^2\ {}^4T_1\ \frac{5}{2}\ U'\kappa\rangle$, or in general as $|\alpha^{2S+1}\Gamma\ \beta\ \Gamma'M'\rangle$ where α is the parent configuration, ${}^{2S=1}\Gamma$ the term under octahedral symmetry, β is a label to distinguish repeated representations of Γ', Γ' itself the representation arising from spin-orbit coupling, and M' the quantum number representing the different rows of the representation Γ' in the octahedral field. The matrix elements will then be of the form

$$\langle \alpha_i\ {}^{2S_i+1}\Gamma_i\beta_i\ \Gamma'_iM'_i\ |\mathcal{H}_s|\ \alpha_j\ {}^{2S_j+1}\Gamma_j\beta_j\ \Gamma'_jM'_j\rangle$$

The spin-orbit coupling operator, $\mathcal{H}_s$, belongs to the representation A_1 of O* and so the matrix will be diagonal in Γ' and M'. Hence, the five-by-five matrix is immediately reduced to a three-by-three involving the U' levels and two one-by-one matrices for the E' and E" levels.

In order to calculate these matrix elements in terms of ζ, the spin-orbit coupling constant, it is necessary to trace back to find specifically the determinantal wave functions from which the levels are derived. As an example, this will be carried out step by step for the 5/2U'($^4T_1$) level.

Because of the diagonalization in M', it is only necessary to select a particular M' and work within it, the result being the same no matter which M' is selected. For reasons which will become apparent later, the 5/2U' level is designated ϕ_3 and the κ component is

$$\phi_3^{\kappa} = \left|t_2{}^5 e^2\ {}^4T_1\ \tfrac{5}{2}\ U'\kappa\right\rangle$$

The first step is to find how the 5/2U'κ component arises. This was previously shown to be a result of coupling the spin representation of ${}^4T_1$ with the space representation, and was U' x T_1 where this particular U' is the representation for 3/2 spin. In Appendix D are tables reproduced from Griffith [57] of coupling coefficients for the octahedral group. In essence, these coupling coefficients are the expansion coefficients $\langle S\Gamma M_S M_\Gamma | S\Gamma\beta\Gamma'M'\rangle$ in the transformation from the $S\Gamma M_S M_\Gamma$ system of quantization to the $S\Gamma\beta\Gamma'M'$ system:

$$|S\Gamma\beta\Gamma'M'\rangle = \sum_{M_S M_\Gamma} \langle S\Gamma M_S M_\Gamma \mid S\Gamma\beta\Gamma'M'\rangle | S\Gamma M_S M_\Gamma\rangle$$

Referring to Appendix D, it can be seen that the 5/2U'κ component can arise from three different possible combinations of U' x T_1. A linear combination of all three is used. Hence

$$\left|t_2{}^5 e^2\ {}^4T_1\ \tfrac{5}{2}\ U'\kappa\right\rangle = -\frac{1}{\sqrt{15}}\left|\tfrac{3}{2}\ T_1\,\kappa\ 0\right\rangle - \frac{1}{\sqrt{10}}\left|\tfrac{3}{2}\ T_1\lambda 1\right\rangle - \sqrt{\tfrac{5}{6}}\left|\tfrac{3}{2}\ T_1\,\nu\, {-1}\right\rangle \qquad (36)$$

where the terms on the right are in the $|S \Gamma M_S M_\Gamma\rangle$ system of quantization.

It is now necessary to find the source of each of the three new functions of equation (36). From previous explanations, it is known that the $^4T_1$ term arose from a coupling of the terms for the t_2^5 and e^2 configurations. It was seen that t_2^5 gives rise to a $^2T_2$ term and e^2 gives rise to a $^3A_2$ plus several singlet terms. However, only the triplet is needed here. Thus the $^4T_1$ term arises from a coupling of $^2T_2$ and $^3A_2$. It is essential to recall that the space coupling is basically independent of the spin coupling. Looking first at the space part, it is necessary to see from which components of T_2 x A_2 the specific T_1 functions of equation (36) arise. These are given in Appendix D.

For the spin part, the T_2 term is a doublet so S = 1/2 which transforms as E'; the A_2 term is a triplet so S = 1 which transforms as T_1. Appendix D contains the coupling coefficients for E' x T_1, and from this the possible combinations to give the needed components for a U' (3/2) spin are found. Thus,

$$\left|\tfrac{3}{2}\ T_1\ \kappa\ 0\right\rangle = \left|{}^2T_2\ \tfrac{1}{2}\ 0,\ {}^3A_2\ 1\ a_2\right\rangle$$

where it is seen that the space part, $T_1 0$ arises from $T_2 0$ x $A_2 a_2$, and the spin part, $3/2\ \kappa$, arises from $E'\alpha'$ x $T_i 1$, α' being the +1/2 component of an E' spin. For the other functions,

$$\left|\tfrac{3}{2}\ T_1 \lambda 1\right\rangle = \sqrt{\tfrac{2}{3}}\left|{}^2T_2\ \tfrac{1}{2} 1, {}^3A_2 0 a_2\right\rangle + \frac{1}{\sqrt{3}}\left|{}^2T_2\ -\tfrac{1}{2}\ 1, {}^3A_2 1 a_2\right\rangle$$

$$\left|\tfrac{3}{2}\ T_1 \nu\ {-1}\right\rangle = \left|{}^2T_2\ -\tfrac{1}{2}\ {-1}, {}^3A_2 {-1} a_2\right\rangle$$

Each of these of course must be multiplied by the appropriate coefficient for each of the three original functions of equation (36).

Again it is necessary to find how each of these four new functions arises. They are combinations of terms from the t_2^5 and e^2 configurations (${}^2T_2$ from t_2^5 and ${}^3A_2$ from e^2). These configurations arise from certain combinations of determinantal wave functions which are given in Appendix D. Thus,

$$\left|{}^2T_2\ \tfrac{1}{2}\ 0, {}^3A_2 1 a_2\right\rangle = -\left|1^2 {-1}^2\ \zeta_1^+\ \theta^+\ \epsilon^+\right\rangle .$$

The function on the right is a determinantal wave function made up of seven single-electron functions where 1^2 represents 1^+1^- , etc., and $\zeta_1 = 1/\sqrt{2}(|2\rangle - |-2\rangle)$, $\theta = |0\rangle$, and $\epsilon = 1/\sqrt{2}(|2\rangle + |-2\rangle)$. Each ket is $|m_1^{\pm}\rangle$ with 1 understood to be 2. Care must be taken with the function containing $|{}^3A_2 0 a_2\rangle$ for this is a triplet with $M_s = 0$ which is the combination $1/\sqrt{2}(\alpha\beta+\beta\alpha)$. Coupling this with the space part of $\theta\epsilon$ gives $1/\sqrt{2}(\theta^+\epsilon^- + \theta^-\epsilon^+)$, so

$$\left|{}^2T_2\ \tfrac{1}{2}\ 1,{}^3A_2 0 a_2\right\rangle = -1/\sqrt{2}\left|1^+ -1^2\ \zeta_1^2\ \theta^+\ \epsilon^-\right\rangle$$

$$-1/\sqrt{2}\left|1^+ -1^2\ \zeta^2\ \theta^-\ \epsilon^+\right\rangle$$

and

$$\left|{}^2T_2 - \tfrac{1}{2}\ 1,{}^3A_2 1 a_2\right\rangle = -\left|1^- -1^2\ \zeta_1^2\ \theta^+\ \epsilon^+\right\rangle .$$

For the remaining function,

$$\left|{}^2T_2 - \tfrac{1}{2}\ -1,{}^3A_2 -1 a_2\right\rangle = \left|1^2 -1^-\ \zeta_1^2\ \theta^-\ \epsilon^-\right\rangle$$

Collecting all the coefficients, the final functions which make up ϕ_3^{κ} are

A. $1/\sqrt{15}\left|1^2 -1^2\ \zeta_1^+\ \theta^+\ \epsilon^+\right\rangle$
B. $1/\sqrt{30}\left|1^+ -1^2\ \zeta_1^2\ \theta^+\ \epsilon^-\right\rangle$
C. $1/\sqrt{30}\left|1^+ -1^2\ \zeta_1^2\ \theta^-\ \epsilon^+\right\rangle$
D. $1/\sqrt{30}\left|1^- -1^2\ \zeta_1^2\ \theta^+\ \epsilon^+\right\rangle$
E. $-\sqrt{5/6}\ \left|1^2 -1^-\ \zeta_1^2\ \theta^-\ \epsilon^-\right\rangle$

In Appendix E are presented the combinations of single-electron determinantal functions which compose the rows of each representation used herein.

The problem now is to evaluate the matrix element $\langle\phi_3|\mathcal{H}_s|\phi_3\rangle$ where $\phi_3 = A + B + C + D + E$. The Hamiltonian operator $\mathcal{H}_s$ is expressible as $\mathcal{H}_s = \sum_i h_s(i)$ where

$$h_s = \zeta(r)\,\underset{\sim}{l}\cdot\underset{\sim}{s} = \zeta\left(\tfrac{1}{2}\,l^+ s^- + \tfrac{1}{2}\,l^- s^+ + l_z s_z\right) \quad (37)$$

and

$$\underset{\sim}{l}^{\pm}|lm\rangle = \left\{\,l(l+1) - m(m\pm 1)\right\}^{1/2}|l\,m\pm 1\rangle$$

$$\underset{\sim}{l}_z|lm\rangle = m\,|\,lm\rangle \quad (38)$$

$$\underset{\sim}{s}^{-}\alpha = \beta \qquad \underset{\sim}{s}^{+}\alpha = 0 \qquad \underset{\sim}{s}_{z}\alpha = 1/2\alpha \qquad \text{(38 cont'd)}$$

$$\underset{\sim}{s}^{-}\beta = 0 \qquad \underset{\sim}{s}^{+}\beta = \alpha \qquad \underset{\sim}{s}_{z}\beta = -1/2\beta$$

As an example of a typical calculation, the term $\langle A|\mathcal{H}_s|D\rangle$ will now be examined. This can be viewed in general as an evaluation of

$$\left\langle a_1(1)a_2(2)a_3(3)a_4(4)a_5(5)a_6(6)a_7(7)\right| \sum_{i=1}^{7} A_i \left| a_8(1)a_9(2)a_{10}(3) \right.$$

$$\left. a_{11}(4)a_{12}(5)a_{13}(6)a_{14}(7)\right\rangle$$

where the a_i's represent single-electron functions belonging to electron (i), and A_i is a single-electron operator. Since these single-electron functions are all orthogonal, the above integral is zero if the bra and ket differ in more than one function. For instance, if all are the same, the above becomes

$$\sum_i \quad \langle a_i(i)|A_i|a_i(i)\rangle$$

and if one pair is different, there is only one term,

$$\langle a_j(j)|A_j|b_j(j)\rangle$$

where a and b are the non-equivalent pair. It is often necessary to permute the functions to achieve a maximum amount of correspondence, care being taken to evaluate the correct parity of the permutation.

Returning to the specific example of $\langle A|\mathcal{H}_s|D\rangle$, this is

$$\frac{1}{15\sqrt{2}}\left\langle 1^+(1)1^-(2)\text{-}1^+(3)\text{-}1^-(4)\,\zeta_1^+(5)\,\theta^+(6)\,\epsilon^+(7)\,\middle|\,\mathcal{H}_s\,\middle|\,1^-(1)\text{-}1^-(2)\text{-}1^+(3)\,\zeta_1^-(4)\,\zeta_1^+(5)\,\theta^+(6)\,\epsilon^+(7)\right\rangle$$

where it is noted that performing the permutation P = [14]·[12] on D puts it equal to A except for the function belonging to electron (1). Therefore, the above integral reduces to

$$\frac{1}{15\sqrt{2}}\left\langle 1^+\middle|\mathcal{H}_s\middle|\zeta_1^-\right\rangle$$

Table F1 of Appendix F lists the eigenvalues belonging to the ten single-electron functions of the d subshell as calculated from the relations of (38). The above integral calculates out to be $1/30\,\zeta$. The results of the entire level are

$$\langle A|\mathcal{H}_s|D\rangle = \langle D|\mathcal{H}_s|A\rangle = 1/30\,\zeta$$
$$\langle B|\mathcal{H}_s|B\rangle = 1/60\,\zeta$$
$$\langle C|\mathcal{H}_s|C\rangle = 1/60\,\zeta$$
$$\langle D|\mathcal{H}_s|D\rangle = -1/60\,\zeta$$
$$\langle E|\mathcal{H}_s|E\rangle = 5/12\,\zeta$$

with all other combinations giving zero. Totalling these values it is found that

$$\langle \phi_3|\mathcal{H}_s|\phi_3\rangle = 1/2\,\zeta$$

The results for the other four levels are

$$\begin{aligned} U'(^2E):&\quad \langle \phi_1 | \mathcal{H}_s | \phi_1 \rangle = 0 \\ 3/2U'(^4T_1):&\quad \langle \phi_2 | \mathcal{H}_s | \phi_2 \rangle = -1/3\,\zeta \\ E'(^4T_1):&\quad \langle \phi_4 | \mathcal{H}_s | \phi_4 \rangle = -\,5/6\,\zeta \\ E''(^4T_1):&\quad \langle \phi_5 | \mathcal{H}_s | \phi_5 \rangle = 1/2\,\zeta \end{aligned}$$

Note that the 5/2U' and E" are degenerate in the absence of further interaction and the situation at this point is as depicted in Figure 5. The energy difference between the $^4T_1$ and ^2E terms is defined by the arbitrary parameter δ which will be positive to the right of the cross-over point and negative to the left.

In the vicinity of the cross-over point, the relationship

$$\Delta = \pi + \delta \tag{39}$$

should hold, where Δ is the crystal-field splitting energy and π is the mean pairing energy. No attempt has been made to quantitatively relate δ to Δ for two reasons: (1) Δ is not required for the calculation of magnetic susceptibilities; (2) there does not seem to be any general agreement on a value for the mean pairing energy of cobalt(II) (see [5] and the discussion therein).

The U' level arising from ^2E has off-diagonal elements with the 3/2U' and 5/2U' levels of $^4T_1$ and these are calculated to be

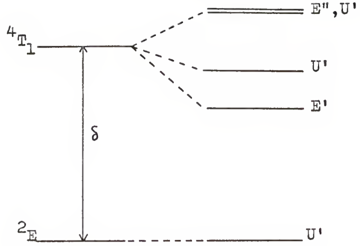

Fig. 5.-Splitting of the $^4T_1$ and ^2E terms under spin-orbit coupling.

$$\langle \phi_1 | \mathcal{H}_s | \phi_2 \rangle = \langle \phi_2 | \mathcal{H}_s | \phi_1 \rangle = 1/\sqrt{5}\,\zeta$$
$$\langle \phi_1 | \mathcal{H}_s | \phi_3 \rangle = \langle \phi_3 | \mathcal{H}_s | \phi_1 \rangle = 3/\sqrt{5}\,\zeta$$

If the zero of energy is taken as the unperturbed energy of the ^2E term, one has the matrix shown in Table 2. Diagonalizing the matrix[+] and plotting the energies of the five levels as a function of δ gives the diagram depicted in Figure 6. These are the W_0 energies required by equation (13). This diagram is consistent with that of Liehr [49] who has presented the entire energy-level diagram for an octahedral d^7 ion.

The last perturbation to be considered is the interaction of the several electronic levels with an external magnetic field. The effect of such a field is, in general, to remove the remaining degeneracy present in each level. If J is a good quantum number, a magnetic field will produce 2J + 1 equally spaced magnetic states. The Hamiltonian for this energy perturbation is

$$\mathcal{H}_1 = \hbar^{-1}\beta H(\underset{\sim}{L} + 2\underset{\sim}{S}) \qquad (40)$$

which is the quantum mechanical analog of equation (10) of

[+] Diagonalization, plus all other nontrivial numerical computations discussed herein, were performed on an IBM 709 at the University of Florida Computing Center. Listings of the pertinent programs are given in Appendix I.

TABLE 2

SPIN-ORBIT COUPLING MATRIX FOR d^7 IN UNITS OF ζ

	$U'(^2E)$	$3/2U'(^4T_1)$	$5/2U'(^4T_1)$	$E'(^4T_1)$	$E''(^4T_1)$
$U'(^2E)$	0	$1/\sqrt{5}$	$3/\sqrt{5}$	0	0
$3/2U'$	$1/\sqrt{5}$	$\delta -1/3$	0	0	0
$5/2U'$	$3/\sqrt{5}$	0	$\delta +1/2$	0	0
E'	0	0	0	$\delta -5/6$	0
E''	0	0	0	0	$\delta +1/2$

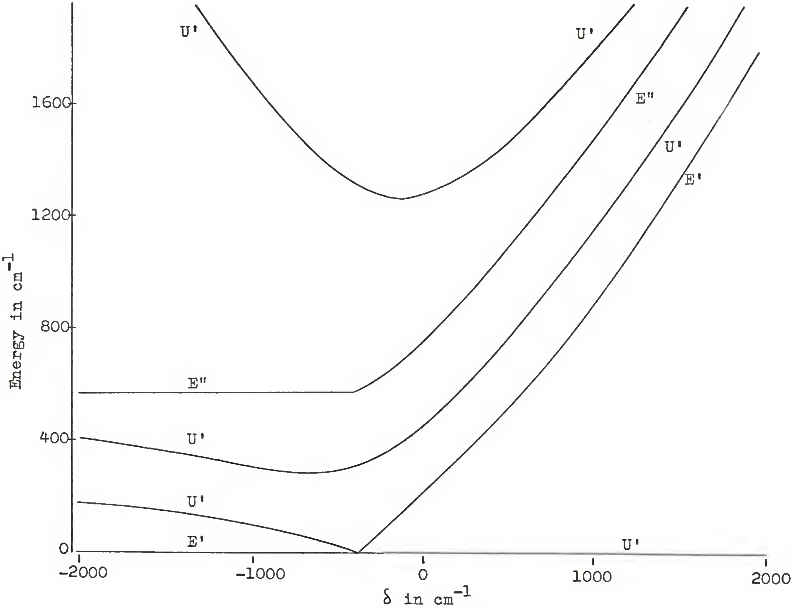

Fig. 6.-Zero-field energy levels for a d^7 system at the cross-over point in an octahedral field.

Appendix B. Since in an octahedral field the susceptibility is independent of the field direction, the magnetic field is taken to be coincidental with the z axis, and equation (40) becomes

$$\mathcal{H}_1 = \hbar^{-1}\beta H_z \sum_i (l_{z_i} + 2s_{z_i}) \ . \qquad (41)$$

The relationships of (38) show that this operator is diagonal in M, so the matrix elements needed are of the form

$$A_{ij} \equiv \langle \Psi_i^M | \mathcal{H}_1 | \Psi_j^M \rangle$$

where Ψ represents the functions belonging to the levels of Figure 6.

The first-order Zeeman effect involves magnetic states within a particular level, thus

$$E^{(1)} = HW_1 = A_{ii} \qquad (42)$$

from which it can be seen that

$$W_1 = \langle \Psi_i^M | \sum_j (l_{z_j} + 2s_{z_j}) | \Psi_i^M \rangle$$

where W_1 is in units of β.

The second-order Zeeman effect arises from off-diagonal terms which allow mixing of magnetic states of different levels. The result is either a raising or lowering of all the magnetic states of a given level. Second-order perturbation theory yields the expression

$$E_i^{(2)} = \sum_{j \neq i} \frac{A_{ij}A_{ji}}{W_{0_i}-W_{0_j}} \qquad (43)$$

for the necessary energies. The desired term, W_2, is then $E_i^{(2)}/H^2$.

As a check, the first-order Zeeman energies are derived for the individual ϕ_i^m states, that is, in the absence of interaction between the U' levels under spin-orbit coupling. This is easily accomplished using the form of the Hamiltonian given in equation (41), and the table of functions in Appendix E. In Table F2 are listed the eigenvalues belonging to the single-electron functions.

Table 3a gives the results for each of the five levels. The energies are given in units of βH and the splittings will be $g\beta H$ where g is the Lande splitting factor. The unequal splitting of the 5/2U' level is the result of neglecting the degeneracy of this level with the E" level. The J = 5/2 level of Figure 5 is actually a linear combination of ϕ_3 and ϕ_5, and so are the magnetic states. Under the operator $\mathcal{H}_1$, ϕ_3^{κ} interacts with $\phi_5^{\beta''}$, and ϕ_3^{ν} interacts with $\phi_5^{\alpha''}$. The particular linear combination is readily calculated, and the new functions, designated by S, are given in Table 3b. It is seen that there are now six equally spaced states. The g values of Tables 3a and 3b are the same as calculated by Griffith [60].

TABLE 3a

FIRST-ORDER ZEEMAN ENERGIES FOR ϕ STATES

	Units of βH
ϕ_1^{κ}	-1
ϕ_1^{λ}	1
ϕ_1^{μ}	-1
ϕ_1^{ν}	1
ϕ_2^{κ}	9/5
ϕ_2^{λ}	3/5
ϕ_2^{μ}	-3/5
ϕ_2^{ν}	-9/5
ϕ_3^{κ}	-22/15
ϕ_3^{λ}	2/5
ϕ_3^{μ}	-2/5
ϕ_3^{ν}	22/15

Table 3a (cont'd)

	Units of βH
$\phi_4^{\alpha'}$	2
$\phi_4^{\beta'}$	-2
$\phi_5^{\alpha''}$	-2/3
$\phi_5^{\beta''}$	2/3

TABLE 3b

FIRST-ORDER ZEEMAN ENERGIES FOR LINEAR COMBINATION OF ϕ_3 AND ϕ_5

	Units of βH
$S_1 = 1/\sqrt{6}(\phi_3^{\kappa} + \sqrt{5}\,\phi_5^{\beta''})$	6/5
$S_2 = 1/\sqrt{6}(-\sqrt{5}\,\phi_3^{\kappa} + \phi_5^{\beta''})$	-2
$S_3 = \phi_3^{\lambda}$	2/5
$S_4 = \phi_3^{\mu}$	-2/5
$S_5 = 1/\sqrt{6}(\sqrt{5}\,\phi_3^{\nu} + \phi_5^{\alpha''})$	2
$S_6 = 1/\sqrt{6}(\phi_3^{\nu} - \sqrt{5}\,\phi_5^{\alpha''})$	-6/5

Each of the three U' levels of Figure 6 is a linear combination of ϕ_1, ϕ_2, and ϕ_3, and it is the W_1 and W_2 values for these levels, as well as for the E' and E" levels, which are needed. For the three U' levels, the desired matrix elements are of the general form

$$A_{ij} = \langle \psi_i^M | \mathcal{H}_1 | \psi_j^M \rangle =$$

$$\langle a_{1i}\, \phi_1^M + a_{2i}\, \phi_2^M + a_{3i}\, \phi_3^M | \mathcal{H}_1 | a_{1_j}\, \phi_1^M + a_{2_j}\, \phi_2^M + a_{3_j}\, \phi_3^M \rangle .$$

The coefficients of the linear combinations are already available from the diagonalization process of the spin-orbit coupling matrix. All parameters necessary for determining W_0, W_1, and W_2, and hence χ, have now been determined.

A brief discussion of units is appropriate at this point. It is shown in Appendix B that a convenient unit for $\hat{\mu}$, the magnetic moment, is erg-gauss^{-1}. From equations (2), (3), and (5), it can be seen that χ then has the units of erg-gauss^{-2} per gram-ion. Equation (13) is used to calculate χ which means that W_0 must have the same units as kT, and the term $(W_1^2/kT - 2W_2)$ must have the units of erg-gauss^{-2}-ion^{-1}.

The W_0 values are calculated in terms of ξ, the spin-orbit coupling constant, which is usually expressed in cm^{-1}. Thus, for the exponential terms, k is expressed as $0.6952 \mathrm{cm}^{-1}$-deg^{-1}-ion^{-1}. As calculated, W_1 is in units of β, the Bohr magneton, and per ion. β is 0.9273×10^{-20} erg-gauss^{-1} so W_1^2 has the units erg^2-gauss^{-2}-ion^{-2}. This is divided by kT, and here, k is expressed as 1.38047×10^{-16}erg-deg^{-1}-ion^{-1}, so W_1^2/kT has the same units as χ. The units of W_2 are β^2 per ion, divided by the units of W_0. Converting the cm^{-1} of W_0 to ergs, leaves W_2 with the units erg-gauss^{-2}-ion^{-1} which is what is needed.

Results and Discussion

The susceptibility, as calculated from equation (13), is dependent on three variables, ζ, δ, and T, these not being necessarily independent of each other. The W's are functions of ζ and δ.

The one-electron spin-orbit coupling parameter, ζ, has a free-ion value of 515cm^{-1} for Co(II) [61], but this is expected to be smaller for ions in a crystalline field [62]. Several test computations were made using a range of values for ζ; however, the susceptibilities were found to be relatively insensitive to these variations and the general shapes of the $\chi^{-1}(T)$ curves were not affected at all. Liehr [49] used a value of 450cm^{-1} which has been adopted for the calculations, treating ζ as a constant independent of the electronic state.

Initial susceptibility calculations were made holding δ constant and curves of the form shown in Figure 7 resulted. For a δ value of $+4000\text{cm}^{-1}$, corresponding to a very strong crystalline field (sufficiently far from the cross-over point that the system can be considered essentially low-spin), one finds the $\chi^{-1}(T)$ plot to be linear from 0°K to well above room temperature. As the value of δ is reduced from large positive values, through the cross-over point and to large negative values, the curves show a continual decrease in slope. Concomitantly,

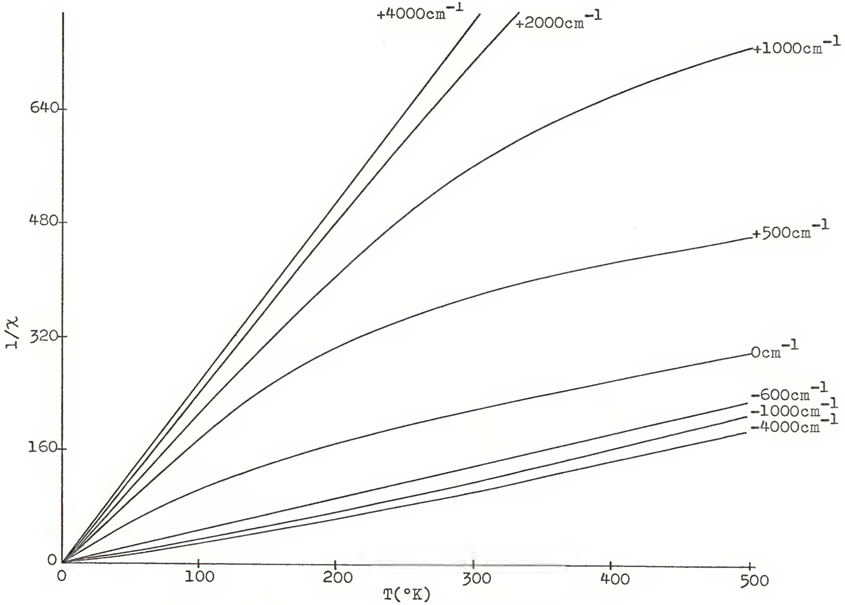

Fig. 7.- χ^{-1} vs T for various values of constant δ.

there is a small degree of curvature incipient at high temperatures. The appearance of this curvature occurs at lower and lower temperatures as the overall slope decreases (with decreasing δ), the high-temperature portion reverting to straight-line behavior. At a δ value of approximately -600cm^{-1}, the plot is essentially straight-line over the entire temperature range. With a further decrease in δ, the general slope continues to decrease but the curvature reverses, that is, it turns away from the temperature axis and its point of appearance begins to shift back toward higher temperatures.

The curvature is caused by two factors operating in equation (2): 1) the second-order Zeeman energies, W_2, which tend to decrease the slope as the temperature increases since W_2 is always negative for the ground level; 2) the influence of the Boltzmann factor which will tend to decrease the slope with increasing temperature to the right of the cross-over point where contributions from excited levels will increase the value of χ (decreases $1/\chi$) and increase the slope with increasing temperature to the left of the cross-over point where the contributions from excited levels decrease the value of χ. With either one of both effects operating, there is significant deviation from the normal Curie-Weiss behavior, and evaluation of a Weiss constant is meaningless.

Recently, Barraclough [63] performed calculations similar to those described herein, and derived curves analogous to those of Figure 7. His results differ significantly from the present ones only in the vicinity of $\delta = 0$. He takes into account the contribution to χ only from the ground electronic level, neglecting the contributions from the other four levels (see Figure 5).

Using equation (20) at a δ value of -4000cm^{-1}, a room-temperature magnetic moment of 4.64 BM is calculated which lies toward the lower limit of the range customarily quoted (4.8 to 5.6 BM) for pure high-spin complexes [8]. This lower value may be attributed in part to the neglect of mixing of high-energy terms other than ^2E with the ground term $^4T_1$ (see Figure 4), a reasonable omission in the vicinity of the cross-over point, but a less and less valid approximation as one proceeds to weaker and weaker fields. Presumably then, if one were to include matrix elements of interaction with higher energy terms, sufficient additional orbital angular momentum would be introduced into the resultant ground level at large negative values of δ to produce the moments more frequently encountered experimentally. At a δ value of $+4000\text{cm}^{-1}$, a room-temperature magnetic moment of 1.76 BM is calculated, in excellent agreement with the spin-only (strong field) moment of low-spin octahedral d^7 complexes. Thus, increasing δ, which corresponds to increasing the crystalline field, causes the effective magnetic moment to decrease in the fashion shown in Figure 8. The important point to be noted is that a smooth decrease in room-temperature magnetic moments from high-spin to low-spin values for Co(II) complexes, concomitant with increasing crystal-field strength, should be regarded as an expected phenomenon.

A very interesting and apparently unreported phenomenon has resulted from the calculation of the separate contributions to the overall susceptibility from each of the five levels of Figure 6, namely, the existence of negative contributions to χ from excited (thermally accessible) levels. Individual percentage contributions of the levels at various values of δ and T, as calculated from equation (13), are reported in Table 4. The unexpected negative contributions are the direct result of the inclusion of the second-order Zeeman energy, W_2, in the computation. Examination of equation (13) reveals that a large positive value for W_2 can give rise to a negative contribution to χ for a particular level should $2W_2$ be larger than $W_1{}^2/kT$. The increasing size and frequency of occurrence of negative contributions with increasing T, as a result of the inverse temperature dependence of the term $W_1{}^2/kT$, is apparent in Table 4. Positive values of W_2 arise for certain excited levels because of the form of equation (43). If the shift

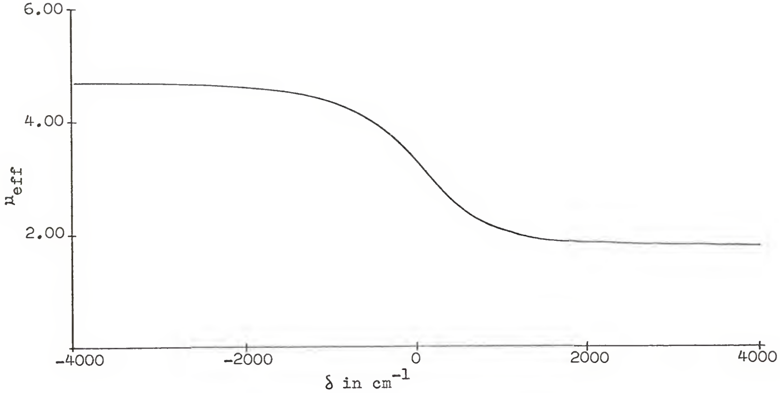

Fig. 8.-Room-temperature magnetic moment vs δ.

TABLE 4

INDIVIDUAL PERCENTAGE CONTRIBUTIONS OF THE FIVE LEVELS TO χ

		δ in cm^{-1}								
		4000	3000	2000	1000	0	-1000	-2000	-3000	-4000
	E'	...	...	...	...	8.6	95.5	97.7	98.2	98.3
	U'	100.0	100.0	100.0	100.0	91.4	4.7	2.3	1.8	1.7
T=100°	U'	...	...	...	...	...	-0.2	...	...	...
	E"	...	...	...	...	...	...	...	...	...
	U'	...	...	...	...	...	...	...	...	...
	E'	...	...	...	5.7	39.5	102.6	98.9	98.8	98.7
	U'	100.0	100.0	100.0	94.5	61.4	2.3	4.3	2.9	2.3
T=300°	U'	...	...	...	...	...	-3.5	-0.9	1.2	2.6
	E"	...	...	...	...	...	-1.4	-2.3	-2.9	-3.6
	U'	...	...	...	...	...	...	...	...	...
	E'	...	0.1	4.4	32.9	53.8	122.0	112.0	111.0	110.0
	U'	100.0	99.9	96.0	70.5	54.8	-5.0	0.7	-1.8	-2.8
T=500°	U'	...	...	-0.3	-2.5	-5.2	-10.5	-3.4	3.0	7.3
	E"	...	...	-0.1	-0.6	-3.4	-6.5	-9.3	-12.2	-14.9
	U'	...	...	...	-0.3	...	...	...	...	...

in energy due to the second-order Zeeman effect for a particular level is primarily the result of mixing of the magnetic states from a level of lower energy, then the denominator on the right of equation (41) determines that $E^{(2)}$, and hence W_2, will be positive.

It is evident from Table 4 that the contributions to χ from excited energy levels due to a Boltzmann distribution are significant, at least in the vicinity of the cross-over point. For example, at a δ value of zero and a temperature of 300°K, the E' level, lying approximately 190cm^{-1} above the U' ground level, contributes 39.5 per cent to the overall susceptibility. At a δ value of $+1000\text{cm}^{-1}$ where the energy separation is about 900cm^{-1}, the contribution from E' has dropped to 5.7 per cent.

Although the mathematical model thus far presented affords an explanation of the existence of intermediate magnetic moments, it does not lead to susceptibility curves containing maxima and minima as are observed experimentally (Figures 1 and 2). In order to extend the theory further, in the hope of resolving the problem while remaining within the formalism already developed, it is necessary to examine some of the assumptions inherent in the calculations.

The curves of Figure 7 were calculated for constant values of δ. However, it is unreasonable to presume that δ remains constant over a large temperature range, and in fact it is much more logical to expect the crystal-field potential to be a function of temperature. As the temperature of the sample increases, the populations of the various excited vibrational levels are increased. An harmonicity of the vibrations would thereby increase the average ligand-metal distance, and hence decrease the potential around the metal ion [64]. Such shifts in Δ (and thus δ) should be observable in the vibrational spectra of transition-metal complexes, and this has apparently been observed for some ions [65]. Also, in an EPR study of anomalous cobalt(II) complexes [54], data are presented which strongly indicate that δ is very temperature dependent.

To determine the dependence of δ on T from first principles would require an intimate knowledge of both inter- and intra-molecular interactions as well as their interdependence, internuclear separations, and in general, detailed information which is not presently available and which can be obtained only by rather lengthy and involved experiments. It was therefore decided to assume a general equation for δ as a function of temperature of the form

$$\delta = \delta_0 + aT + bT^2 + cT^3 \qquad (44)$$

The coefficients were chosen such that the overall shift in δ over a 400°K temperature range would be on the order of 1200cm^{-1} at a maximum. Shifts in the optical spectra of some crystalline hydrated transition-metal ions have been observed to be 200 to 500cm^{-1} over a 200°K temperature range [65]. The cobalt(II) salt studied was $CoSO_4 \cdot 7H_2O$, for which a rather large shift of the absorption assigned to a superposition of $T_1(^4F) \rightarrow T_1(^4P)$ and $T_1(^4F) \rightarrow A_2(^4F)$ transitions was observed. A shift of 500cm^{-1} for this band would correspond to a change of crystal-field potential of approximately 600cm^{-1} (maximum). Over a 400°K range, one might therefore expect a shift upward of 1200cm^{-1}.

With the above criterion in mind, various values for the coefficients a, b, and c were selected. By varying δ_0, the value of δ at 0°K, and embodying equation (44) into the computation of χ, curves such as those shown in Figure 9 were produced. The values of δ_0 and the coefficients for each curve of Figure 9 are given in Table 5. In general, reducing the value of a, b, or c, results in a broadening of the curves and a shift of the maximum toward higher reciprocal susceptibility and higher temperatures. Also, as would be expected, the lower the value of δ_0, the lower the temperature at which the maximum appears. There are innumerable values, and combinations of values, which can be used for δ_0 and the coefficients. The curves depicted in Figure 9 are intended only to indicate that it is possible to explain the general structure of the experimental $\chi^{-1}(T)$ curves by allowing the crystal-field potential

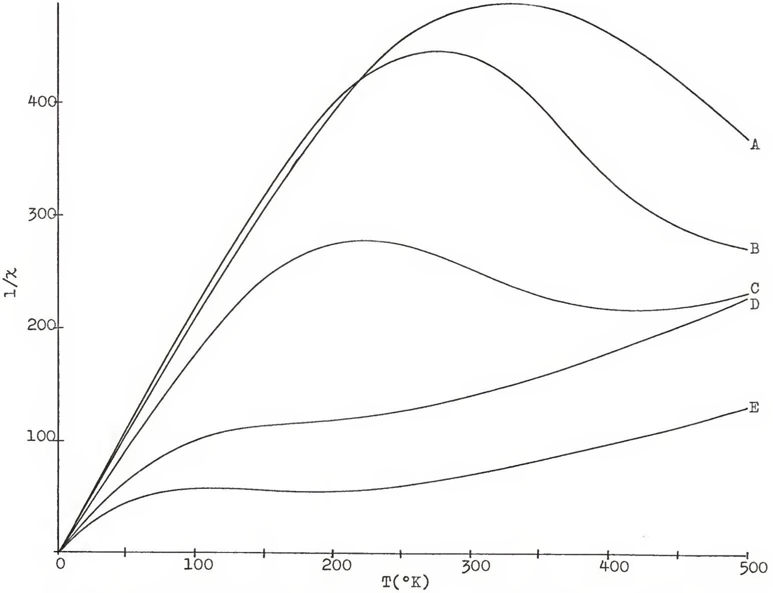

Fig. 9.- χ^{-1} vs T with $\delta = f(T)$. Parameters for curves given in Table 5.

TABLE 5

PARAMETERS OF EQUATION (44) USED TO CALCULATE THE CURVES OF FIGURE 9

Curve	δ_o	a	b	c
A	1000	-2.0	$+8.0 \times 10^{-3}$	-1.4×10^{-5}
B	1000	0	-3.0×10^{-3}	-4×10^{-6}
C	500	0	-3.0×10^{-3}	-4×10^{-6}
D	100	-2.0	0	0
E	500	-6.0	0	$+1.0 \times 10^{-5}$

to be a function of temperature. A reasonable fit for all experimental curves can be obtained by varying the four parameters.

Ewald, Martin, Ross, and White [50] have attempted to explain anomalous $\chi^{-1}(T)$ behavior in iron(III) complexes using arguments not too different from those used herein for cobalt(II) complexes. Iron(III) is a d^5 ion, and the Tanabe and Sugano diagram [58] for a d^5 system is shown in Figure 10. Ewald et al. restrict themselves to a discussion of only the $^2T_2$ and $^6A_1$ terms in the vicinity of the cross-over point, although it may be argued that the $^4T_1$, being only about 7000cm^{-1} higher in energy at the cross-over point, will have a significant effect on the form of the $^2T_2$ and $^6A_1$ terms.

These authors include spin-orbit coupling within $^2T_2$, but do not take into account possible mixing of levels between terms. The $^2T_2$ term splits into two levels, an E" and a U'. The $^6A_1$ does not split, but does transform under octahedral symmetry as degenerate E" and U' levels. Thus, there should be considerable mixing of levels which Ewald et al. failed to take into consideration. It should also be remarked that both the higher-energy $^4T_1$ and $^4T_2$ terms contain an E" and a U' capable of interaction with both the $^2T_2$ and $^6A_1$.

Because of the above assumptions, Ewald et al. were able to use the equations of Kotani [66], wherein J remains

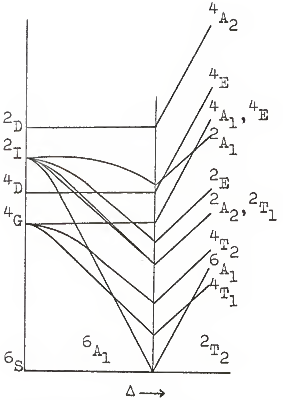

Fig. 10. Energy level diagram for a d^5 ion in an octahedral field.

a good quantum number and second-order Zeeman interactions are confined to magnetic states arising from different levels within a single term. Their equation is

$$\mu^2 = \frac{3/4g^2 + 105e^{-(1+E/\zeta)x} + 8x^{-1}[1-e^{-3x/2}]}{1 + 2e^{-3x/2} + 3e^{-(1+E/\zeta)x}} \qquad (45)$$

where $x = \zeta/kT$, and E is the difference in energy between the $^6A_1$ and $^2T_2$ terms, being completely equivalent to δ of this dissertation. This equation encompasses the contributions from the two levels of $^2T_2$ arising from spin-orbit coupling, and the single level of $^6A_1$. These are in the ratio

$$2 : 4e^{-3x/2} : 6e^{-(1+E/\zeta)x} \qquad (46)$$

The calculations yielded a series of curves for various values of the $^2T_2$-$^6A_1$ energy separation, somewhat analogous to the curves for the d^7 system presented in Figure 7. Due to the nature of the approximations used, the Lande splitting factor g was an independent parameter. The calculations for the d^7 system inherently included the splittings of the magnetic states as a function of δ, and no further adjustment of g was necessary.

The curves of Ewald et al. do show considerable curvature and, somewhat surprisingly, do contain maxima and minima, but, as in the cobalt(II) case, do not resemble the experimental curves, the maxima and minima appearing at too low values of the temperature. They propose that the main reason for the failure of their simplified model to quantitatively yield results consistent with experimental data is an expected difference between the metal-ligand vibration frequencies of the $^2T_2$ and $^6A_1$ terms. It is asserted that the metal-ligand stretching and bending frequencies should be considerably lower in the $^6A_1$ term than in $^2T_2$. As a result, the vibrational partition functions will be different for the two terms, and Ewald *et al*. take this into account by multiplying the contribution of the $^6A_1$ term to the magnetic moment by the ratio of the partition functions, Q_a/Q_t, altering the ratios of (46) to

$$2 : 4e^{-3x/2} : 6(Q_a/Q_t)e^{-(1+E/\zeta)x}$$

where the subscripts a and t refer to the $^6A_1$ and $^2T_2$ terms. Then, for further simplification, this ratio is set equal to a constant, c. By using various values for this constant, the maxima and minima of their basic curves are shifted toward higher temperatures, and they find it possible to approximate their experimental curves. Unfortunately, they do not give values for this constant which must be used to obtain a fit, or justify the magnitude required.

If one examines the curves of Figure 7, it is evident that from a mathematical point of view, any factor which increases the proportion or importance of high-spin levels mixed into the ground level as the temperature increases, will accentuate the curvature already present even to the point of developing maxima and minima. This is essentially what reducing δ with increasing temperature accomplished for the d^7 model presented in this dissertation. It is also the reason that the original simplified curves of Ewald et al. contain maxima and minima. As was previously mentioned, part of the curvature of the plots of Figure 7 is due to the Boltzmann factor whereby higher levels become more populated with increasing temperature. For the d^5 system, this means that a sextet level is becoming increasingly more important with respect to a doublet, whereas in d^7 it is a quartet level over a doublet. It is because the sextet level of d^5 is able to exert a greater influence on the magnetic moment than can the comparable quartet level of d^7, that maxima and minima appear for the d^5 case and not for the d^7 case. The possibility of maxima and minima being produced this way was first expressed by Guha in 1963 [67].

The basis for the direction in which Ewald et al. proceeded is the very pertinent observation that the Tanabe and Sugano diagrams represent electronic energy differences, and calculations should be based on total molecular energies, including vibrational contributions. However, as noted, only differences in vibrational frequencies between the various terms will have any effect on the relative energies. Differences arise from changes in force constants, both stretching and bending, from one term to another, and force constants are functions of the shape of the potential energy curves. Ewald et al. present some highly qualitative potential energy curves "...calculated on the basis of a trivial generalization of a treatment given by Jorgensen (1957) of the $Mn(H_2O)_6^{2+}$ ion."[+] And, although these curves do have different shapes for the $^2T_2$ and $^6A_1$ terms, Ewald et al. inexplicably stress the differences in the equilibrium metal-ligand distance for the two term states for the ion which, to a first approximation, will have no effect on the vibrational partition functions. Nevertheless, their main point is valid, and for completeness the d^7 system should be examined using their model.

To apply the Ewald model to the d^7 system, it is necessary to simplify the original calculations so as not to include mixing of levels under spin-orbit coupling. If the high-spin contribution is to be weighted because of differences in vibrational partition functions, this simplification will allow such a modification to be applied easily, whereas if mixing is included, the determination of the amount each level is to be weighted becomes unduly complicated.

[+] From p. 357 of [50]. The Jorgensen reference is Acta. Chem. Scand., 11, 53(1957).

The equation used to calculate μ^2 for the d^7 system has been derived by Griffith [68] and is

$$\begin{aligned}\mu^2 = \{&c[300(x+5) + 6(45x-88)e^{-x/2} + 12(35x-81)e^{-4x/3}] \\ &+ 150xe^{-(\delta/\zeta\ -1/8)x}\}/\{c[25x(1+2e^{-x/2} + 3e^{-4x/3})] \\ &+ 50xe^{-(\delta/\zeta\ -1/8)x}\}\end{aligned} \tag{47}$$

where c is the weighting factor for the ${}^4T_1$ contribution. From equation (20)

$$\chi^{-1} = \frac{3kT}{N\beta^2\mu^2}, \tag{48}$$

and setting c equal to unity, curves at various values of δ/ζ are produced as shown in Figure 11.

If one compares the curves of Figure 11 with those of Figure 7, it is apparent that to the left of the cross-over point there is little difference; but, to the right of the cross-over point ($\delta > 0$), the range of δ in which are produced curves intermediate between low-spin and high-spin behavior is considerably smaller for the Ewald model. This is simply a consequence of neglecting mixing under spin-orbit coupling.

In Figure 12 are presented some representative curves derived from the curves of Figure 11 by using a weighting factor. As would be expected, the variation in shape is not as diverse as for the curves of Figure 9. Nevertheless, the curves presented in both Figures 9 and 12 indicate that

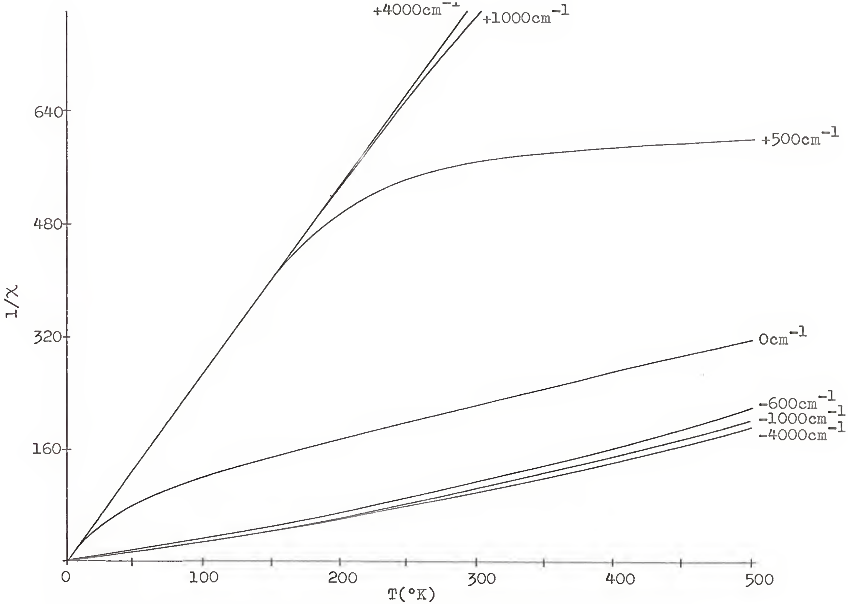

Fig. 11.- χ^{-1} vs T calculated by the Ewald model for values of δ with $\overline{c} = 1$.

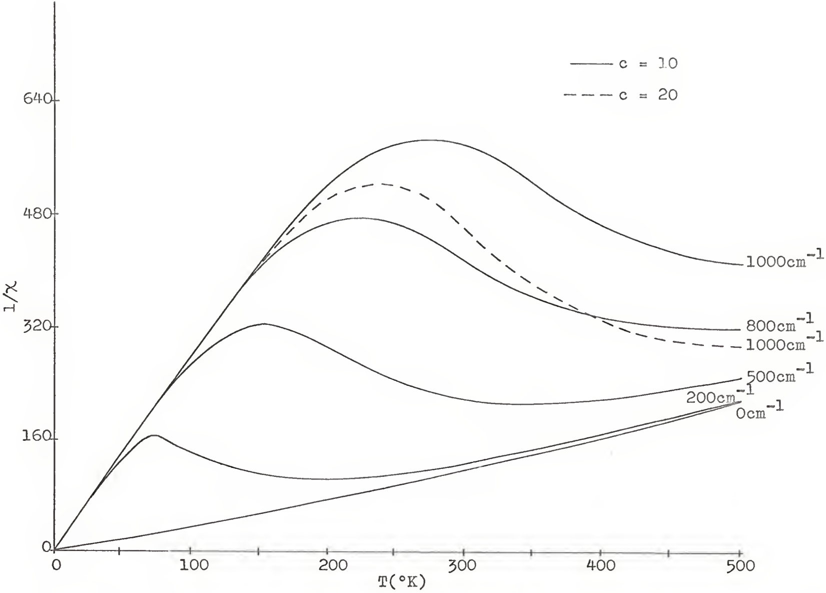

Fig. 12.- χ^{-1} vs T calculated by the Ewald model for values of δ with c = 10 and c = 20.

there are at least two distinct modifications to the basic theoretical model, each of which will allow reasonable fitting of the experimental curves. It would be advantageous at this point to attempt at least a qualitative examination of the Ewald model and examine the pertinent factors therein.

The major criticism which can be leveled at the Ewald model is its inherent necessity for simplifying assumptions. The inclusion of mixing of levels under spin-orbit coupling would, admittedly, severely complicate the computations, but its neglect serves to limit their usefulness. Exactly of what magnitude are these differences cannot be determined from knowledge presently at hand; this is also the stumbling block to determining exactly how δ is a function of temperature. Ewald et al. do make an attempt to derive values for their constant c in a semiquantitative fashion, although again, the necessity for simplifying assumptions puts the results in serious doubt. Briefly, their arguments are as follows.

An equilibrium constant, K_1, is defined as the ratio of the populations in the $^6A_1$ level and the lower, doubly degenerate component of $^2T_2$, that is,

$$K_1 = \frac{2}{6(Q_a/Q_t)e^{-(E+\xi)/kT}} , \qquad (49)$$

and thus

$$\ln \tfrac{1}{3} K_1 = \ln(Q_a/Q_t) - (E+ \zeta)/kT \qquad (50)$$

If Q_a/Q_t is constant, then a plot of log K_1 versus T^{-1} will be a straight line. They state that by assuming values for g and ζ, the relative populations of the two levels of $^2T_2$ are established, and then experimental values of μ^2 are used to calculate apparent values of K_1. By varying g and ζ, it is possible to get straight line relationships between log K_1 and T^{-1}, and from these, c and E can be found within a certain range.

The weakest part of the entire argument is the assumption that the ratio Q_a/Q_t is constant, although these authors do acknowledge that this is an over simplification and attempt to show how the theory could be refined if the ratio were made a function of temperature. This will be examined shortly. By defining K_1 as an equilibrium constant for two levels only, they have essentially reasserted the idea of a two-state equilibrium. At least for the cobalt(II) systems, it has previously been shown that such a simple equilibrium is an inadequate model [47,69], and the multilevel contributions to the susceptibility as reported herein in Table 4 further confirm this.

Ewald et al. examine the Q_a/Q_t ratio as a function of temperature although they do not incorporate their findings into their model. They first limit the contributions to Q_a and Q_t to the six Fe-S stretching and nine

S-Fe-S bending modes, and then assume that for each term, all six stretching modes have the same frequency and all nine bending modes have the same frequency. This assumption of course has no basis in fact, and it is difficult to perceive how their subsequent results can have any meaning. For example, the stretching modes of an XY_6 octahedral molecule will exhibit three independent frequencies (A_{1g}, E_g, and T_{1u}) as will the bending modes (T_{1u}, T_{2g}, and T_{2u}). As an illustration the three stretching frequencies of SeF_6 as given by Nakamoto [70], are 708, 662, and 437cm^{-1} while the bending frequencies are 780, 405, and 260cm^{-1}. Most of the other examples of XY_6 octahedral molecules given by Nakamoto have even more disparate frequencies.

Ewald _et al_. further choose to interpret the Tanabe and Sugano diagrams as including zero-point vibrational energy, and thus any differences in the zero-point vibrational frequencies between the two terms is not included.

It must be concluded that, although the original idea of Ewald _et al_. certainly merits consideration, that is, that there may be significant differences in the total molecular energies of the high-spin and low-spin terms, their subsequent attempt at a semi-theoretical justification involves far too many simplifications to be of use. It is for just this reason that an attempt to determine _a priori_ how δ may be a function of temperature has been avoided in this dissertation.

It is evident from the discussion thus far that at the present level of knowledge, the criterion that the crystal-field potential is a function of temperature stands out as an important factor causing the specific anomalous behavior of the cobalt(II) complexes. It is not unreasonable to suspect that this also applies to the anomalous iron(III) complexes and possibly other anomalous transition metal compounds. However, it is undoubtedly true that there are many contributing factors, some major and some minor, which could play a role in determining magnetic behavior. Ewald *et al*. investigated one of these; other possibilities include the effect of the electronic state on the metal-ligand distance, the effect of covalency, and the effect of distortions from octahedral symmetry.

In a transition from a low-spin to a high-spin term, it has been postulated that there will be an increase in the metal-ligand internuclear distance caused by an electron jumping from a t_2 orbital to an e orbital [71]. As a result, Δ will be different for different levels. However, a recent paper [72] investigating cobalt bond lengths has concluded that the spin state probably has only a very small effect on the metal-ion radius. It is therefore concluded that if differences in radii between the various levels is a factor at all, it is probably a minor one.

All the calculations presented in this work have been based on a simple crystal-field model which does not take into account any covalency which may be present. Evidence has been presented by Fisher and Stoufer [73] which indicates that the strong crystalline field present in these anomalous cobalt(II) compounds is the result of extensive π interaction. This implies a significant amount of covalent bonding. Since magnetic moments arise from orbital and spin angular momenta, it is the effect of covalency on these properties which could limit the usefulness of the calculations. However, a partial covalency due to an admixture of ligand orbitals into the metal-ion wave functions will not change the number of unpaired electrons of a particular level, and hence will not alter the spin angular momentum. Additional orbital angular momentum will not be added, and so the total effect can only be further quenching of the orbital angular momentum associated with the metal ion. This has been partially taken into account by using a value for the spin-orbit coupling constant lower than its free-ion value. Furthermore, the actual magnitude of the crystal-field splitting, which is seriously affected by covalency, does not directly enter the calculations. Hence, although covalency is certainly present in these compounds, it is unlikely that it plays a significant role in determining their specific magnetic behavior.

Another very possible factor which must be considered is distortions from cubic symmetry. For the model presented herein, pure octahedral symmetry has been assumed, although some Jahn-Teller distortion might be expected. However, a study of the structure of the low-spin cobalt(II) compound $K_2Ba[Co(NO_2)_6]$ by Bertrand and Carpenter [74] reveals that the cobalt ion is surrounded by six nitrogens undistorted from octahedral geometry. An EPR study [54] revealed an experimental g value around 2.1 for this compound and also for several of the anomalous compounds listed in Table 1. Also, Van Vleck [75] has shown that if the low symmetry matrix elements are small compared with kT, the average calculated susceptibility will not be very different if such low-symmetry elements are neglected entirely. The experimental values of the susceptibilities of the compounds listed in Table 1 were all taken from solid, microcrystalline materials; no single-crystal measurements have yet been made. Therefore, from an experimental point of view, any anisotropy present has been averaged. Thus, until single-crystal studies are made, the degree to which distortion from octahedral symmetry influences the magnetic behavior remains indeterminate. There is the possibility that such distortions are temperature dependent and this factor has been implicitly allowed for by assuming δ to be a function of temperature.

In a concurrent study of these cobalt(II) systems, Fisher [5] discussed the role played by the non-coordinated anion in influencing magnetic behavior. He found some correlation between anion size and the amount of low-spin character present in the complex. His general conclusion was that different types of crystal packing will have varying effects on the amount of distortion from octahedral symmetry experienced by the complex cation. The important point to be drawn from Fisher's work is that solid state effects are of major importance in determining the magnetic properties of these systems.

The only manner by which more light may be shed on this problem is by further experimental investigation, both in the solid state and solution. One very powerful tool is electron paramagnetic resonance whereby it is possible to investigate individual electronic energy levels. Part II of this dissertation reports just such a study.

PART II

ELECTRON PARAMAGNETIC RESONANCE STUDIES

Introduction

In Part I, theoretical calculations of magnetic susceptibility as a function of temperature were carried out for a d^7 ion in an octahedral field. Using a model involving an equilibrium distribution of magnetic ions over several low-lying electronic levels, and incorporating the hypothesis that the crystal-field potential be a function of temperature, reasonable agreement was achieved between the theoretical calculation and the experimental results of magnetic susceptibility for a group of anomalous cobalt(II) complexes. However, it was concluded that there are undoubtedly several interacting effects influencing the magnetic behavior of these complexes in addition to the temperature dependence of the crystal field, and that further experimental work is necessary to give more explicit direction to the theoretical analysis. One promising experimental technique is electron paramagnetic resonance.

Electron paramagnetic resonance involves transitions between individual magnetic states that are associated with one electronic level, whereas magnetic susceptibility is a weighted average of contributions from all populated levels. Thus, while susceptibility measurements can provide a considerable amount of information concerning the gross molecular structure of a complex, EPR provides a means of studying the characteristics of individual electronic levels.

For the particular anomalous cobalt(II) complexes discussed in Part I, several effects should be observable by EPR if the theoretical model presented is a reasonable description of the molecular structure. First, examination of Table 4 indicates that at certain values of δ, at least the first excited electronic level should be sufficiently populated that distinct transitions involving the magnetic states of both the ground level and first excited level should be observable. Second, if δ is a function of temperature, then the changes in the relative populations of the various levels with temperature would not be fully accountable by the Boltzmann factor. The population of a level is related to the intensity of the EPR signal (*vide infra*). Third, the energy separations between the magnetic states (g values) are functions of δ because of the mixing of levels under spin-orbit coupling and the mixing of states through the second-order Zeeman effect. Thus, the energy of the EPR transitions should be a function of temperature. It is therefore the object of Part II to attempt to observe these three effects for the anomalous cobalt(II) systems.

A previous EPR study of some of these anomalous cobalt(II) complexes by Schmidt, Brey, and Stoufer [54,77] was plagued with considerable instrumental difficulties and arrived at inconclusive results. Only transitions within the ground level were observed; no transitions attributable to an excited level were found. The g values found for the compounds studied were all approximately 2.1, and on this basis the ground level was assigned as the low-spin ^2E. Although the g values were not found to be constant over a wide temperature range, the uncertainty in their value was too large to determine any systematic trend. The approximate population of the ground level was calculated from the average normalized signal intensity of a standard compound, $K_2Ba[Co(NO_2)_6]\cdot H_2O$, which is believed to be sufficiently far to the right of the cross-over point to be considered 100 per cent low-spin. The signal intensities of the anomalous compounds were found to decrease markedly with increasing temperature, indicating a significant decrease in the population of the ground level. By assuming a simple two term, high-spin $\rightleftharpoons$ low-spin equilibrium, and comparing the calculated population decrease with the measured effective magnetic-moment increase over the same temperature range, the researchers were led to conclude that the energy separation between the high-spin and low-spin terms (δ) was decreasing with increasing temperature. However, they qualified their conclusions by stating the belief that there was a large systematic error in the population values which increased with increasing temperature because of broadening of the absorption curve.

In order to quantitatively test the mathematical model established in Part I, it is necessary to calculate the actual energy splittings (g values) of the magnetic states of each of the pertinent levels (see Figure 6) as a function of δ. The usual selection rule for magnetic dipole (EPR) transitions is $\Delta M_J = \pm 1$, but because of mixing of states through the second-order Zeeman effect, it is possible that other transitions will be allowed, and thus it is necessary to calculate transition probabilities for the various states involved. The method and results of these computations are given in the Calculations section.

It is not the purpose of this dissertation to investigate or expound upon the theoretical aspects of electron paramagnetic resonance. Only a brief description of the pertinent concepts will be presented here. For a more complete discourse of EPR theory, the reader is referred to Bersohn and Baird [78] and Pake [79].

The total angular momentum J of a free ion can exist in all possible orientations in the absence of an external field, and there will be no resultant magnetization of a sample. When this ion is placed in a magnetic field, the level will split into 2J+1 magnetic states with energies equal to $Mg\beta H$, where M is the quantum number designating the various spatial orientations of J, g is the experimental splitting factor or the Lande factor, β is the Bohr magneton, and H is the external magnetic field. $Mg\beta$ is the first-order energy coefficient W_1 discussed in Part I. An alternating radiofrequency magnetic field applied at right angles to H will induce magnetic dipole transitions according to the selection rule $\Delta M = \pm 1$. Thus, the energy of the transition will be

$$h\nu = g\beta H \tag{51}$$

where ν is the frequency of absorbed energy and h is Planck's constant. The *a priori* transition probabilities are equal for absorption and emission, but because of a thermal distribution, the state of lower energy has the larger population, and absorption should occur more often than emission. The upper state would soon become saturated, however, and the net absorption would diminish to zero if it were not for radiationless decay whereby the energy is released through vibrational, rotational, or translational motion. This is known as spin-lattice relaxation.

Resonance will occur when the radiofrequency waves have exactly the right amount of energy to excite an electron from one state to another. The instrumental procedure normally followed is to hold the r.f. field constant and sweep the applied magnetic field.

The quantity g is defined by equation (51) and is simply a proportionality constant between the frequency and the field at which resonance occurs. Thus, the location of the maximum in the EPR absorption spectrum yields the g value.

The intensity of an EPR signal is the total energy absorbed by the sample at resonance and is proportional to the area under the absorption curve. It is determined by the frequency used, the concentration of the paramagnetic sample, the power of the applied resonance radiation, the transition probability, and the temperature. For a given sample, the first three factors mentioned will usually remain constant over a wide temperature range, and it is the transition probability and temperature which are important in determining relative areas of any one sample as a function of temperature. The signal intensity is inversely proportional to the absolute temperature. This is proved in Appendix G.

The nucleus of an atom may have a magnetic moment which can influence the magnetic energy of the electron and split each EPR signal into 2I + 1 lines where I represents the angular momentum of the nucleus. Usually this "hyperfine" splitting is observed only at low temperatures where the overall spectral envelope is narrow and resolution is possible.

Experimental

All electron paramagnetic resonance spectra were obtained by using a Varian Associates EPR spectrometer system, V-4502-14. This system consists of a V-4501 console, a V-4500-41A microwave bridge, a V-4560 100Kc field modulation and control unit, a V-3601 twelve-inch magnet, and a V-FR2503 magnet power supply. A V-4531 Multi-purpose cavity was used in conjunction with a variable temperature accessory, V-4557, which includes a V-4540 variable temperature controller. The temperature dial calibration accuracy as specified by Varian Associates is ±3°C. The nominal klystron operating frequency is 9.5 gigacycles with a maximum power output of no less than 300 milliwatts.

The instrument system was standardized with a benzene solution of diphenyl picryl hydrazyl (DPPH), a stable free radical with a known g value of 2.00354 ± 0.00003. With the frequency constant, $h\nu$ is constant, having the same value for both sample and standard. The g value of the sample is then obtained from

$$g_{sample} = g_{std} H_{std} / H_{sample} \qquad (52)$$

where H is the field strength at which resonance occurs. In order to minimize instrumental effects, all spectra were recorded over five-minute sweep times, leakage current was set at 300 milliamps, attenuation at 6 decibels, and field strength at 3100 gauss. Sweep rates were 10,000, 5000, 2500, or 1000 gauss per five minutes. A g_{std} was established for each sweep rate.

Whenever a spectrum was so broad that a reasonable base line could not be established, it was often possible to approximate H as being located one half the distance between the field-strength values at the maximum and minimum of the first derivative curve. Because these peaks are not sharp in a broad spectrum, and because the spectrum need not necessarily be symmetrical, this method is not as accurate as is that which utilizes a true base line.

To obtain an EPR spectrum as a function of temperature, the sample tube is inserted into a quartz dewar which has been previously inserted into the resonance cavity. The temperature is controlled by electrical heaters counteracting a stream of nitrogen gas flowing through the dewar and cooled by having passed through a coil immersed in liquid nitrogen. In addition, room-temperature dry nitrogen gas is allowed to flow through the cavity to prevent condensation.

All samples used, with the exception of the tris(o-phenanthroline)cobalt(II) perchlorate, were supplied by Harold M. Fisher. The o-phenanthroline salt was supplied by Dr. R. C. Stoufer.

Calculations

The method of calculating the W_1 and W_2 coefficients of the energy expansion of equation (7) has been presented in Part I. The W_1 term represents the diagonal elements of the z component of the magnetic Hamiltonian matrix, and W_2 is a function of the off-diagonal elements. To calculate the energies of the magnetic states, it is necessary to diagonalize this matrix. The resultant eigenvalues will be designated by W', and the energies will be W'H. The functions belonging to these eigenvalues will be designated $|\Gamma "M"\rangle$. The energies will also be expressible as M"gβH, and the energy splittings given by

$$\Delta M''g = \Delta W' \tag{53}$$

if W' is expressed in units of β. Since there is extensive mixing of states through the second-order Zeeman mechanism, ΔM" is not necessarily restricted to ±1. However, if g is taken to be an experimental quantity, ΔM" may be assumed to be included in it, and therefore

$$g = \Delta W' \ . \tag{54}$$

The computer program developed for the computations of Part I calculates the elements of the z component of the magnetic Hamiltonian matrix as a function of δ. By diagonalizing the matrix, the W' values are obtained as a function of δ.

The allowed EPR transitions are proportional to

$$P_\epsilon = \left| \left\langle \Gamma''_i M''_i \middle| \underset{\sim}{L}_\epsilon + 2\underset{\sim}{S}_\epsilon \middle| \Gamma''_j M''_j \right\rangle \right|^2 \qquad (55)$$

for transitions between states i and j where ϵ represents the component along the direction of the magnetic vector of the incident radiation [59]. The $|\Gamma''M''\rangle$ functions are diagonal for $\epsilon = z$, and since x and y are equivalent in an octahedral field, it is only necessary to calculate P_x.

To find the eigenvalues of L_x and S_x, use is made of the raising and lowering operators,

$$\begin{aligned} \underset{\sim}{L}^+ &= \underset{\sim}{L}_x + i\underset{\sim}{L}_y \\ \underset{\sim}{L}^- &= \underset{\sim}{L}_x - i\underset{\sim}{L}_y \end{aligned} \qquad (56)$$

where

$$\begin{aligned} \underset{\sim}{L}^+|LM\rangle &= [L(L+1) - M(M+1)]^{1/2}|\underset{\sim}{L}M{+}1\rangle \\ \underset{\sim}{L}^-|LM\rangle &= [L(L+1) - M(M-1)]^{1/2}|\underset{\sim}{L}M{-}1\rangle \end{aligned}$$

$$(57)$$

The equations for $\underset{\sim}{S}^+$ and $\underset{\sim}{S}^-$ are analogous. Adding the two equations of (56), and rearranging,

$$\underset{\sim}{L}_x = 1/2(\underset{\sim}{L}^+ + \underset{\sim}{L}^-) , \qquad (58)$$

and similarly

$$2\underset{\sim}{S}_x = \underset{\sim}{S}^+ + \underset{\sim}{S}^- . \qquad (59)$$

Calling the $|\Gamma''M''\rangle$ functions Λ, each is a linear combination of four Ψ functions where Ψ represents the $|\Gamma'M'\rangle$ functions determined in Part I. More specifically,

$$\Lambda^{j}{}_{b} = b^{j}{}_{1}\,\Psi^{\kappa}_{1} + b^{j}{}_{2}\,\Psi^{\kappa}_{2} + b^{j}{}_{3}\,\Psi^{\kappa}_{3} + b^{j}{}_{4}\,\Psi^{\rho''}_{5}$$

$$\Lambda^{j}{}_{c} = c^{j}{}_{1}\,\Psi^{\lambda}_{1} + c^{j}{}_{2}\,\Psi^{\lambda}_{2} + c^{j}{}_{3}\,\Psi^{\lambda}_{3} + c^{j}{}_{4}\,\Psi^{\alpha'}_{4}$$

$$\Lambda^{j}{}_{d} = d^{j}{}_{1}\,\Psi^{\nu}_{1} + d^{j}{}_{2}\,\Psi^{\lambda}_{2} + d^{j}{}_{3}\,\Psi^{\nu}_{3} + d^{j}{}_{4}\,\Psi^{\rho'}_{4}$$

$$\Lambda^{j}{}_{e} = e^{j}{}_{1}\,\Psi^{\mu}_{1} + e^{j}{}_{2}\,\Psi^{\mu}_{2} + e^{j}{}_{3}\,\Psi^{\mu}_{3} + e^{j}{}_{4}\,\Psi^{\alpha''}_{5}$$

The Ψ's are linear combinations of the ϕ functions as described in Part I, and the ϕ's are given in terms of the single-electron functions in Appendix E. The coefficients for the various linear combinations are available from the diagonalization process, and so it is only necessary to obtain the eigenvalues belonging to $\underset{\sim}{L}_x + 2\underset{\sim}{S}_x$ for the ten single-electron functions of the d subshell. The eigenvalues are given in Table F3 of Appendix F.

In general,

$$P_x = \Big| \sum_{i=j} \alpha_i \alpha_j \left\langle \phi_i \middle| L_x + 2S_x \middle| \phi_j \right\rangle \Big|^2 \qquad (60)$$

where α encompasses all coefficients. The values for the integrals are presented in Table 6.

The g values and transition probability numbers (equation (55) yields only values proportional to transition probabilities) have been calculated for the E' and lowest U' levels as a function of δ by means of the computer program listed in Appendix I2. The other levels would not be

TABLE 6

EIGENVALUES FOR $\langle \phi_i | \underset{\sim}{L}_x + 2\underset{\sim}{S}_x | \phi_j \rangle$

	ϕ_1^{κ}	ϕ_1^{λ}	ϕ_1^{μ}	ϕ_1^{ν}
ϕ_1^{κ}	0	0	0	-1
ϕ_1^{λ}	0	0	-1	0
ϕ_1^{μ}	0	-1	0	0
ϕ_1^{ν}	-1	0	0	0

$$\langle \phi_1 | \underset{\sim}{L}_x + 2\underset{\sim}{S}_x | \phi_2 \rangle = 0$$

$$\langle \phi_1 | \underset{\sim}{L}_x + 2\underset{\sim}{S}_x | \phi_3 \rangle = 0$$

$$\langle \phi_1 | \underset{\sim}{L}_x + 2\underset{\sim}{S}_x | \phi_4 \rangle = 0$$

$$\langle \phi_1 | \underset{\sim}{L}_x + 2\underset{\sim}{S}_x | \phi_5 \rangle = 0$$

Table 6 (cont'd)

	ϕ_2^κ	ϕ_2^λ	ϕ_2^μ	ϕ_2^ν
ϕ_2^κ	0	$\frac{3}{5}\sqrt{3}$	0	0
ϕ_2^λ	$\frac{3}{5}\sqrt{3}$	0	$\frac{6}{5}$	0
ϕ_2^μ	0	$\frac{6}{5}$	0	$\frac{3}{5}\sqrt{3}$
ϕ_2^ν	0	0	$\frac{3}{5}\sqrt{3}$	0

	ϕ_2^κ	ϕ_2^λ	ϕ_2^μ	ϕ_2^ν
ϕ_3^κ	0	$\frac{3}{10}\sqrt{3}$	0	$-\frac{3}{2}$
ϕ_3^λ	$\frac{3}{10}\sqrt{3}$	0	$-\frac{9}{10}$	0
ϕ_3^μ	0	$-\frac{9}{10}$	0	$\frac{3}{10}\sqrt{3}$
ϕ_3^ν	$-\frac{3}{2}$	0	$\frac{3}{10}\sqrt{3}$	0

Table 6 (cont'd)

	ϕ_2^{κ}	ϕ_2^{λ}	ϕ_2^{μ}	ϕ_2^{ν}
$\phi_4^{\alpha'}$	$-\frac{1}{2}\sqrt{15}$	0	$\frac{1}{2}\sqrt{5}$	0
$\phi_4^{\beta'}$	0	$-\frac{1}{2}\sqrt{5}$	0	$\frac{1}{2}\sqrt{15}$
$\phi_5^{\alpha''}$	$-\frac{3}{10}\sqrt{5}$	0	$-\frac{3}{10}\sqrt{5}$	0
$\phi_5^{\beta''}$	0	$\frac{3}{10}\sqrt{15}$	0	$\frac{3}{10}\sqrt{5}$

	ϕ_3^{κ}	ϕ_3^{λ}	ϕ_3^{μ}	ϕ_3^{ν}
ϕ_3^{κ}	0	$-\frac{4}{15}\sqrt{3}$	0	$-\frac{2}{3}$
ϕ_3^{λ}	$-\frac{4}{15}\sqrt{3}$	0	$-\frac{6}{5}$	0
ϕ_3^{μ}	0	$-\frac{6}{5}$	0	$-\frac{4}{15}\sqrt{3}$
ϕ_3^{ν}	$-\frac{2}{3}$	0	$-\frac{4}{15}\sqrt{3}$	0

Table 6 (cont'd)

	ϕ_3^{κ}	ϕ_3^{λ}	ϕ_3^{μ}	ϕ_3^{ν}
$\phi_4^{\alpha'}$	0	0	0	0
$\phi_4^{\beta'}$	0	0	0	0
$\phi_5^{\alpha''}$	$\frac{4}{15}\sqrt{5}$	0	$\frac{4}{15}\sqrt{15}$	0
$\phi_5^{\beta''}$	0	$-\frac{4}{15}\sqrt{15}$	0	$-\frac{4}{15}\sqrt{5}$

	$\phi_4^{\alpha'}$	$\phi_4^{\beta'}$	$\phi_5^{\alpha''}$	$\phi_5^{\beta''}$
$\phi_4^{\alpha'}$	0	2	0	0
$\phi_4^{\beta'}$	2	0	0	0
$\phi_5^{\alpha''}$	0	0	0	$-\frac{2}{3}$
$\phi_5^{\beta''}$	0	0	$-\frac{2}{3}$	0

sufficiently populated at reasonable temperatures to give an observable EPR signal.

For the E' level, the calculations yield an essentially constant g value of 4.000 and a transition probability number of 324. The transition is between the states $\Lambda^4{}_c$ and $\Lambda^4{}_d$.

There are four transitions with a finite probability within the U' levels, $\Lambda_b \rightleftarrows \Lambda_c$, $\Lambda_b \rightleftarrows \Lambda_e$, $\Lambda_c \rightleftarrows \Lambda_d$, and $\Lambda_d \rightleftarrows \Lambda_e$. The g values and transition probability numbers for these transitions within the U' ground level are presented in Table 7 for δ values from 3000cm^{-1} to -2000cm^{-1}. For δ values larger than 400cm^{-1}, the transition probabilities for the $\Lambda_b \rightleftarrows \Lambda_c$ and $\Lambda_d \rightleftarrows \Lambda_e$ transitions become negligible relative to the $\Lambda_b \rightleftarrows \Lambda_e$ and $\Lambda_c \rightleftarrows \Lambda_d$ transitions. The variations in the g values for all the transitions as a function of δ are readily understood by an examination of Figure 13 where the splittings of the magnetic states of the lowest U' level have been plotted as a function of δ. From the cross-over point to large values of δ, the four magnetic states tend to merge into two doubly degenerate states with a splitting corresponding to a g value of 2.0 as is expected for an essentially pure U'(^{2}E) level (see Table 3a). To the left of the cross-over point, however, the extensive mixing of states results in considerable variation in the energies of the states. Even

TABLE 7

EPR g VALUES AND TRANSITION PROBABILITY NUMBERS FOR TRANSITIONS OF THE LOWEST U'

	$\Lambda_b \rightleftarrows \Lambda_e$		$\Lambda_c \rightleftarrows \Lambda_d$		$\Lambda_b \rightleftarrows \Lambda_c$		$\Lambda_d \rightleftarrows \Lambda_e$	
δ in cm^{-1}	g	P_x	g	P_x	g	P_x	g	P_x
3000	2.033	1.041	2.044	1.036				
2800	2.037	1.047	2.050	1.040				
2600	2.041	1.053	2.057	1.045				
2400	2.046	1.062	2.065	1.052				
2200	2.052	1.072	2.076	1.059				
2000	2.060	1.084	2.090	1.068				
1800	2.068	1.100	2.107	1.079				
1600	2.079	1.120	2.129	1.093				
1400	2.091	1.146	2.158	1.110				
1200	2.105	1.181	2.197	1.132				
1000	2.121	1.229	2.249	1.159				
800	2.138	1.293	2.320	1.192				
600	2.152	1.382	2.418	1.230				
400	2.156	1.506	2.554	1.272	2.354	0.008	2.356	0.007
200	2.136	1.676	2.740	1.307	2.436	0.018	2.439	0.016
0	2.061	1.898	2.987	1.313	2.521	0.043	2.527	0.037
- 200	1.884	2.161	3.292	1.244	2.578	0.109	2.598	0.078
- 400	1.540	2.407	3.649	0.011	2.306	1.302	2.882	0.107
- 600	0.977	2.513	3.901	0.712	2.481	0.293	2.397	0.526
- 800	0.232	2.357	4.017	0.342	2.162	0.563	2.087	0.790
-1000	0.555	1.973	3.931	0.078	1.725	0.824	1.651	1.071
-1200	1.239	1.524	3.706	0.001	1.268	1.019	1.199	1.280
-1400	1.765	1.138	3.433	0.055	0.865	1.137	0.803	1.402
-1600	2.148	0.848	3.172	0.169				
-1800	2.425	0.641	2.944	0.296				
-2000	2.627	0.495	2.751	0.415				

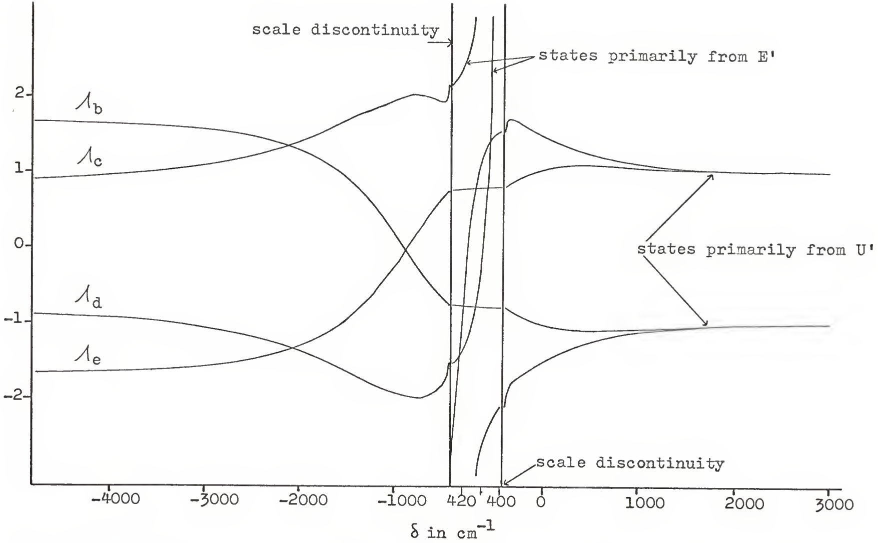

Fig. 13.-Splittings of magnetic states of lowest U' as a function of δ, with cross-over of E' states.

at $\delta = -5000\text{cm}^{-1}$, the states have not yet achieved the splittings corresponding to the g value of 1.2 for a pure $3/2U'(^4T_1)$ level.

In Figure 13, the region in the vicinity of $\delta = -410\text{cm}^{-1}$ has been enlarged in order to illustrate the interaction between the Λ_c and Λ_d states of the U' with the Λ_c and Λ_d states of the E'.

Results

The electronic paramagnetic resonance spectra of five microcrystalline terpyridine derivatives of cobalt(II) have been obtained as a function of temperature. All five show strong resonance absorptions corresponding to g values in the range 2.05 to 2.23. In addition, at low temperatures these compounds also give a second resonance absorption with g values all approximately 4.25. This secondary absorption is some 1800 times weaker than the primary one. The signal intensities for the primary absorptions were obtained for all five compounds, but only for $[Co(terpy)_2]SO_4 \cdot 2H_2O$ could the signal intensities for the secondary absorption be obtained. This is due to lack of resolution for the other four compounds. The g values and intensities are tabulated in Tables 8-12. Two typical spectra (sulfate at 193°K) are shown in Figures 14 and 15.

TABLE 8

THE TEMPERATURE DEPENDENCE OF THE EPR SPECTRUM OF $[Co(terpy)_2]SO_4 \cdot 2H_2O$

Temperature °K	U' g Value ±0.005	E' g Value ±0.05	U' Signal Intensity	E' Signal Intensity
93.2	2.063	4.216	4260	2.46
113.2	2.068	4.257	4630	2.49
133.2	2.068	4.216	4740	2.45
153.2	2.069	4.271	4920	2.49
173.2	2.069	4.257	4830	2.49
193.2	2.071	4.229	4850	2.43
213.2	2.070	4.271	4880	2.35
233.2	2.070		4420	
243.2	2.072		3880	
253.2	2.072		3380	
263.2	2.076		2800	
273.2	2.076		2260	
283.2	2.082		1880	
293.2	2.091		1390	
303.2	2.094		1070	

TABLE 9

THE TEMPERATURE DEPENDENCE OF THE EPR SPECTRUM OF $[Co(terpy)_2]Cl_2 \cdot 5H_2O$

Temperature °K	U' g Value ±0.005	E' g Value ±0.05	U' Signal Intensity
93.2	2.093	4.229	1200
113.2	2.090		1220
133.2	2.093		1260
153.2	2.090		1170
173.2	2.100		1010
193.2	2.099		834
213.2	2.104		550
233.2	2.112		353
243.2	2.115		
253.2	2.129		
263.2	2.129		
273.2	2.129		
283.2	2.125		

TABLE 10

THE TEMPERATURE DEPENDENCE OF THE EPR SPECTRUM OF $[Co(terpy)_2](ClO_4)_2 \cdot H_2O$

Temperature °K	U' g Value ±0.005	E' g Value ±0.05	U' Signal Intensity
103.2	2.090	4.257	3850
113.2	2.086	4.257	3850
133.2	2.081		3525
173.2	2.104		1628
193.2	2.111		800
213.2	2.135		
233.2	2.214		
253.2	2.233		
263.2	2.231		

TABLE 11

THE TEMPERATURE DEPENDENCE OF THE EPR SPECTRUM OF $[Co(terpy)_2]I_2 \cdot H_2O$

Temperature °K	U' g Value ±0.005	E' g Value ±0.05	U' Signal Intensity
83.2	2.086	4.257	3090
93.2	2.089	4.271	2770
133.2	2.096		2420
173.2	2.099		1720
213.2	2.114		742
233.2	2.121		
253.2	2.124		
263.2	2.127		
273.2	2.126		
283.2	2.131		

TABLE 12

THE TEMPERATURE DEPENDENCE OF THE EPR SPECTRUM OF $[Co(terpy)_2](NO_3)_2$

Temperature °K	U' g Value ±0.005	E' g Value ±0.05	U' Signal Intensity
93.2	2.103	4.285	3530
103.2	2.101	4.257	3410
113.2	2.102	4.243	3560
133.2	2.100	4.243	3460
153.2	2.104		2990
173.2	2.104		2330
193.2	2.104		1470
213.2	2.113		458
233.2	2.104		
243.2	2.104		

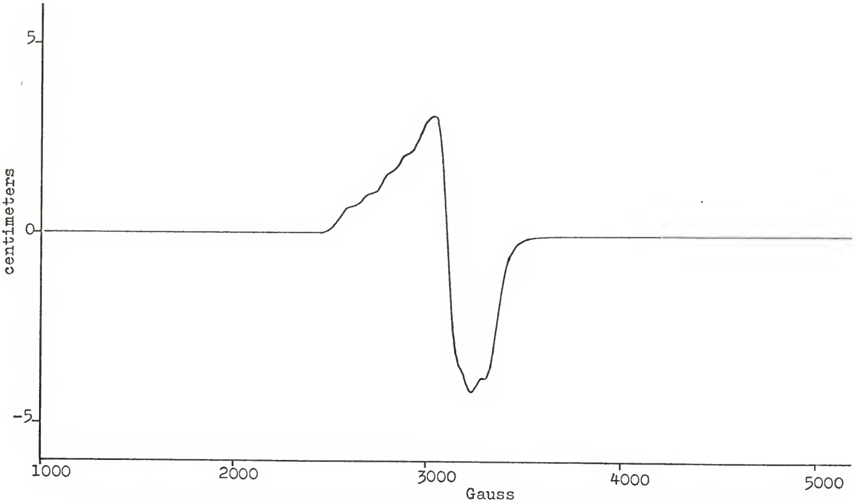

Fig. 14.-EPR spectrum of $[Co(terpy)_2]SO_4 \cdot 2H_2O$ at 193°K. Signal amplitude = 250.

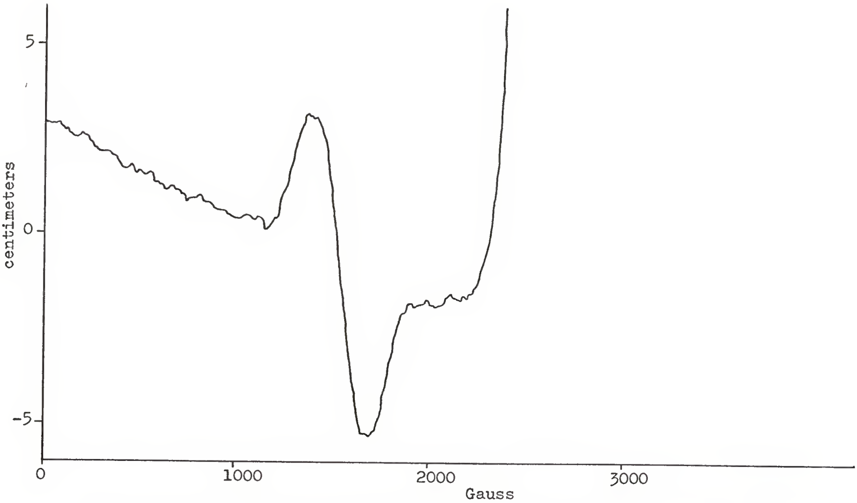

Fig. 15.-EPR spectrum of $[Co(terpy)_2]SO_4 \cdot 2H_2O$ at 193°K. Signal amplitude = 400,000.

The incipient fine structure apparent in Figure 14 is the result of hyperfine interaction. At lower temperatures, this hyperfine splitting becomes further resolved, and eight peaks are observed. This is consistent with a known nuclear spin for cobalt of 7/2.

Spectra for $[Co(o\text{-}phen)_3](ClO_4)_2$ were obtained at 173°, 133°, and 93°K. Again, two resonance absorptions are present. The primary absorption gives such a broad signal that only at 93°K can a reasonable estimate of g be made. It is 4.30 ± 0.1. The secondary absorption appears as a weak signal superimposed upon the primary absorption, and is observed at 173° and 133°K; it is completely hidden at 93°K. The g value at 173°K is 2.03 ± 0.1, and at 133°K is 2.04 ± 0.1. The spectra at 133° and 93°K are shown in Figures 16 and 17.

The general characteristics of the spectra of the terpyridine salts are very broad, weak absorptions at or near room temperature, but with subsequent narrowing and increasing intensity at lower temperatures. A typical broadened spectrum is shown in Figure 18. Instrumental and physical measurement factors lead to an uncertainty in the g values of approximately ± 0.005. Values having uncertainties much larger than this cannot accurately indicate differences between values at two different temperatures, and so have not been reported.

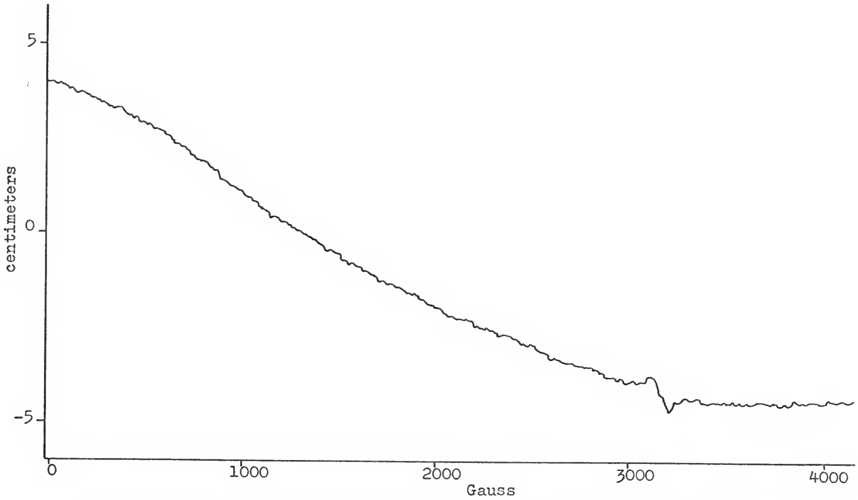

Fig. 16.-EPR spectrum of $[Co(o\text{-}phen)_3](ClO_4)_2$ at 133°K. Signal amplitude = 160,000.

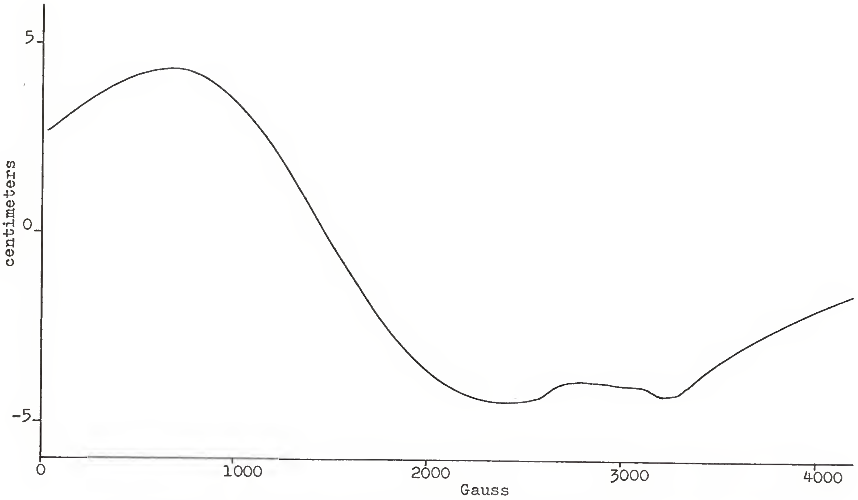

Fig. 17.-EPR spectrum of [Co(o-phen)$_3$](ClO$_4$)$_2$ at 93°K. Signal amplitude = 25,600.

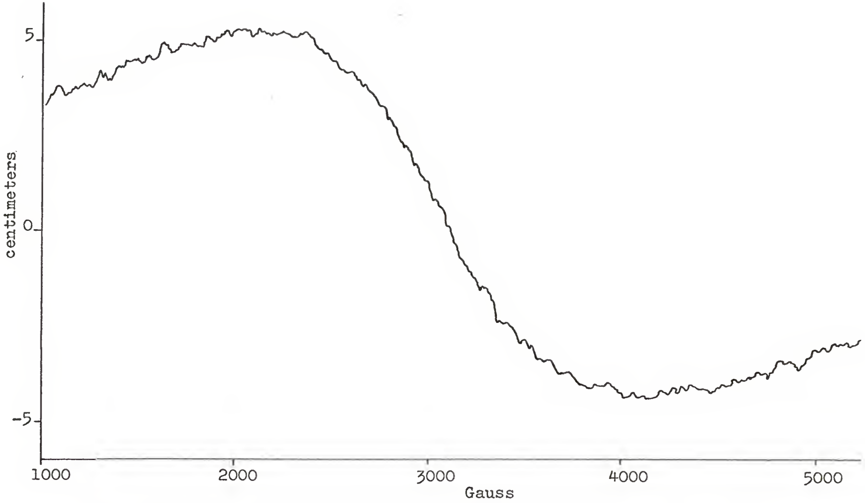

Fig. 18.-EPR spectrum of $[Co(terpy)_2](NO_3)_2$ at 0°K. Signal amplitude = 63,000.

The broadness and necessarily large signal amplification at the higher temperatures decreases the precision of the g values, and only for the sulfate are the spectra narrow enough at the higher temperatures to allow reasonable measurements of signal intensities above 233°K. This results from the electrons being in a chemical environment and interacting magnetically with this environment in a more or less random fashion. As a consequence, the resultant magnetic field experienced by a population of electron spins is not entirely homogeneous, though the applied magnetic field may be. Hence, resonance is achieved over a range of applied field strengths giving a finite width to the EPR absorption curve. Radiationless decay will occur more rapidly at higher temperatures because of increases in vibrational, rotational, and translational energies, and therefore, because of the Heisenberg uncertainty principle, the energy at which resonance occurs will be less certain, and this will lead to a broadening of the spectrum.

Because of differences in sample concentrations, comparisons between the magnitudes of the signal intensities of two different complexes will have no meaning. However, for the sulfate, the intensities for the two resonances are comparable. The numbers given are in arbitrary units. The signal intensities are obtained from measuring the areas under the two halves of the first-derivative curve. The approximate error in measuring these areas is between 5 and 10 per cent.

Discussion

The appearance of two distinct EPR absorptions for the terpyridine complexes confirms the existence of an equilibrium distribution of magnetic ions over at least two electronic levels. Observation of the same phenomenon in the "normal high-spin" o-phenanthroline complex indicates that such an equilibrium may exist in a large number of octahedral cobalt(II) complexes previously thought to be 100 per cent either high-spin or low-spin. The existence of an equilibrium should at least qualitatively establish the proximity of the crystal-field potential of the complex to the cross-over point.

The respective g values of the two absorptions for the terpyridine series leave little doubt that the two levels involved are the E' and the lowest U'. The calculations indicate that a g value of about 2.1 - 2.3 is expected for the U' level to the right of the cross-over point, and this is approximately what has been found. The average g value of 4.25 found for the secondary absorptions is somewhat higher than the 4.000 predicted for the E' level in the strong-field approximation. However, Low reports a g value of 4.2785 for Co^{2+} ions in a MgO single crystal, and assigns this to the E' level [80]. If one calculates the expected g value for the E' level using the weak-field scheme, the value 4.333 is obtained. It is gratifying that the experimental g value is between the theoretical limits of the strong- and weak-field approximations and so near to the value found by Low. One explanation for the discrepancy between 4.25 and 4.00 is the possibility that the transition from the U' to the excited E' level may not be vertical. This could arise because of a difference in the metal-ligand internuclear distance between the U' and E' levels, and thus the value of Δ, and hence δ, would be different for the different ions of the two levels. The possibility of this was mentioned in the Discussion of Part I. The E' level, arising wholly from the $^4T_1$ term, would be expected to have a δ value less than the one for the U' level which, to the right of the cross-over point, arises predominately from the ^2E term. The applicability of the strong-field scheme is uncertain to the left of the cross-over point, and it is not unreasonable that calculations designed to consider systems to the right of the cross-over point may begin to break down.

The ground level of the o-phenanthroline complex is the E' level, and the g value found of 4.3 ± 0.1 is consistent with this, and consistent with a weak-field formulation. The first excited level is a U', presumably predominately $3/2U'(^4T_1)$ if a vertical transition is assumed. The g value of 2.0 ± 0.1 is not consistent with a pure 3/2U' level in either the weak-field or strong-field scheme; the weak-field g value is 1.067 [81] and the strong-field g value is 1.2. However, as shown in Figure 13, mixing of states is significant to a far greater degree and over a far larger range of δ to the left of the cross-over point than to the right of the cross-over point; the value of 2.0 gives no indication of the location of the transition in terms of δ.

With the exception of the nitrate, the terpyridine salts show a shift in g value with temperature for the primary absorption, the g values decreasing with decreasing temperature. Close examination of Tables 8-11 reveals that the largest differential occurs at the higher temperatures. For example, the sulfate g value drops 0.022 units from 303° to 243°, but only 0.009 units from 243° to 93°; the chloride g value drops 0.021 units from 283° to 213°, but only 0.011 units from 213° to 93°; the perchlorate g value drops 0.120 units from 263° to 193°, but only 0.021 units from 193° to 103°; and the iodide g value drops 0.32 units from 283° to

173°, but only 0.013 units from 173° to 83°. The corresponding signal intensities increase with decreasing temperature, but again, the largest changes occur at the higher temperatures with an apparent leveling off of the signal intensities at the lower temperatures. This type of behavior is qualitatively what is expected. The shift in g values and signal intensities was predicted on the hypothesis that δ is a function of temperature which would be a result of increasing the population of excited, anharmonic vibrational levels with increasing temperature. The degree of anharmonicity of the vibrational levels is expected to increase with the vibrational quantum number as the potential energy curve deviates more and more from a parabolic shape. Therefore, as the temperature increases, the shift in the equilibrium metal-ligand distance should monotonically increase, and hence the g values and signal intensities should shift to a greater degree at higher temperatures than at lower temperatures.

Examination of Table 7 reveals that to the right of the cross-over point, there are two transitions predicted within the U' level with similar g values and probabilities. Since only one transition is observed experimentally, it is reasonable to expect that it is a composite of the two predicted transitions, and that the resultant g value is an average of the two calculated ones. The transition probability numbers are not too different for the two transitions and are taken to be equal. The effect of these numbers in determining the relative strengths of the two transitions is discussed below and in Appendix H. Table 13 lists the expected g values from $\delta = 0$ to 3000cm^{-1} for an average of the two g values for the $\Lambda_b \approx \Lambda_e$ and $\Lambda_c \approx \Lambda_d$ transitions. The g values for the two transitions are seen to diverge as δ approaches zero, and this effect could be a contributing factor to the broadening of the spectra at higher temperatures.

A quantitative comparison of the experimental and calculated g values would indicate room-temperature values for the terpyridine complexes of between 800 and 2000cm^{-1}. These are somewhat larger than expected from the magnetic susceptibility results, but are at least in semi-quantitative agreement.

Although the shifts in the signal intensities are qualitatively consistent with what is expected, the quantitative aspects are not. As δ decreases from values to the right of the cross-over point to the point where the E' and lowest U' levels are of equal energy, the population of the U' ground level can decrease to 67 per cent of the total population at a maximum. A further decrease would demand that the E' level become the ground level. The

TABLE 13

AVERAGE g VALUES OF $\Lambda_b \rightleftharpoons \Lambda_e$ AND $\Lambda_c \rightleftharpoons \Lambda_d$ TRANSITIONS

in cm^{-1}	g
3000	2.039
2800	2.044
2600	2.049
2400	2.056
2200	2.064
2000	2.075
1800	2.088
1600	2.104
1400	2.125
1200	2.151
1000	2.185
800	2.229
600	2.285
400	2.355
200	2.438
0	2.524

decrease in signal intensity reported for the primary absorption of the terpyridine cases is in every instance larger than 33 per cent. This result is identical to the results reported by Schmidt _et al_. [54] who explained the large decrease in signal intensity to a systematic error in measuring the areas under the spectral curves at the higher temperatures. At these temperatures the spectra are broad and the base lines not easily established. As a result, a large amount of the signal may be lost in the "tails" of the spectra, leading to an erroneously low value for the signal intensity.

The possibility that the E' level becomes the ground level at certain values of temperature is not completely ruled out, although it is highly unlikely that the E' level is much more than a few wave numbers lower than the U' level. At the higher temperatures, the signals are very broad and an EPR absorption due to a transition within the E' level could be hidden beneath the spectral envelope. A distinct possibility is that the presence of this E' absorption is actually contributing to the broadness of the spectra. Spectra for the compound $K_2Ba[Co(NO_2)_6]$, considered to be 100 per cent low-spin, were used as a standard by Schmidt _et al_. No extensive broadening was observed, and the signal intensity remained constant as a function of temperature.

The signal intensity from the E' level might easily be expected to be considerably weaker than the intensity from the U' level, even though they be of comparable energies. The degeneracy of the respective levels favors the U' by a factor of two. Also, within a given sample and assuming apparatus effects caused by different instrument settings are constant, the intensity is proportional to the square of the magnetic field at which resonance is observed [82]. Since the E' resonance is observed at a field strength approximately one-half that at which the U' resonance is observed, the relative signal intensity would be reduced further by a factor of four.

The exact role played by transition probabilities in influencing the signal intensity is not readily apparent, nor is it discussed in the common EPR references. The signal intensity is a direct function of the net absorption of the sample which is proportional to the small difference in population between the two states involved. Since the probability for an absorption is equal to that of an emission, the difference in population is dependent upon the amount of radiationless decay. Thus, it is the relative difference in the probabilities of radiationless decay and emission which influences the signal intensity. This is demonstrated in Appendix H. A comparison of the transition probability number of 324 given previously for the E' transitions with the numbers for the U' transitions is therefore not significant. More specifically, it is not unreasonable to presume that even when the E' level is in close proximity to the U' level that the signal intensity for the E' transitions is less than for the U' transitions.

The EPR absorptions for $[Co(terpy)_2]SO_4 \cdot 2H_2O$ remain reasonably narrow even near room temperature. A general comparison of the g values for all the terpyridine complexes reveals that the sulfate g values are relatively smaller than those of the other complexes. This would seem to imply that in general the δ value for the sulfate complex is located farther to the right of the cross-over point than are the δ values for the other complexes. If this is the case, then the E' absorption would be weaker at the higher temperatures than for the other complexes. An examination of the $\chi^{-1}(T)$ curve for the sulfate given in Figure 2 shows that the maximum appears at a higher temperature than for the other terpyridine salts, again indicating that it is farther removed from the cross-over point than the others.

A comparison of signal intensities for the two absorptions for the sulfate is probably not meaningful for the reasons mentioned previously. However, the intensities for the E' absorption are seen to remain approximately constant over the same range of temperature as do the U' intensities.

CONCLUSIONS

Certain predictions concerning the expected EPR behavior of the anomalous octahedral cobalt(II) complexes were made based upon the theoretical model developed in Part I. These were the existence of two distinct resonance absorptions corresponding to transitions within the E' and lowest U' levels, a shift in g values with temperature, and a shift in signal intensity with temperature. All three phenomena were observed and good qualitative and even semi-quantitative agreement with the theoretical model was obtained. The lack of close quantitative agreement only serves to underscore the point made in Part I that, although the model presented goes far toward characterizing the behavior of these complexes, it remains incomplete.

It must be recalled that the model developed in Part I was designed to explain the variation in magnetic susceptibility as a function of temperature, and that its application to predicting EPR behavior should not be expected to yield quantitative results. Magnetic susceptibility measurements involve an average result taken over a number of energy levels and magnetic states, and is not as sensitive to certain parameters as are EPR measurements which involve transitions between distinct energy states. Therefore, assumptions which may be suitable for predicting susceptibility behavior may not be valid for predicting EPR behavior. For example, very small amounts of magnetic exchange between different ions has little effect on the magnetic susceptibility, but often such amounts can interfere markedly with the interpretation of EPR data [83]. Also, covalency effects, which were thought to affect the susceptibility results to only a minor degree, would lead to a lowering of the experimental g value of a complex [84]. Another consideration is that small distortions from octahedral symmetry could easily alter the relative splittings of the magnetic states without affecting susceptibility behavior. This latter point is dramatically evident to the left of the cross-over point where Figure 13 shows considerable fluctuation in the magnetic state splittings while no anomalies are evident for the susceptibility calculations in that region.

It can be concluded, therefore, that the EPR studies of Part II serve to add further credence to the theoretical model of Part I and at the same time emphasize the need for further study of these anomalous complexes. Single-crystal EPR measurements would aid considerably in determining the distortion, if any, from octahedral symmetry, and the role it plays in influencing the magnetic behavior. Extensive solution experiments should aid in illuminating the influence of the anion, and in general, crystal-lattice effects.

Also, optical measurements as a function of temperature would be very helpful.

There is much which remains to be learned about these anomalous systems, and it is hoped that this work will provide a foundation from which further studies may proceed.

SUMMARY

The magnetic susceptibilities of certain six-coordinate octahedral cobalt(II) complexes were studied from a theoretical point of view. Calculations of magnetic susceptibility as a function of temperature were made for a d^7 ion in an octahedral field, in order to explain the magnetic moments of these cobalt complexes, moments which are observed to be intermediate between the usual "high-spin" and "low-spin" values normally found. In addition, their magnetic behavior is anomalous, that is, their reciprocal susceptibility is not a linear function of the temperature. Using the strong-field approximation, a model based upon an equilibrium distribution of magnetic ions over several electronic levels arising from the $^4T_1$ and ^2E terms in the vicinity of the cross-over point yielded calculated magnetic moments which smoothly increased in value from the "low-spin" limit to near the "high-spin" limit as the crystal-field potential was decreased from strong-field values to weak-field values. Incorporating into the model the hypothesis that the crystal-field potential is a function of temperature, theoretical reciprocal susceptibility curves as a function of temperature were calculated. These curves are in reasonable agreement with the experimental curves.

In an effort to further characterize the anomalous complexes, an electron paramagnetic resonance study was conducted. The theoretical model predicted that two distinct resonance absorptions should be observed, that the g values should vary with temperature, and that the signal intensities should shift with temperature. All three phenomena were observed experimentally. In addition, the nature of the shifts was consistent with the hypothesis that the variation of the crystal-field potential with temperature is a result of anharmonic metal-ligand vibrations.

It was concluded that the model forms a reasonable basis by which to characterize these anomalous systems and this model further indicates several unresolved factors which could influence the magnetic behavior and which remain to be investigated.

APPENDICES

APPENDIX A

ALTERNATIVE DEFINITIONS FOR SOME MAGNETIC RELATIONSHIPS

The magnetic field within a substance, termed the magnetic induction $\hat{B}$, is different from the free-space field $\hat{H}$. They are related by

$$\hat{B} = \hat{H} + 4\pi\hat{I} \qquad \text{(A-1)}$$

where $\hat{I}$ is the intensity of magnetization per unit volume. The ratio of B/H is the magnetic permeability, often symbolized by μ_o . From the equation (A-1), the relationship

$$B/H = 1 + 4\pi\kappa \qquad \text{(A-2)}$$

is obtained where

$$\kappa = I/H \qquad \text{(A-3)}$$

and is the magnetic susceptibility per unit volume. Occasionally there is used the specific susceptibility, χ_{sp}, related to κ via the density D of the substance,

$$\chi_{sp} = \kappa/D \ . \qquad \text{(A-4)}$$

More commonly is used the susceptibility per gram ion, gram atom, or mole, which is simply χ_{sp} times the gram-ionic, gram-atomic, or gram-molecular weight. For example,

$$\chi_{g-i} = \chi_{sp}(\text{gram-ionic weight}). \qquad \text{(A-5)}$$

In this dissertation, the symbol χ without subscripts is used for the susceptibility per gram ion. This definition for χ is completely equivalent to the one given by equation (5) of the Introduction.

APPENDIX B

DISCUSSION OF MAGNETIC MOMENTS AND DERIVATION OF EQUATION (6)

Magnetic fields are generated by moving electric charges. A positive electric current moving in a coil will produce a magnetic field whose direction is given by the right-hand rule. In a very simplified manner, an electron moving around a nucleus can be thought of as a tiny current loop. The product of the current i and the area described by this electron loop, A, is defined as the orbital magnetic moment, $\hat{\mu}_L$, where A is the area vector whose direction is also given by the right-hand rule. In cgs units,

$$\hat{\mu}_L = \frac{i\hat{A}}{c} \qquad (B\text{-}1)$$

where c is the velocity of light. The current i is charge per second, and the cgs unit of charge divided by c is 10 coulombs. Thus, in equation (B-1), $\hat{u}$ has the units of $10\text{clb-cm}^2\text{-sec}^{-1}$. For convenience, this is converted to erg-gauss^{-1} by the relationship

$$1 \text{ gauss} = 10^{-1} \text{ erg-sec-clb}^{-1}\text{-cm}^{-2} \ . \qquad (B\text{-}2)$$

Since the current due to an electron moving in an orbit with velocity v is simply the electronic charge multiplied by the number of times it traverses a complete loop per second, $i = -ev/2\pi r$, with the area of the orbit being πr^2. Then the orbital magnetic moment summed over all the discrete charges of a molecule is

$$\hat{\mu}_L = -\frac{1}{2c} \Sigma e_i(\hat{r}_i \times \hat{v}_i) . \qquad \text{(B-3)}$$

Note that because the current i is due to negative electrons, the direction of $\hat{\mu}_i$ as defined in equation (B-1) is opposite that of both $\hat{A}$ and the generated magnetic field. Thus it is in a north-to-south direction.

Momentum p_i equals $m\hat{v}_i$, and orbital angular momentum $\hat{L}$ is $\Sigma\hat{r}_i \times \hat{p}_i$ giving the relation

$$\hat{\mu}_L = -\frac{e}{2mc}\hat{L} \qquad \text{(B-4)}$$

where e now represents the total charge. The intrinsic spin of the electron gives rise to a spin magnetic moment, $\hat{\mu}_s$, which can be related to the spin angular momentum, $\hat{S}$, by

$$\hat{\mu}_s = -\frac{e}{mc}\hat{S} . \qquad \text{(B-5)}$$

This relationship is derived from relativistic considerations [76]. The total magnetic moment is then

$$\hat{\mu} = \hat{\mu}_L + \hat{\mu}_s . \qquad \text{(B-6)}$$

In the direction of an applied external magnetic field (z direction), the above equations become

$$\mu_{L_z} = -\frac{e}{2mc} L_z$$

$$\mu_{s_z} = -\frac{e}{mc} S_z$$

$$\mu_z = \mu_{L_z} + \mu_{s_z} \qquad \text{(B-7)}$$

The energy of interaction of a system with an external magnetic field may be taken as the classical form of that part of the Hamiltonian due to a magnetic field [1].

$$E_1 = \sum_{i=1} \left\{ \frac{e_i}{2mc} \hat{H} \times \hat{r}_i \cdot \hat{p}_i + \frac{e_i^{\,2}}{8mc^2} \left| \hat{H} \times \hat{r}_i \right|^2 + \frac{e_i}{mc} \hat{H} \cdot \hat{s}_i \right\} \qquad \text{(B-8)}$$

where E_1 is that part of the energy dependent on H. The first and third parts of equation (B-8) represent the contributions from the interaction of the orbital and spin angular momenta, respectively, with the magnetic field. The second part of the equation is due to an induced interaction and gives rise to diamagnetism. It is negligible relative to the other two and will not be considered. Rearranging slightly gives

$$E_1 = \sum_{i=1} \left\{ \frac{e_i}{2mc} \hat{H} \cdot \hat{r}_i \times \hat{p}_i + \frac{e_i}{mc} \hat{H} \cdot \hat{s}_i \right\}, \qquad \text{(B-9)}$$

which is further simplified to

$$E_1 = \frac{e}{2mc} \hat{H} \cdot \hat{L} + \frac{e}{mc} \hat{H} \cdot \hat{S} \qquad \text{(B-10)}$$

with $\hat{S} = \Sigma \hat{s}_i$. Taking the field to be in the z direction and differentiating with respect to H,

$$\frac{\partial E}{\partial H} = \frac{e}{2mc} L_z + \frac{e}{mc} S_z \qquad \text{(B-11)}$$

which, from the relations of (B-7), yields

$$\frac{\partial E}{\partial H} = -\mu_{L_z} - \mu_{S_z} \qquad \text{(B-12)}$$

or

$$\mu_z = -\frac{\partial E}{\partial H} \qquad \text{(B-13)}$$

where E can now be taken as the total energy for an atom in a magnetic field in a given electronic state.

APPENDIX C

TABLE OF DIRECT PRODUCTS FOR THE GROUP O

O	A_1	A_2	E	T_1	T_2	E'	E''	U'
A_1	A_1	A_2	E	T_1	T_2	E'	E''	U'
A_2	A_2	A_1	E	T_2	T_1	E''	E'	U'
E	E	E	A_1+A_2+E	T_1+T_2	T_1+T_2	U'	U'	$E'+E''+U'$
T_1	T_1	T_2	T_1+T_2	$A_1+E+T_1+T_2$	$A_2+E+T_1+T_2$	$E'+U'$	$E''+U'$	$E'+E''+2U'$
T_2	T_2	T_1	T_1+T_2	$A_2+E+T_1+T_2$	$A_1+E+T_1+T_2$	$E''+U'$	$E'+U'$	$E'+E''+2U'$
E'	E'	E''	U'	$E'+U'$	$E''+U'$	A_1+T_1	A_2+T_2	$E+T_1+T_2$
E''	E''	E'	U'	$E''+U'$	$E'+U'$	A_2+T_2	A_1+T_1	$E+T_1+T_2$
U'	U'	U'	$E'+E''+U'$	$E'+E''+2U'$	$E'+E''+2U'$	$E+T_1+T_2$	$E+T_1+T_2$	$A_1+A_2+E+2T_1+2T_2$

APPENDIX D

COUPLING COEFFICIENTS FOR THE OCTAHEDRAL GROUP

$T_1 x U'$	E'		E''		$\frac{3}{2}U'$				$\frac{5}{2}U'$			
	α'	β'	α''	β''	κ	λ	μ	ν	κ	λ	μ	ν
1 κ	.	.	$\frac{1}{\sqrt{6}}$	.	.	.	.	.	.	.	.	$\frac{\sqrt{5}}{\sqrt{6}}$
0 κ	.	.	.	$-\frac{1}{\sqrt{3}}$	$\frac{\sqrt{3}}{\sqrt{5}}$	.	.	.	$-\frac{1}{\sqrt{15}}$	.	.	.
-1 κ	$\frac{1}{\sqrt{2}}$	.	.	.	.	$\frac{\sqrt{2}}{\sqrt{5}}$	.	.	.	$\frac{1}{\sqrt{10}}$	.	.
1 λ	.	.	.	$-\frac{1}{\sqrt{2}}$	$-\frac{\sqrt{2}}{\sqrt{5}}$	.	.	.	$-\frac{1}{\sqrt{10}}$	.	.	.
0 λ	$-\frac{1}{\sqrt{3}}$	.	.	.	.	$\frac{1}{\sqrt{15}}$	.	.	.	$\frac{\sqrt{3}}{\sqrt{5}}$	.	.
-1 λ	.	$\frac{1}{\sqrt{6}}$	.	.	.	.	$\frac{2\sqrt{2}}{\sqrt{15}}$	.	.	.	$-\frac{\sqrt{3}}{\sqrt{10}}$	.

Appendix D (cont'd)

$T_1 x U'$	E'		E''		$\frac{3}{2}U'$				$\frac{5}{2}U'$			
	α'	β'	α''	β''	κ	λ	μ	ν	κ	λ	μ	ν
1 μ	$\frac{1}{\sqrt{6}}$	.	.	.	.	$-\frac{2\sqrt{2}}{\sqrt{15}}$	.	.	.	$\frac{\sqrt{3}}{\sqrt{10}}$	.	.
0 μ	.	$-\frac{1}{\sqrt{3}}$	.	.	.	.	$-\frac{1}{\sqrt{15}}$	.	.	.	$-\frac{\sqrt{3}}{\sqrt{5}}$	.
-1 μ	.	.	$-\frac{1}{\sqrt{2}}$	.	.	.	.	$\frac{\sqrt{2}}{\sqrt{5}}$	.	.	.	$\frac{1}{\sqrt{10}}$
1 ν	.	$\frac{1}{\sqrt{2}}$	.	.	.	.	$-\frac{\sqrt{2}}{\sqrt{5}}$	.	.	.	$-\frac{1}{\sqrt{10}}$	.
0 ν	.	.	$-\frac{1}{\sqrt{3}}$	.	.	.	.	$-\frac{\sqrt{3}}{\sqrt{5}}$	.	.	.	$\frac{1}{\sqrt{15}}$
-1 ν	.	.	.	$\frac{1}{\sqrt{6}}$	.	.	.	.	$-\frac{\sqrt{5}}{\sqrt{6}}$	.	.	.

Appendix D (cont'd)

A_2 x T_2		T_1 1	0	−1
a_2	1	1	.	.
a_2	0	.	1	.
a_2	−1	.	.	1

T_1 x E'		E' α'	β'	U' κ	λ	μ	ν
1	α'	.	.	1	.	.	.
0	α'	$\frac{1}{\sqrt{3}}$	.	.	$\frac{\sqrt{2}}{\sqrt{3}}$	.	.
−1	α'	.	$\frac{\sqrt{2}}{\sqrt{3}}$	.	.	$\frac{1}{\sqrt{3}}$	.
1	β'	$-\frac{\sqrt{2}}{\sqrt{3}}$	.	.	$\frac{1}{\sqrt{3}}$	.	.
0	β'	.	$-\frac{1}{\sqrt{3}}$	.	.	$\frac{\sqrt{2}}{\sqrt{3}}$	.
−1	β'	.	.	.	.	.	1

$$
\begin{array}{ll}
t_2^{5} & \left\{\begin{array}{l}
\left|{}^2T_2\ \tfrac{1}{2}\ 1\right\rangle = -\left|1^{+}\ -1^{2}\ \xi^{2}_{,}\right\rangle \\
\left|{}^2T_2\ \tfrac{1}{2}\ 0\right\rangle = -\left|1^{2}\ -1^{2}\ \xi^{+}_{,}\right\rangle \\
\left|{}^2T_2\ \tfrac{1}{2}\ -1\right\rangle = \left|1^{2}\ -1^{+}\ \xi^{2}_{,}\right\rangle
\end{array}\right. \\
t_2^{6} & \left|{}^1A_1\ 0\ 0\right\rangle = \left|1^{2}\ -1^{2}\ \xi^{2}_{,}\right\rangle \\
e^{2} & \left|{}^3A_2\ 1\ a_2\right\rangle = \left|\theta^{+}\ \epsilon^{+}\right\rangle
\end{array}
$$

APPENDIX E

TABLE OF FUNCTIONS

$$\left|\phi_1^{\kappa}\right\rangle = \left|1^2-1^2\zeta_1^2\epsilon^-\right\rangle$$

$$\left|\phi_1^{\lambda}\right\rangle = -\left|1^2-1^2\zeta_1^2\theta^+\right\rangle$$

$$\left|\phi_1^{\mu}\right\rangle = \left|1^2-1^2\zeta_1^2\theta^-\right\rangle$$

$$\left|\phi_1^{\nu}\right\rangle = -\left|1^2-1^2\zeta_1^2\epsilon^+\right\rangle$$

$$\left|\phi_2^{\kappa}\right\rangle = -\sqrt{\tfrac{3}{5}}\left|1^2-1^2\zeta_1^+\theta^+\epsilon^+\right\rangle + \sqrt{\tfrac{2}{15}}\left|1^+-1^2\zeta_1^2\theta^+\epsilon^-\right\rangle$$

$$+\sqrt{\tfrac{2}{15}}\left|1^+-1^2\zeta_1^2\theta^-\epsilon^+\right\rangle + \sqrt{\tfrac{2}{15}}\left|1^--1^2\zeta_1^2\theta^+\epsilon^+\right\rangle$$

$$\left|\phi_2^{\lambda}\right\rangle = \sqrt{\tfrac{2}{5}}\left|1^2-1^+\zeta_1^2\theta^+\epsilon^+\right\rangle - 1/\sqrt{45}\left|1^2-1^2\zeta_1^+\theta^+\epsilon^-\right\rangle$$

$$- 1/\sqrt{45}\left|1^2-1^2\zeta_1^+\theta^-\epsilon^+\right\rangle - 1/\sqrt{45}\left|1^2-1^2\zeta_1^-\theta^+\epsilon^+\right\rangle$$

$$\frac{2\sqrt{2}}{\sqrt{45}}\left|1^+-1^2\zeta_1^2\theta^-\epsilon^-\right\rangle + \frac{2\sqrt{2}}{\sqrt{45}}\left|1^--1^2\zeta_1^2\theta^+\epsilon^-\right\rangle$$

$$- \frac{2\sqrt{2}}{\sqrt{45}}\left|1^--1^2\zeta_1^2\theta^-\epsilon^+\right\rangle$$

$$\left|\phi_2^{\mu}\right\rangle = \frac{2\sqrt{2}}{\sqrt{45}}\left|1^2-1^+\zeta_1^2\theta^+\epsilon^-\right\rangle + \frac{2\sqrt{2}}{\sqrt{45}}\left|1^2-1^+\zeta_1^2\theta^-\epsilon^+\right\rangle$$

$$+ \frac{2\sqrt{2}}{\sqrt{45}}\left|1^2-1^-\zeta_1^2\theta^+\epsilon^+\right\rangle + \frac{1}{\sqrt{45}}\left|1^2-1^2\zeta_1^+\theta^-\epsilon^-\right\rangle$$

$$1/\sqrt{45}\left|1^2-1^2\zeta_1^-\theta^+\epsilon^-\right\rangle + 1/\sqrt{45}\left|1^2-1^2\zeta_1^-\theta^-\epsilon^+\right\rangle$$

$$+ \sqrt{\tfrac{2}{5}}\left|1^--1^2\zeta_1^2\theta^-\epsilon^-\right\rangle$$

$$\left|\phi_2^{\nu}\right\rangle = \sqrt{\tfrac{2}{15}}\left|1^2-1^+\zeta_1^2\theta^-\epsilon^-\right\rangle + \sqrt{\tfrac{2}{15}}\left|1^2-1^-\zeta_1^2\theta^+\epsilon^-\right\rangle + \sqrt{\tfrac{3}{5}}\left|1^2-1^2\zeta_1^-\theta^-\epsilon^-\right\rangle$$

$$+ \sqrt{\tfrac{2}{15}}\left|1^2-1^-\zeta_1^2\theta^-\epsilon^+\right\rangle$$

Appendix E (cont'd)

$$\begin{aligned}|\phi_3^{\kappa}\rangle = {} & \frac{1}{\sqrt{15}}|1^2\text{-}1^2\xi_1^+\theta^+\epsilon^+\rangle + \frac{1}{\sqrt{30}}|1^+\text{-}1^2\xi_1^2\theta^+\epsilon^-\rangle \\ & + \frac{1}{\sqrt{30}}|1^+\text{-}1^2\xi_1^2\theta^-\epsilon^+\rangle + \frac{1}{\sqrt{30}}|1^-\text{-}1^2\xi_1^2\theta^+\epsilon^+\rangle \\ & - \sqrt{\frac{5}{6}}|1^2\text{-}1^-\xi_1^2\theta^-\epsilon^-\rangle\end{aligned}$$

$$\begin{aligned}|\phi_3^{\lambda}\rangle = {} & \frac{1}{\sqrt{10}}|1^2\text{-}1^+\xi_1^2\theta^+\epsilon^+\rangle - \frac{1}{\sqrt{5}}|1^2\text{-}1^2\xi_1^+\theta^+\epsilon^-\rangle \\ & - \frac{1}{\sqrt{5}}|1^2\text{-}1^2\xi_1^+\theta^-\epsilon^+\rangle - \frac{1}{\sqrt{5}}|1^2\text{-}1^2\xi_1^-\theta^+\epsilon^+\rangle \\ & - 1/\sqrt{10}|1^+\text{-}1^2\xi_1^2\theta^-\epsilon^-\rangle - 1/\sqrt{10}|1^-\text{-}1^2\xi_1^2\theta^+\epsilon^-\rangle \\ & - 1/\sqrt{10}|1^-\text{-}1^2\xi_1^2\theta^-\epsilon^+\rangle\end{aligned}$$

$$\begin{aligned}|\phi_3^{\mu}\rangle = {} & - \frac{1}{\sqrt{10}}|1^2\text{-}1^+\xi_1^2\theta^+\epsilon^-\rangle - \frac{1}{\sqrt{10}}|1^2\text{-}1^+\xi_1^2\theta^-\epsilon^+\rangle \\ & - \frac{1}{\sqrt{10}}|1^2\text{-}1^-\xi_1^2\theta^+\epsilon^+\rangle + \frac{1}{\sqrt{5}}|1^2\text{-}1^2\xi_1^+\theta^-\epsilon^-\rangle \\ & + 1/\sqrt{5}|1^2\text{-}1^2\xi_1^-\theta^+\epsilon^-\rangle + 1/\sqrt{5}|1^2\text{-}1^2\xi_1^-\theta^-\epsilon^+\rangle \\ & + 1/\sqrt{10}|1^-\text{-}1^2\xi_1^2\theta^-\epsilon^-\rangle\end{aligned}$$

$$\begin{aligned}|\phi_3^{\nu}\rangle = {} & - \sqrt{\frac{5}{6}}|1^+\text{-}1^2\xi_1^2\theta^+\epsilon^+\rangle + \frac{1}{\sqrt{30}}|1^2\text{-}1^+\xi_1^2\theta^-\epsilon^-\rangle \\ & + \frac{1}{\sqrt{30}}|1^2\text{-}1^-\xi_1^2\theta^+\epsilon^-\rangle + \frac{1}{\sqrt{30}}|1^2\text{-}1^-\xi_1^2\theta^-\epsilon^+\rangle \\ & - 1/\sqrt{15}|1^2\text{-}1^2\xi_1^-\theta^-\epsilon^-\rangle\end{aligned}$$

$$\begin{aligned}|\phi_4^{\alpha'}\rangle = {} & 1/\sqrt{2}|1^2\text{-}1^+\xi_1^2\theta^+\epsilon^+\rangle + \frac{1}{3}|1^2\text{-}1^2\xi_1^+\theta^+\epsilon^-\rangle \\ & + \frac{1}{3}|1^2\text{-}1^2\xi_1^+\theta^-\epsilon^+\rangle + \frac{1}{3}|1^2\text{-}1^2\xi_1^-\theta^+\epsilon^+\rangle - \frac{1}{3\sqrt{2}}|1^+\text{-}1^2\xi_1^2\theta^-\epsilon^-\rangle \\ & - \frac{1}{3\sqrt{2}}|1^-\text{-}1^2\xi_1^2\theta^+\epsilon^-\rangle - \frac{1}{3\sqrt{2}}|1^-\text{-}1^2\xi_1^2\theta^-\epsilon^+\rangle\end{aligned}$$

Appendix E (cont'd)

$$
\begin{aligned}
|\phi_4^{\beta'}\rangle = {} & \frac{1}{3\sqrt{2}}|1^2 -1^+ \xi_1^2 \theta^+ \epsilon^-\rangle + \frac{1}{3\sqrt{2}}|1^2 -1^+ \xi_1^2 \theta^- \epsilon^+\rangle \\
& + \frac{1}{3\sqrt{2}}|1^2 -1^- \xi_1^2 \theta^+ \epsilon^+\rangle + \frac{1}{3}|1^2 -1^2 \xi_1^+ \theta^- \epsilon^-\rangle + \frac{1}{3}|1^2 -1^2 \xi_1^- \theta^+ \epsilon^-\rangle \\
& + \frac{1}{3}|1^2 -1^2 \xi_1^- \theta^- \epsilon^+\rangle - \frac{1}{\sqrt{2}}|1^- -1^2 \xi_1^2 \theta^- \epsilon^-\rangle
\end{aligned}
$$

$$
\begin{aligned}
|\phi_5^{\alpha''}\rangle = {} & -1/\sqrt{6}|1^+ -1^2 \xi_1^2 \theta^+ \epsilon^+\rangle - 1/\sqrt{6}|1^2 -1^+ \xi_1^2 \theta^- \epsilon^-\rangle \\
& - 1/\sqrt{6}|1^2 -1^- \xi_1^2 \theta^+ \epsilon^-\rangle - 1/\sqrt{6}|1^2 -1^- \xi_1^2 \theta^- \epsilon^+\rangle \\
& + 1/\sqrt{3}|1^2 -1^2 \xi_1^- \theta^- \epsilon^-\rangle
\end{aligned}
$$

$$
\begin{aligned}
|\phi_5^{\beta''}\rangle = {} & 1/\sqrt{3}|1^2 -1^2 \xi_1^+ \theta^+ \epsilon^+\rangle + 1/\sqrt{6}|1^+ -1^2 \xi_1^2 \theta^+ \epsilon^-\rangle \\
& + 1/\sqrt{6}|1^+ -1^2 \xi_1^2 \theta^- \epsilon^+\rangle + 1/\sqrt{6}|1^- -1^2 \xi_1^2 \theta^+ \epsilon^+\rangle \\
& + 1/\sqrt{6}|1^2 -1^- \xi_1^2 \theta^- \epsilon^-\rangle
\end{aligned}
$$

APPENDIX F

TABLE F1

SPIN-ORBIT COUPLING EIGENVALUES OF THE 3d ORBITALS

$$\mathcal{H}_s = \zeta(\tfrac{1}{2}l^+s^- + \tfrac{1}{2}l^-s^+ + l_zs_z)$$

$$\mathcal{H}_s|1^+\rangle = |2^-\rangle + \tfrac{1}{2}|1^+\rangle$$

$$\mathcal{H}_s|\theta^+\rangle = \frac{\sqrt{6}}{2}|1^-\rangle$$

$$\mathcal{H}_s|-1^+\rangle = \frac{\sqrt{6}}{2}|\theta^-\rangle - \tfrac{1}{2}|-1^+\rangle$$

$$\mathcal{H}_s|\zeta_1^+\rangle = -\frac{1}{\sqrt{2}}|-1^-\rangle + |\epsilon^+\rangle$$

$$\mathcal{H}_s|\epsilon^+\rangle = \frac{1}{\sqrt{2}}|-1^-\rangle + |\zeta_1^+\rangle$$

$$\mathcal{H}_s|1^-\rangle = \frac{\sqrt{6}}{2}|\theta^+\rangle - \tfrac{1}{2}|1^-\rangle$$

$$\mathcal{H}_s|\theta^-\rangle = \frac{\sqrt{6}}{2}|-1^+\rangle$$

$$\mathcal{H}_s|-1^-\rangle = |-2^+\rangle + \tfrac{1}{2}|-1^-\rangle$$

$$\mathcal{H}_s|\zeta_1^-\rangle = \frac{1}{\sqrt{2}}|1^+\rangle - |\epsilon^-\rangle$$

$$\mathcal{H}_s|\epsilon^-\rangle = \frac{1}{2}|1^+\rangle - |\zeta_1^-\rangle$$

TABLE F2

EIGENVALUES FOR THE OPERATOR

$$\mathcal{H}_1 = \hbar\beta H_z(l_z+2s_z)$$

$$\mathcal{H}_1|1^+\rangle = 2|1^+\rangle$$

$$\mathcal{H}_1|\theta^+\rangle = |\theta^+\rangle$$

$$\mathcal{H}_1|-1^-\rangle = 0$$

$$\mathcal{H}_1|\xi_1^+\rangle = 2|\epsilon^+\rangle + |\xi_1^+\rangle$$

$$\mathcal{H}_1|\epsilon^+\rangle = 2|\xi_1^+\rangle + |\epsilon^+\rangle$$

$$\mathcal{H}_1|1^-\rangle = 0$$

$$\mathcal{H}_1|\theta^-\rangle = |\theta^-\rangle$$

$$\mathcal{H}_1|-1^-\rangle = -2|-1^-\rangle$$

$$\mathcal{H}_1|\xi_1^-\rangle = 2|\epsilon^-\rangle - |\xi_1^-\rangle$$

$$\mathcal{H}_1|\epsilon^-\rangle = 2|\xi_1^-\rangle - |\epsilon^-\rangle$$

TABLE F3

EIGENVALUES FOR THE OPERATOR

$$\mathcal{H}_x = \hbar\beta H_x(l_x + 2\underset{\sim}{s}_x)$$

$$\mathcal{H}_x|1^+\rangle = |2^+\rangle + \sqrt{6}/2|\theta^+\rangle + |1^-\rangle$$

$$\mathcal{H}_x|\theta^+\rangle = \sqrt{6}/2|1^+\rangle + \sqrt{6}/2|-1^+\rangle + |\theta^-\rangle$$

$$\mathcal{H}_x|-1^+\rangle = \sqrt{6}/2|\theta^+\rangle + |-2^+\rangle + |-1^-\rangle$$

$$\mathcal{H}_x|1^-\rangle = |2^-\rangle + \sqrt{6}/2|\theta^-\rangle + |1^+\rangle$$

$$\mathcal{H}_x|\theta^-\rangle = \sqrt{6}/2|1^-\rangle + \sqrt{6}/2|-1^-\rangle + |\theta^+\rangle$$

$$\mathcal{H}_x|-1^-\rangle = \sqrt{6}/2|\theta^-\rangle + |-2^-\rangle + |-1^+\rangle$$

$$\mathcal{H}_x|\epsilon^+\rangle = \frac{1}{\sqrt{2}}\left[|1^+\rangle + |2^-\rangle + |-1^+\rangle + |-2^-\rangle\right] = 1/\sqrt{2}|1^+\rangle + 1/\sqrt{2}|-1^+\rangle + |\epsilon^-\rangle$$

$$\mathcal{H}_x|\epsilon^-\rangle = \frac{1}{\sqrt{2}}\left[|1^-\rangle + |2^+\rangle + |-1^-\rangle + |-2^+\rangle\right] = 1/\sqrt{2}|1^-\rangle + 1/\sqrt{2}|-1^-\rangle + |\epsilon^+\rangle$$

$$\mathcal{H}_x|\zeta_1^+\rangle = \frac{1}{\sqrt{2}}\left[|1^+\rangle + |2^-\rangle - |-1^+\rangle - |-2^-\rangle\right] = 1/\sqrt{2}|1^+\rangle - 1/\sqrt{2}|-1^+\rangle + |\zeta_1^-\rangle$$

$$\mathcal{H}_x|\zeta_1^-\rangle = \frac{1}{\sqrt{2}}\left[|1^-\rangle + |2^+\rangle - |-1^-\rangle - |-2^+\rangle\right] = 1/\sqrt{2}|1^-\rangle - 1/\sqrt{2}|-1^-\rangle + |\zeta_1^+\rangle$$

APPENDIX G

PROOF OF THE INVERSE PROPORTIONALITY BETWEEN SIGNAL INTENSITY AND ABSOLUTE TEMPERATURE[+]

Consider a large assembly of unpaired electrons divided into two populations, a +1/2 spin population and a -1/2 spin population. At thermal equilibrium, the ratio of the two populations is governed by the Boltzmann factor,

$$\frac{n(-1/2)}{n(+1/2)} = \exp \frac{E(-1/2) - E(+1/2)}{kT} = e^{g\beta H/kT} \; . \qquad (G\text{-}1)$$

The signal intensity is directly proportional to the difference in population of the two states, Δn, where

$$\Delta n = n(-1/2) - n(+1/2) \; . \qquad (G\text{-}2)$$

Denoting the total population as

$$N = n(-1/2) + n(+1/2) \qquad (G\text{-}3)$$

and combining equations (G-1) - (G-3),

$$\Delta n = \frac{N(e^{g\beta H/kT} - 1)}{e^{g\beta H/kT} + 1} \quad . \qquad (G\text{-}4)$$

The denominator of equation (G-4) is negligibly different from 2, and therefore,

$$\Delta n = \frac{N}{2}(e^{g\beta H/kT} - 1) \quad . \qquad (G\text{-}5)$$

Expanding equation (G-5) as a Taylor series,

[+] Reference [78].

$$\Delta n = \frac{N}{2}\left[\left(1 + \frac{g\beta H}{kT} + \frac{[g\beta H/kT]^2}{2!} + . . .\right) - 1\right] . \tag{G-6}$$

With $g\beta H/kT \ll 1$, all terms second-order and higher can be neglected, and so

$$\Delta n = \frac{Ng\beta H}{2kT} . \tag{G-7}$$

APPENDIX H

DERIVATION OF SIGNAL INTENSITY DEPENDENCE UPON QUANTUM EFFICIENCY[+]

The signal intensity for an absorption may be expressed by

$$I = A \phi N \qquad \text{(H-1)}$$

where A represents all the instrument factors, ϕ is the quantum efficiency to be defined below, and N is the total population. Designating the populations of the ground and excited states by n_1 and n_2 respectively, where $N = n_1 + n_2$, the rate of change of the population of the excited state is

$$\frac{d[n_2]}{dt} = k_a[n_1] - k_e[n_2] - k_r[n_2] \qquad \text{(H-2)}$$

where the rate constants are for absorption (k_a), emission (k_e), and radiationless decay (k_r). At equilibrium,

$$[n_2] = k_a[n_1]/(k_e+k_r) \ . \qquad \text{(H-3)}$$

The quantum efficiency is defined by

$$\phi = k_e[n_2]/k_a[n_1] \ . \qquad \text{(H-4)}$$

Substituting equation (H-3) into (H-4), one obtains

$$\phi = k_e/(k_e+k_r) \ . \qquad \text{(H-5)}$$

[+] Reference [85].

Thus, the quantum efficiency, and hence the signal intensity, is very dependent upon the magnitude of the rate of radiationless decay. The transition probability numbers calculated in Part II are directly proportional to k_a and k_e which are equal for EPR transitions.

APPENDIX I

Computer Programs

Each of the two main programs written for this dissertation may be separated into three parts, the middle part of both being common. The middle part is reproduced here only once. The subroutine JACOBI is a diagonalization subroutine which utilizes only the upper half of a matrix. JACOBI was made available in binary form by Dr. Charles E. Reid of the University of Florida. The plotting subroutine is available on the library tape at the University of Florida Computing Center.

I1

Part 1

```
C     PROGRAM FOR CALCULATING AND PLOTTING MAGNETIC SUSCEPTIBILITIES AS
C     A FUNCTION OF TEMPERATURE FOR VALUES OF SMALL DELTA WITH
C     DELTA AS A FUNCTION OF TEMPERATURE.  P IS DELTA-ZERO.  Q, R, AND S
C     ARE COEFFICIENTS OF THE VIRIAL EXPANSION.
C
      DIMENSION A(3,3), ARRAY(6), VA(3,3), WO(5), W1(5,5), W2(5,5),
     1B(4,4), C(4,4), D(4,4), E(4,4), T(50), TRISH(5), PIKE(4), SLC(5),
     1SSC(50), DEN(50), CHI(50), REC(50), GRAPH(867)
    1 READ INPUT TAPE 5, 10, ZETA, P, Q, R, S
      DO 40 L=1,50
      T(L)=L*10
      DELT(L) = P + Q*T(L) + R*T(L)**2 + S*T(L)**3
      DEL = DELT(L)
```

Part 2

```
C     ELEMENTS OF THE 3X3 SPIN-ORBIT COUPLING MATRIX
C
      A(1,1)=0.
      A(1,2)=0.44721*ZETA
      A(1,3)=1.34164*ZETA
      A(2,1)=A(1,2)
      A(2,2)=DEL-ZETA/3.
      A(2,3)=0.
      A(3,1) = A(1,3)
      A(3,2)=A(2,3)
      A(3,3)=DEL+ZETA/2.
C
C     ARRAY IS THE UPPER HALF OF 'A' MATRIX.  JACOBI IS DIAGONALIZATION
C     SUBROUTINE
C
      K=0
      DO 3 J=1,3
      DO 3 I=1,J
      K=K+1
    3 ARRAY(K) = A(I,J)
      CALL JACOBI (3,ARRAY,VA,ITER,TRACE)
C
```

```
C     W0(I) ARE THE ZERO-ORDER ENERGIES
C
      W0(1)=ARRAY(1)
      W0(2)=ARRAY(3)
      W0(3)=ARRAY(6)
      W0(4)=DEL-0.83333*ZETA
      W0(5)=DEL+0.5*ZETA
C
C     W1(I,J) ARE THE FIRST-ORDER ZEEMAN ENERGIES CALCULATED USING THE
C     EIGENVECTORS, VA, OF THE DIAGONALIZED MATRIX
C
      W1(1,1)=-VA(1,1)**2+1.8*VA(2,1)**2-1.46667*VA(3,1)**2-1.2*VA(2,1)*
     1VA(3,1)
      W1(1,2)= VA(1,1)**2+0.6*VA(2,1)**2+0.40000*VA(3,1)**2+3.6*VA(2,1)*
     1VA(3,1)
      W1(1,3)=-W1(1,2)
      W1(1,4)=-W1(1,1)
      W1(2,1)=-VA(1,2)**2+1.8*VA(2,2)**2-1.46667*VA(3,2)**2-1.2*VA(2,2)*
     1VA(3,2)
      W1(2,2)= VA(1,2)**2+0.6*VA(2,2)**2+0.40000*VA(3,2)**2+3.6*VA(2,2)*
     1VA(3,2)
      W1(2,3)=-W1(2,2)
      W1(2,4)=-W1(2,1)
      W1(3,1)=-VA(1,3)**2+1.8*VA(2,3)**2-1.46667*VA(3,3)**2-1.2*VA(2,3)*
     1VA(3,3)
      W1(3,2)= VA(1,3)**2+0.6*VA(2,3)**2+0.40000*VA(3,3)**2+3.6*VA(2,3)*
     1VA(3,3)
      W1(3,3)=-W1(3,2)
      W1(3,4)=-W1(3,1)
      W1(4,1)=2.
      W1(4,2)=-2.
      W1(5,1)=-0.66667
      W1(5,2)=0.66667
C
C     B(I,J), C(I,J), D(I,J), AND E(I,J) ARE THE OFF-DIAGONAL ELEMENTS
C     OF THE MAGNETIC HAMILTONIAN USED TO CALCULATE THE SECOND-ORDER
```

```
C     ZEEMAN ENERGIES, W2(I,J)
C
      B(1,2)=-VA(1,1)*VA(1,2)+1.8*VA(2,1)*VA(2,2)-1.46667*VA(3,1)*VA(3,2
     1)-0.6*VA(2,1)*VA(3,2)-0.6*VA(3,1)*VA(2,2)
      B(1,3)=-VA(1,1)*VA(1,3)+1.8*VA(2,1)*VA(2,3)-1.46667*VA(3,1)*VA(3,3
     1)-0.6*VA(2,1)*VA(3,3)-0.6*VA(3,1)*VA(2,3)
      B(1,4)=-1.34164*VA(2,1)+1.19256*VA(3,1)
      B(2,1)=B(1,2)
      B(2,3)=-VA(1,2)*VA(1,3)+1.8*VA(2,2)*VA(2,3)-1.46667*VA(3,2)*VA(3,3
     1)-0.6*VA(2,2)*VA(3,3)-0.6*VA(3,2)*VA(2,3)
      B(2,4)=-1.34164*VA(2,2)+1.19256*VA(3,2)
      B(3,1)=B(1,3)
      B(3,2)=B(2,3)
      B(3,4)=-1.34164*VA(2,3)+1.19256*VA(3,3)
      B(4,1)=B(1,4)
      B(4,2)=B(2,4)
      B(4,3)=B(3,4)
      C(1,2)= VA(1,1)*VA(1,2)+0.6*VA(2,1)*VA(2,2)+0.40000*VA(3,1)*VA(3,2
     1)+1.8*VA(2,1)*VA(3,2)+1.8*VA(3,1)*VA(2,2)
      C(1,3)= VA(1,1)*VA(1,3)+0.6*VA(2,1)*VA(2,3)+0.40000*VA(3,1)*VA(3,3
     1)+1.8*VA(2,1)*VA(3,3)+1.8*VA(3,1)*VA(2,3)
      C(1,4)=2.23605*VA(2,1)
      C(2,1)=C(1,2)
      C(2,3)= VA(1,2)*VA(1,3)+0.6*VA(2,2)*VA(2,3)+0.40000*VA(3,2)*VA(3,3
     1)+1.8*VA(2,2)*VA(3,3)+1.8*VA(3,2)*VA(2,3)
      C(2,4)=2.23605*VA(2,2)
      C(3,1)=C(1,3)
      C(3,2)=C(2,3)
      C(3,4)=2.23605*VA(2,3)
      C(4,1)=C(1,4)
      C(4,2)=C(2,4)
      C(4,3)=C(3,4)
      D(1,2)=-C(1,2)
      D(1,3)=-C(1,3)
      D(1,4)= C(1,4)
      D(2,1)=D(1,2)
```

```
D(2,3)=-C(2,3)
D(2,4)= C(2,4)
D(3,1)=D(1,3)
D(3,2)=D(2,3)
D(3,4)= C(3,4)
D(4,1)=D(1,4)
D(4,2)=D(2,4)
D(4,3)=D(3,4)
E(1,2)=-B(1,2)
E(1,3)=-B(1,3)
E(1,4)= B(1,4)
E(2,1)=E(1,2)
E(2,3)=-B(2,3)
E(2,4)= B(2,4)
E(3,1)=E(1,3)
E(3,2)=E(2,3)
E(3,4)= B(3,4)
E(4,1)=E(1,4)
E(4,2)=E(2,4)
E(4,3)=E(3,4)
```

Part 3

```
 W2(1,1)=B(1,2)**2/(WO(1)-WO(2))+B(1,3)**2/(WO(1)-WO(3))+B(1,4)**2/
1(WO(1)-WO(5))
 W2(1,2)=C(1,2)**2/(WO(1)-WO(2))+C(1,3)**2/(WO(1)-WO(3))+C(1,4)**2/
1(WO(1)-WO(4))
 W2(1,3)=D(1,2)**2/(WO(1)-WO(2))+D(1,3)**2/(WO(1)-WO(3))+D(1,4)**2/
1(WO(1)-WO(4))
 W2(1,4)=E(1,2)**2/(WO(1)-WO(2))+E(1,3)**2/(WO(1)-WO(3))+E(1,4)**2/
1(WO(1)-WO(5))
 W2(2,1)=B(1,2)**2/(WO(2)-WO(1))+B(2,3)**2/(WO(2)-WO(3))+B(2,4)**2/
1(WO(2)-WO(5))
 W2(2,2)=C(1,2)**2/(WO(2)-WO(1))+C(2,3)**2/(WO(2)-WO(3))+C(2,4)**2/
1(WO(2)-WO(4))
 W2(2,3)=D(1,2)**2/(WO(2)-WO(1))+D(2,3)**2/(WO(2)-WO(3))+D(2,4)**2/
1(WO(2)-WO(4))
```

```
      W2(2,4)=E(1,2)**2/(WO(2)-WO(1))+E(2,3)**2/(WO(2)-WO(3))+E(2,4)**2/
     1(WO(2)-WO(5))
      W2(3,1)=B(1,3)**2/(WO(3)-WO(1))+B(2,3)**2/(WO(3)-WO(2))+B(3,4)**2/
     1(WO(3)-WO(5))
      W2(3,2)=C(1,3)**2/(WO(3)-WO(1))+C(2,3)**2/(WO(3)-WO(2))+C(3,4)**2/
     1(WO(3)-WO(4))
      W2(3,3)=D(1,3)**2/(WO(3)-WO(1))+D(2,3)**2/(WO(3)-WO(2))+D(3,4)**2/
     1(WO(3)-WO(4))
      W2(3,4)=E(1,3)**2/(WO(3)-WO(1))+E(2,3)**2/(WO(3)-WO(2))+E(3,4)**2/
     1(WO(3)-WO(5))
      W2(4,1)=C(1,4)**2/(WO(4)-WO(1))+C(2,4)**2/(WO(4)-WO(2))+C(3,4)**2/
     1(WO(4)-WO(3))
      W2(4,2)=D(1,4)**2/(WO(4)-WO(1))+D(2,4)**2/(WO(4)-WO(2))+D(3,4)**2/
     1(WO(4)-WO(3))
      W2(5,1)=E(1,4)**2/(WO(5)-WO(1))+E(2,4)**2/(WO(5)-WO(2))+E(3,4)**2/
     1(WO(5)-WO(3))
      W2(5,2)=B(1,4)**2/(WO(5)-WO(1))+B(2,4)**2/(WO(5)-WO(2))+B(3,4)**2/
     1(WO(5)-WO(3))
      DO 5 I=1,5
      DO 5 J=1,4
    5 W2(I,J)=W2(I,J)*8.6586E-25
C
C     VARIABLE TRISH IS FOR EXPONENTIAL TERMS.  DEN IS THE DENOMINATOR
C     OF CHI.  SLC IS SINGLE LEVEL CONTRIBUTION AND SSC IS SINGLE STATE
C     CONTRIBUTION.  PIKE IS THE COEFFICIENT QUANTITY FOR NUMERATOR
C     EXPONENTS.
C
      DO 37 I = 1,5
      TRISH(I) = EXPF(-WO(I)/(T(L)*0.69503))
   37 CONTINUE
      DEN(L) = 4.*TRISH(1) + 4.*TRISH(2) + 4.*TRISH(3) + 2.*TRISH(4)
     1+ 2.*TRISH(5)
      CHI(L)=0.
      DO 39 I=1,5
      SLC(I)=0.
      SSC(L)=0.
      DO 38 J=1,4
      PIKE(J) = W1(I,J)**2*6.22887E-25/T(L) - W2(I,J)
      SSC(L) = SSC(L) + (6.02252E23*PIKE(J))*TRISH(I)
   38 CONTINUE
      SLC(I) = SSC(L)/DEN(L)
   39 CHI(L) = CHI(L)+SLC(I)
      REC(L)=1./CHI(L)
   40 CONTINUE
      WRITE OUTPUT TAPE 6, 22
      WRITE OUTPUT TAPE 6, 28, (T(L), REC(L), DELT(L), L=1,50)
      WRITE OUTPUT TAPE 6, 24, (T(L),REC(L),L=1,50)
      CALL PLOT2(GRAPH,500.,0., 500.,0.)
      CALL PLOT3(1H0,T(1),REC(1),51)
      WRITE OUTPUT TAPE 6, 25
      CALL FPLOT4(22,22H          ONE OVER CHI)
      WRITE OUTPUT TAPE 6, 26
      WRITE OUTPUT TAPE 6, 27, P, Q, R, S
      GO TO 1
   10 FORMAT (F10.4, F10.4, E13.5, E13.5, E13.5)
   22 FORMAT (1H1,11X1HT,11X3HREC,17X3HDEL)
   24 FORMAT (1HP,1XF12.0,5XE13.6)
   25 FORMAT (1H1)
   26 FORMAT (1H0,56X11HTEMPERATURE)
   27 FORMAT (1H0,23X4HP = F10.4,5X4HQ = E13.5,5X4HR = E13.5,5X4HS =
     1E13.5)
   28 FORMAT (1H0,1XF12.0,5XE13.6,8XF9.2)
      END
```

I2

Part 1

```
C      PROGRAM FOR CALCULATING G VALUES AND TRANSITION PROBABILITY
C      NUMBERS AS FUNCTIONS OF SMALL DELTA.  L REPRESENTS THE PSI WHICH
C      PREDOMINATES IN THE LOWEST U PRIME LEVEL.
C
       DIMENSION A(3,3),   ARRAY(6), VA(3,3),   W0(5), W1(5,5), B(4,4),
      1C(4,4), W2(5,5), D(4,4), E(4,4), T(50), CHI(50), REC(50),
      1PV(4,4),QV(4,4),RV(4,4),SV(4,4),PB(4,4),QC(4,4),RD(4,4),SE(4,4),
      1SYLB1(3),SYA1M(3),SYLM(3,3),SYMA2(3),SYB1N(3),SYMN(3,3),SYKA1(3),
      1SYB2L(3),SYKL(3,3),SYKA2(3),SYB2N(3),SYKN(3,3),ELM1PQ(3,3),
      1ELM1PS(3,3),ELM1QR(3,3),ELM1RS(3,3),ELM4QR(3,3),AH(3,3),VAA(3,3),
      1PVR(4,4),QVR(4,4),RVR(4,4),SVR(4,4),PBR(4,4),QCR(4,4),RDR(4,4),
      1SER(4,4),KK(4)
       ZETA = 450.
       DO 500 IDEL = 1,51,2
       DEL = IDEL*100 - 2100
       IF (DEL - 140.0) 160,160,159
  159 L = 1
       GO TO 165
  160 IF (DEL + 140.0) 162,161,161
  161 L = 2
       GO TO 165
  162 IF (DEL + 422.0) 164,163,163
  163 L = 3
       GO TO 165
  164 L = 2
  165 WRITE OUTPUT TAPE 6, 14, DEL, L
```

Part 2 - Same as in I1

Part 3

```
C     B(I,I), C(I,I), D(I,I), AND E(I,I) ARE THE DIAGONAL ELEMENTS OF
C     THE MAGNETIC HAMILTONIAN.
C
      DO 30 I=1,3
      B(I,I) = W1(I,1) + WC(I)
      C(I,I) = W1(I,2) + WC(I)
      D(I,I) = W1(I,3) + WC(I)
      E(I,I) = W1(I,4) + WC(I)
   30 CONTINUE
      B(4,4) = W1(5,2) + WC(5)
      C(4,4) = W1(4,1) + WC(4)
      D(4,4) = W1(4,2) + WC(4)
      E(4,4) = W1(5,1) + WC(5)
C
C     DIAGONALIZATION OF SECOND-ORDER MAGNETIC STATES, CAP LAMBDA.
C     PV, QV, RV, AND SV ARE THE MATRIX ELEMENTS.
C
      DO 51 I=1,4
      DO 51 J=1,4
      PV(I,J) = B(I,J)
      QV(I,J) = C(I,J)
      RV(I,J) = D(I,J)
      SV(I,J) = E(I,J)
   51 CONTINUE
```

```
      WRITE OUTPUT TAPE 6, 85, ((PV(I,J),J=1,4),I=1,4)
      WRITE OUTPUT TAPE 6, 86, ((QV(I,J),J=1,4),I=1,4)
      WRITE OUTPUT TAPE 6, 87, ((RV(I,J),J=1,4),I=1,4)
      WRITE OUTPUT TAPE 6, 88, ((SV(I,J),J=1,4),I=1,4)
C
C     PVR(N), ETC. ARE THE UPPER-HALF ELEMENTS BEFORE DIAGONALIZATION,
C     THE DIAGONALIZED VALUES AFTER.  PB, QC, RD, AND SE ARE THE EIGEN-
C     VECTORS.
C
      N = 0
      DO 299 J=1,4
      DO 299 I=1,J
      N = N + 1
      PVR(N) = PV(I,J)
      QVR(N) = QV(I,J)
      RVR(N) = RV(I,J)
      SVR(N) = SV(I,J)
  299 CONTINUE
      CALL JACOBI (4,PVR,PB,ITER,TRACE)
      CALL JACOBI (4,QVR,QC,ITER,TRACE)
      CALL JACOBI (4,RVR,RD,ITER,TRACE)
      CALL JACOBI (4,SVR,SE,ITER,TRACE)
      WRITE OUTPUT TAPE 6, 95, ((PB(I,J),J=1,4),I=1,4)
      WRITE OUTPUT TAPE 6, 96, ((QC(I,J),J=1,4),I=1,4)
      WRITE OUTPUT TAPE 6, 97, ((RD(I,J),J=1,4),I=1,4)
      WRITE OUTPUT TAPE 6, 98, ((SE(I,J),J=1,4),I=1,4)
      M=0
      DO 180 K=1,4
      M = M + K
      PVR(K)=PVR(M)
      QVR(K)=QVR(M)
      RVR(K)=RVR(M)
      SVR(K)=SVR(M)
  180 CONTINUE
      WRITE OUTPUT TAPE 6, 399
      WRITE OUTPUT TAPE 6, 300, (PVR(K),K=1,4)
      WRITE OUTPUT TAPE 6, 301, (QVR(K),K=1,4)
      WRITE OUTPUT TAPE 6, 302, (RVR(K),K=1,4)
      WRITE OUTPUT TAPE 6, 303, (SVR(K),K=1,4)
      DO 54 K=1,3
      PVR(K) = PVR(K) - WC(K)
      QVR(K) = QVR(K) - WC(K)
      RVR(K) = RVR(K) - WC(K)
      SVR(K) = SVR(K) - WC(K)
   54 CONTINUE
      PVR(4) = PVR(4) - WC(5)
      QVR(4) = QVR(4) - WC(4)
      RVR(4) = RVR(4) - WC(4)
      SVR(4) = SVR(4) - WC(5)
      WRITE OUTPUT TAPE 6, 100, (PVR(K),K=1,4)
      WRITE OUTPUT TAPE 6, 101, (QVR(K),K=1,4)
      WRITE OUTPUT TAPE 6, 102, (RVR(K),K=1,4)
      WRITE OUTPUT TAPE 6, 103, (SVR(K),K=1,4)
C
C     SY OF VARIABLE NAMES REPRESENTS PSI.  K, L, M, AND N REPRESENT
C     KAPPA, LAMBDA, MU, AND NU.  A AND B REPRESENT ALPHA AND BETA.
C     1 AND 2 REPRESENT SINGLE  AND DOUBLE PRIME.
C
C    CALCULATION OF ELEMENTS OF LAMBDA-ONE PQ
C
      DO 55 I=1,3
      SYKA1(I) = -VA(2,I)*1.9365
      SYB2L(I) = VA(2,I)*1.1619 - VA(3,I)*1.0328
      DO 55 J=1,3
      SYKL(I,J) = VA(2,I)*VA(2,J)*1.0392 + VA(2,I)*VA(3,J)*0.5196 +
     1VA(3,I)*VA(2,J)*0.5196 -VA(3,I)*VA(3,J)*0.4619
   55 CONTINUE
C
C     CALCULATION OF ELEMENTS OF LAMBDA-ONE PS
C
      SYB2A2 = -2./3.
      DO 56 I=1,3
      SYKA2(I) = -VA(2,I)*0.6708 + VA(3,I)*0.5963
      SYB2N(I) = VA(2,I)*0.6708 - VA(3,I)*0.5963
      DO 56 J=1,3
      SYKN(I,J) = -VA(2,I)*VA(3,J)*1.5 - VA(3,I)*VA(2,J)*1.5 -
     1VA(3,I)*VA(3,J)*2./3. - VA(1,I)*VA(1,J)
   56 CONTINUE
C
C     CALCULATION OF ELEMENTS OF LAMBDA-ONE AND LAMBDA-FOUR QR
C
      SYA1B1 = 2.
      DO 60 I=1,3
      SYLB1(I) = -VA(2,I)*1.118
      SYA1M(I) = VA(2,I)*1.118
      DO 60 J=1,3
      SYLM(I,J) = -VA(1,I)*VA(1,J) + VA(2,I)*VA(2,J)*1.2 - VA(2,I)*
     1VA(3,J)*0.9 -VA(3,I)*VA(2,J)*0.9 - VA(3,I)*VA(3,J)*1.2
   60 CONTINUE
C
C     CALCULATION OF ELEMENTS LAMBDA-ONE RS
C
      DO 61 I=1,3
      SYMA2(I) = -VA(2,I)*1.1619 + VA(3,I)*1.0328
      SYB1N(I) = VA(2,I)*1.9365
      DO 61 J=1,3
      SYMN(I,J) = VA(2,I)*VA(2,J)*1.0392 + VA(2,I)*VA(3,J)*0.5196 +
     1VA(3,I)*VA(2,J)*0.5196 - VA(3,I)*VA(3,J)*0.4619
   61 CONTINUE
C
C     ELM1 REPRESENTS ELEMENTS OF LOWEST U PRIME, ELM4 OF E PRIME.  TLM
C     IS TOTAL OF ALL ELEMENTS.  PLM IS TRANSITION PROBABILITY NUMBERS.
C
C     CALCULATION OF LAMBDA-ONE PQ
C
      TLM1PQ = 0.
      DO 72 I=1,3
      DO 72 J=1,3
      ELM1PQ(I,J) = PB(I,L)*(QC(J,L)*SYKL(I,J) + QC(4,L)*SYKA1(I)) +
     1PB(4,L)*(QC(J,L)*SYB2L(J))
      TLM1PQ = TLM1PQ + ELM1PQ(I,J)
   72 CONTINUE
C
C     CALCULATION OF LAMBDA-ONE PS
C
      TLM1PS = 0.
      DO 73 I=1,3
      DO 73 J=1,3
      ELM1PS(I,J) = PB(I,L)*(SE(J,L)*SYKN(I,J) + SE(4,L)*SYKA2(I)) +
     1PB(4,L)*(SE(J,L)*SYB2N(J)) + PB(4,L)*SE(4,L)*SYB2A2
      TLM1PS = TLM1PS + ELM1PS(I,J)
   73 CONTINUE
C
C     CALCULATION OF LAMBDA-ONE QR
C
      TLM1QR = 0.
      DO 74 I=1,3
      DO 74 J=1,3
      ELM1QR(I,J) = QC(I,L)*(RD(J,L)*SYLM(I,J) + RD(4,L)*SYLB1(I)) +
     1QC(4,L)*(RD(J,L)*SYA1M(J)) + QC(4,L)*RD(4,L)*SYA1B1
      TLM1QR = TLM1QR + ELM1QR(I,J)
   74 CONTINUE
C
C     CALCULATION OF LAMBDA-ONE RS
C
      TLM1RS = 0.
      DO 75 I=1,3
      DO 75 J=1,3
      ELM1RS(I,J) = RD(I,L)*(SE(J,L)*SYMN(I,J) + SE(4,L)*SYMA2(I)) +
     1RD(4,L)*(SE(J,L)*SYB1N(J))
      TLM1RS = TLM1RS + ELM1RS(I,J)
   75 CONTINUE
C
C     CALCULATION OF LAMBDA-FOUR QR
```

```
C
      TLM4QR = 0.
      DO 76 I=1,3
      DO 76 J=1,3
      ELM4QR(I,J) = QC(I,4)*(RD(J,4)*SYLM(I,J) + RD(4,4)*SYLB1(I)) +
     1QC(4,4)*(RD(J,4)*SYA1M(J)) + QC(4,4)*RD(4,4)*SYA1B1
      TLM4QR = TLM4QR + ELM4QR(I,J)
   76 CONTINUE
      PLM1PS = TLM1PS**2
      PLM1QR = TLM1QR**2
      PLM1RS = TLM1RS**2
      PLM1PQ = TLM1PQ**2
      PLM4QR = TLM4QR**2
      WRITE OUTPUT TAPE 6, 104
      WRITE OUTPUT TAPE 6, 105, PLM1PQ, PLM1PS, PLM1QR, PLM1RS, PLM4QR
  500 CONTINUE
      CALL EXIT
  399 FORMAT (1H1,1X18HBEFORE SUBTRACTION)
  300 FORMAT (1H0, 3HPVR//3X4E15.6//)
  301 FORMAT (1H0, 3HQVR//3X4E15.6//)
  302 FORMAT (1H0, 3HRVR//3X4E15.6//)
  303 FORMAT (1H0, 3HSVR//3X4E15.6//)
   10 FORMAT  (F10.4)
   14 FORMAT (1H1,11H DEL EQUALS F10.4,5X8HL EQUALS I4)
   12 FORMAT (1H0,3H VA/1X3F12.6/1X3F12.6/1X3F12.6)
   13 FORMAT (1H0,29H SPIN-ORBIT COUPLING ENERGIES/1X5F12.6)
  104 FORMAT (1H0,4X6HPLM1PQ,9X6HPLM1PS,9X6HPLM1QR,9X6HPLM1RS,9X6HPLM4QR
     1)
  105 FORMAT (1H0,5E15.6)
  100 FORMAT (1H0,15HPV(I,J)--B(I,J)//1X,4E15.6//)
  101 FORMAT (1H0,15HQV(I,J)--C(I,J)//1X,4E15.6//)
  102 FORMAT (1H0,15HRV(I,J)--D(I,J)//1X,4E15.6//)
  103 FORMAT (1H0,15HSV(I,J)--E(I,J)//1X,4E15.6//)
   85 FORMAT (1H0,2HPV/1X4E15.6/1X4E15.6/1X4E15.6/1X4E15.6)
   86 FORMAT (1H0,2HQV/1X4E15.6/1X4E15.6/1X4E15.6/1X4E15.6)
   87 FORMAT (1H0,2HRV/1X4E15.6/1X4E15.6/1X4E15.6/1X4E15.6)
```

```
 88 FORMAT (1H0,2HSV/1X4E15.6/1X4E15.6/1X4E15.6/1X4E15.6)
 95 FORMAT (1H0,2HPB/1X4E15.6/1X4E15.6/1X4E15.6/1X4E15.6)
 96 FORMAT (1H0,2HQC/1X4E15.6/1X4E15.6/1X4E15.6/1X4E15.6)
 97 FORMAT (1H0,2HRD/1X4E15.6/1X4E15.6/1X4E15.6/1X4E15.6)
 98 FORMAT (1H0,2HSE/1X4E15.6/1X4E15.6/1X4E15.6/1X4E15.6)
200 FORMAT (1H1,21HDIAG. BEFORE ORDERING)
201 FORMAT (1H0,4E15.6//)
202 FORMAT  (1H0,43HDIAG. AFTER ORDERING, BEFORE WO SUBTRACTION)
    END
```

BIBLIOGRAPHY

1. J. S. Griffith, "The Theory of Transition Metal Ions," Cambridge University Press, 1961, chapter 5.

2. J. H. Van Vleck, "Electric and Magnetic Susceptibilities," Oxford University Press, 1932, chapter 2.

3. B. N. Figgis, "Introduction to Ligand Fields," Interscience Publishers, New York, 1966.

4. R. C. Stoufer, D. W. Smith, E. A. Clevenger, and T. E. Norris, Inorg. Chem., 5, 1167(1966).

5. H. M. Fisher, Ph.D. Dissertation, University of Florida, 1966.

6. P. Langevin, Annales de Chemie et Physique (8), 5, 70(1905).

7. P. Curie, Annales de Chemie et Physique (7), 5, 289 (1895).

8. B. N. Figgis and R. S. Nyholm, J. Chem. Soc., 1954, 12.

9. D. H. Busch, "Cobalt," Ed. by R. S. Young, A.C.S. Monograph Series, Reinhold Publishing Co., New York, 1960, chapter 6.

10. L. C. Jackson, Phil. Trans., 224, 1(1924).

11. L. Cambi and L. Szego, Ber., 66, 656(1933).

12. A. H. White, R. Roper, E. Kokot, H. Waterman, and R. L. Martin, Australian J. Chem., 17, 294(1964).

13. G. Bozza, Gazz. chim. ital., 63, 778(1933); cf. reference 31.

14. L. Cambi, Congr. Intern. quim. pura apl., 9°, Madrid, 2, 199(1934); cf. Chem. Abstr., 29, 6858(1935).

15. R. B. Janes, Phys. Rev., 48, 78(1935).

16. M. Calvin and C. H. Barkelew, J. Am. Chem. Soc., 68, 2267(1946).

17. B. N. Figgis and R. S. Nyholm, J. Chem. Soc., 1959, 338.

18. H. S. French, M. Z. Magee, and E. Sheffield, J. Am. Chem. Soc., 64, 1924(1942).

19. J. B. Willis and D. P. Mellor, J. Am. Chem. Soc., 69, 1237(1947).

20. F. Basolo and W. R. Matoush, J. Am. Chem. Soc., 75, 5663(1953).

21. L. Sacconi, P. Paoletti, and G. Del Re, J. Am. Chem. Soc., 79, 4062(1957).

22. L. M. Venanzi, J. Chem. Soc., 1958, 719.

23. G. Maki, J. Chem. Phys., 28, 651(1958).

24. G. Maki, J. Chem. Phys., 29, 1129(1958).

25. C. J. Ballhausen and A. D. Liehr, J. Am. Chem. Soc., 81, 538(1959).

26. J. S. Griffith, J. Inorg. Nucl. Chem., 2, 229(1956).

27. L. Sacconi, R. Cini, M. Ciampolini, and F. Maggio, J. Am. Chem. Soc., 82, 3487(1960).

28. J. P. Fackler, Jr. and F. A. Cotton, J. Am. Chem. Soc., 82, 5005(1960).

29. R. H. Holm and T. M. McKinney, J. Am. Chem. Soc., 82, 5506(1960).

30. F. A. Cotton and J. P. Fackler, Jr., J. Am. Chem. Soc., 83, 2818(1961).

31. G. A. Melson and D. H. Busch, J. Am. Chem. Soc., 86, 4830(1964).

32. D. R. Eaton, W. D. Phillips, and D. J. Caldwell, J. Am. Chem. Soc., 85, 397(1963).

33. R. H. Holm and K. Swaminathan, Inorg. Chem., 2, 181 (1963).

34. R. H. Holm, A. Chakravorty, and G. O. Dudek, J. Am. Chem. Soc., 86, 379(1964).

35. G. W. Everett, Jr. and R. H. Holm, J. Am. Chem. Soc., 87, 5266(1964).

36. G. W. Everett, Jr. and R. H. Holm, J. Am. Chem. Soc., 88, 2442(1966).

37. H. C. A. King, E. Körös, and S. M. Nelson, J. Chem. Soc., 1963, 5449.

38. H. C. A. King, E. Körös, and S. M. Nelson, J. Chem. Soc., 1964, 4832.

39. L. Sacconi, M. Ciampolini, and G. P. Speroni, Inorg. Chem., 4, 1116(1965).

40. K. Madeja and E. König, J. Inorg. Nucl. Chem., 25, 377(1963).

41. W. A. Baker, Jr. and H. M. Bobonich, Inorg. Chem., 3, 1184(1964).

42. W. A. Baker, Jr. and G. J. Long, Chem. Commun., 1965, 368.

43. E. König and K. Madeja, Chem. Commun., 1966, 61.

44. P. E. Figgins and D. H. Busch, J. Am. Chem. Soc., 82, 820(1960).

45. R. C. Stoufer, D. H. Busch, and W. B. Hadley, J. Am. Chem. Soc., 83, 3732(1961).

46. P. Cossee, Mol. Phys., 3, 125(1960).

47. R. Hogg and R. G. Wilkins, J. Chem. Soc., 1962, 340.

48. O. Ramirez, Ph.D. Dissertation, University of Florida, 1965.

49. A. D. Liehr, J. Phys. Chem., 67, 1314(1963).

50. A. H. Ewald, R. L. Martin, I. G. Ross, and A. H. White, Proc. Roy. Soc., A280, 235(1964).

51. H. Theorell and A. Ehrenberg, Acta. Chem. Scand., 5, 823(1951).

52. P. George, J. Beetlestone, and J. S. Griffith, "Haematin Enzymes," Pergamon Press, New York, 1961, p. 105.

53. P. A. M. Dirac, "The Principles of Quantum Mechanics," Oxford University Press, 1958.

54. J. G. Schmidt, W. S. Brey, Jr., and R. C. Stoufer, Inorg. Chem., in press.

55. Ref. 1, chapter 9.

56. J. H. M. Thornley, C. G. Windsor, and J. Owen, Proc. Roy. Soc. A284, 252(1965).

57. Ref. 1, Appendix 2.

58. Y. Tanabe and S. Sugano, J. Phys. Soc. Japan, 9, 753 (1954).

59. Ref. 1, p. 107.

60. Ref. 1, p. 271.

61. T. M. Dunn, Trans. Farad. Soc., 57, 1441(1961).

62. J. Owen, Proc. Roy. Soc., A227, 183(1955).

63. C. G. Barraclough, Trans. Farad. Soc., 62, 1033(1966).

64. T. M. Dunn, "Modern Coordination Chemistry," Ed. by J. Lewis and R. G. Wilkins, Interscience Publishers, Inc., New York, 1963, p. 284.

65. O. G. Holmes and D. S. McClure, J. Chem. Phys., 26, 1686(1957).

66. M. Kotani, J. Phys. Soc. Japan, 4, 293(1949).

67. B. C. Guha, Nature, 197, 1093(1963).

68. J. S. Griffith, Trans. Farad. Soc., 54, 1109(1958).

69. E. A. Clevenger, Master's Thesis, University of Florida, 1961.

70. K. Nakamoto, "Infrared Spectra of Inorganic and Coordination Compounds," John Wiley and Sons, Inc., New York, 1963, p. 119.

71. J. H. van Santen and J. S. van Wieringen, Rec. Trav. Chim. Pays-Bas, 71, 420(1952).

72. M. T. Barnet, B. M. Craven, H. C. Freeman, N. E. Kime, and J. A. Ibers, Chem. Commun., 1966, 307.

73. H. M. Fisher and R. C. Stoufer, Inorg. Chem., 5, 1172 (1966).

74. J. A. Bertrand and D. A. Carpenter, Inorg. Chem., 5, 514(1966).

75. Ref. 2, chapter 7.

76. Ref. 53, chapter 11.

77. J. G. Schmidt, Ph. D. Dissertation, University of Florida, 1965.

78. M. Bersohn and J. C. Baird, "An Introduction to Electron Paramagnetic Resonance," W. A. Benjamin, Inc., New York, 1966.

79. G. E. Pake, "Paramagnetic Resonance," W. A. Benjamin, Inc., New York, 1962.

80. W. Low, "Paramagnetic Resonance in Solids," Academic Press, Inc., New York, 1960, p. 91.

81. Ref. 1, chapter 12.

82. Ref. 78, p. 74.

83. Ref. 3, chapter 11.

84. K. W. H. Stevens, Proc. Roy. Soc., A219, 542(1953).

85. W. J. McCarthy, Ph.D. Dissertation, University of Florida, 1966.

BIOGRAPHICAL SKETCH

David Lloyd Williams was born March 12, 1939, in Newton, Massachusetts. He graduated from Newton High School in June, 1957. In June, 1961, he received a Bachelor of Science degree from The Massachusetts Institute of Technology. He received a Master of Science degree in August, 1963, from the University of Vermont. In September, 1963, he enrolled in the University of Florida where he has pursued studies toward the degree of Doctor of Philosophy until the present time.

This dissertation was prepared under the direction of the chairman of the candidate's supervisory committee and has been approved by all members of that committee. It was submitted to the Dean of the College of Arts and Sciences and to the Graduate Council, and was approved as partial fulfillment of the requirements for the degree of Doctor of Philosophy.

December 17, 1966

E. Ruffin Jones
Dean, College of Arts and Sciences

Dean, Graduate School

Supervisory Committee:

R. Carl Stoufer
Chairman

Darwin W. Smith

R. D. Dresdner

J. D. Winefordner

T. D. Carr